TRAINING AND ASSESSMENT OF HAND-EYE COORDINATION WITH ELECTROENCEPHALOGRAPHY

LEE CHUN SIONG

(B.Eng.(Hons.), NUS)

A THESIS SUBMITTED

FOR THE DEGREE OF DOCTOR OF PHILOSOPHY

DEPARTMENT OF MECHANICAL ENGINEERING

NATIONAL UNIVERSITY OF SINGAPORE

2015

DECLARATION

I hereby declare that this thesis is my original work and it has been written by me in its entirety. I have duly acknowledged all the sources of information which have been used in the thesis.

This thesis has also not been submitted for any degree in any university previously.

Lee Chun Siong

14 Jan 2015

Acknowledgments

First of all, I would like to express my deepest gratitude for my supervisor, Associate Prof Chui Chee Kong, for his guidance over the years. This thesis would not be possible if not for his constant guidance and encouragement.

I would like to thank my family, friends and colleagues at NUS for helping me through the period of my studies and encouraging me throughout this arduous journey.

I would also like to thank the various collaborators and mentors who have also helped me to accomplish this work:

- Associate Prof Stephen Chang (NUH)
- Dr Guan Cuntai (AStar I2R)
- Mr Wang Chuan Chu (AStar I2R)
- Dr Tan Bhing Leet (IMH)
- Dr Joseph Leong (IMH)
- Dr Eu Pui Wai (IMH)

Summary

Hand-eye coordination (HEC) is a complex system of perceptual processing of visual information, proprioceptive feedback of our hands and arms and the cognitive controller that manages these sensory inputs and executive motion. It is a natural function taken for granted in the simple common tasks in everyday life. However, in some people such as mentally ill patients, their hand-eye coordination may become impaired and require exhaustive rehabilitative treatments. At the other end of the spectrum, professionals such as athletes and surgeons require excellent HEC to function.

The objective of this thesis is to investigate the visual, motor and neural aspects of HEC through neural and motor performance analysis of subjects performing visual cue driven HEC tasks such as pointing and tracing in order to examine a person's hand eye coordination capability thereby leading to methods for more effective assessment and training. This research approaches each aspect of HEC and develops appropriate simulation games to study the hand eye coordination skills of subjects. Specific investigations include identifying pertinent Electroencephalography (EEG) markers correlating to motor skill mastery, analysing and correlating motor performance with neural activity.

The effect of visual cues influencing HEC was studied upon. Visual cues provide significant perceptual information that can affect performance. In some scenarios such as surgical endoscopy, some cues are lost or diminished, leading to reduced HEC ability and diminished motor performance. In our study, we investigated the influence of attenuating and augmenting various visual cues such as dynamic depth shadowing to improve HEC capability, reducing execution time and number of errors.

The effect of robotic haptic guidance on motor skill mastery of two HEC tasks through a robotic manipulator was also investigated. Through two separate tasks, one

designed for testing accuracy of motion and another designed for testing consistency in motion, detailed motion analysis breakdown in factors such as cumulative trajectory error and cumulative joint angle motion show that robotic guidance improves motor skill mastery more than autonomous practice. Haptic guidance also elicited a larger change in neural signal complexity in the subjects.

Conventional physical motor task performance metrics, when insufficient in differentiating the overall performance, can be augmented with neural analysis. Utilizing non-invasive EEG readings, we compared task performance against EEG readings to identify possible neural markers for gauging mental activity pertinent to motor skill mastery of a simple folding task. Through power spectrum and signal complexity analysis, results identify signal complexity values and activity in the theta and low alpha frequency band in the central, occipital and parietal regions as suitable neural markers.

Further experiments with a rapid-fire pointing task within an interactive game on a touch-screen panel demonstrated the correlation between task performance learning curves with neural activity and the effect of colour in the visual cues presented to the subjects. Epoched extraction of consecutive event related EEG data enabled neural analysis at shorter time scales, revealing significant differences in intra-task waveforms for different scenarios.

Table of Contents

Author's Publications

Book Chapters

C.S. Lee and C.K. Chui. "Training and Measuring the Hand–Eye Coordination Capability of Mentally Ill Patients" in Advances in Therapeutic Engineering. CRC Press ISBN 9781439871737. pp. 45-82, 2012.

C. S. Lee, C. K. Chui, C. T. Guan, P. W. Eu, B. L. Tan, and J. Leong, "Integrating EEG Modality in Serious Games for Rehabilitation of Mental Patients," in Simulations, Serious Games And Their Applications, Y. Cai and S. L. Goei, Eds. Singapore, pp. 51–68, 2014.

Article in Journal

C.S. Lee and C.K. Chui, "EEG Analysis of Hand-eye Coordination with Simulation Games", Simulation & Gaming (submitted)

C.S. Lee, C.K. Chui, and S. K. Y. Chang. "Influence of Dynamic Shadowing on 2D and 3D Laparoscopic Visualization Under Visible Light and Infrared Light", Journal of Laparoendoscopic & Advanced Surgical Techniques A, vol. 23, pp. 561-569, 2013.

S. K. Y. Chang, C. S. Lee, W. W. Hlaing, and C. K. Chui, "Vascularised porcine liver model for surgical training", Medical Education, vol. 45, pp. 520, 2011.

Conference Paper

C. S. Lee, L. Yang, T. Yang, C. K. Chui, J. Liu, W. Huang, Y. Su, and S. K. Y. Chang, "Designing an active motor skill learning platform with a robot-assisted laparoscopic trainer," in Engineering in Medicine and Biology Society, EMBC, pp. 4534-4537, 2011.

List of Tables

List of Figures

List of Abbreviations

2D	Two-Dimensional
3D	Three-Dimensional
ABS	Acrylonitrile Butadiene Styrene
ADHD	Attention Deficit/Hyperactivity Disorder
ANOVA	Analysis of Variance
CBFELM	Cerebellar Feedback-Error-Learning Model
CELTS	Computer-Enhanced Laparoscopic Training System
CMOS	Complementary Metal-Oxide Semiconductor
CNS	Central Nervous System
DC	Direct Current
DOFs	Degrees of Freedom
ECoG	Electrocorticography
EEG	Electroencephalography
EMG	Electromyography
EOG	Electrooculography
EPSP	Excitatory Postsynaptic Potential
ERP	Event-Related Potential
FFT	Fast Fourier Transform
FIR	Finite Impulse Response
FLS	Fundamentals of Laparoscopic Surgery
fMRI	Functional Magnetic Resonance Imaging
HD	High-Definition
HEC	Hand-Eye Coordination
ICA	Independent Component Analysis
IRL	Infrared Light
LED	Light-Emitting Diode

LZC	Lempel-Ziv Complexity
MEG	Magnetoencephalography
MIS	Minimally Invasive Surgery
MsI	Primary Motor Cortex
NASA	National Aeronautics and Space Administration
NIRS	Near-Infrared Spectroscopy
OT	Occupational Therapy
PCCR	Pupil Centre Corneal Reflection
PLV	Phase-Locking Value
PMC	Premotor Cortex
POG	Point-of-Gaze
RGB	Red Green Blue
SMA	Supplementary Motor Area
SmI	Somatosensory Cortex
SMR	Sensorimotor Rhythm
SQUID	Superconducting Quantum Interference Device
USB	Universal Serial Bus

1 Introduction

1.1 Background and Motivations

Hand-Eye Coordination (HEC) is a complex system of perceptual processing of visual information, proprioceptive feedback of our hands and arms and the cognitive controller that manages these sensory inputs and executive motion. It is a natural fine motor skill function that is learned in early childhood and taken for granted in the execution of simple common tasks in everyday life.

However, in some instances of neurological trauma such as bilateral lesions of the parieto-occiptal lobe in people suffering from Bálint's syndrome [1] or psychological disorder such as children suffering from developmental coordination disorder [2], the brain's ability to coordinate visual input and proprioception with executive function is impaired, leading to significant deterioration in HEC ability. In such patients, the conventional route of therapy is lengthy and continual occupational rehabilitation in order to ameliorate the deficit in HEC ability. This effectually puts a large strain on the manpower and resources needed to operate the rehabilitative programs. At the other end of the spectrum, professionals such as athletes and surgeons require excellent HEC to function and they spend countless hours practicing in order to achieve skill mastery. At both ends of the spectrum, there lies a need for HEC training and current methods often involve the need for manpower-intensive experienced coaching in order to improve the efficacy of the training.

In this thesis, HEC is organized into three aspects: vision, haptics and cognition. The visual aspect covers visual perception and eye gaze motion. The haptic aspect covers executive motion of the hand/arm along with proprioception and haptic feedback. The cognition aspect covers the synergy between the visual and haptic aspects coupled with memory and learning.

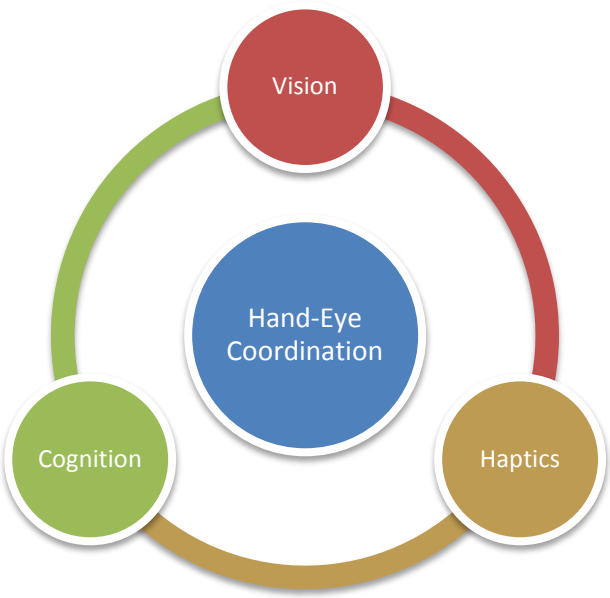

Figure 1.1: Aspects of Hand-Eye Coordination.

Much of the earlier research into HEC involves fields such as the study of human gaze behaviour, eye saccade/fixation strategies and analysis of human arm motion, including task-specific gaze behaviour with the eyes leading the hand motion and providing optimal spatial feedback of the hand's motion in completion of the task, highlighting the synergy between visual inputs and motor output being the core of a person's HEC ability. The effects of visual cues and haptic cues on HEC have also been explored thoroughly.

In more recent times, with the advancement and proliferation of brain monitoring methods, especially non-invasive ones, such as Electroencephalography (EEG), Functional Magnetic Resonance Imaging (fMRI) and Near-Infrared Spectroscopy (NIRS), research into brain functions has been exponentially growing but still, very little is known about the various neural mechanisms in the brain that support HEC. That is because HEC requires almost every aspect of the central nervous system such as the occipital lobe that processes visual inputs, frontal lobe for planning and parietal lobe for sensory integration. In addition, current state of the art brain monitoring

devices are also unable to provide the level of spatio-temporal resolution needed to fully monitor the billions of neurons and trillions of synapses in a single brain.

The notion of monitoring the brain for HEC task mastery stems from two general facts from neuroscience research into brain function: Firstly, the cerebral cortex can be spatially generalized into functional lobes [3]. Measuring activity at specific regions of the brain therefore relates to particular brain function. Secondly, neuroplasticity which is the generalized term for induced plastic changes in the neurons and synapses occurs as a result of task mastery [4]. Therefore, there should be a correlation between the changes in brain activities of a person with the consolidation of skill over practice.

The broad aim of this research is to probe the nature of this correlation by controlling inbound cues to the subject (visual and haptic cues) and observing resultant outbound changes from the subject (motor performance and neural activity). By first developing an understanding of this correlation, we hope to eventually apply this knowledge and achieve a better means of training and assessment of HEC tasks.

To achieve the aim of this research, hypotheses are constructed and a series of experiments have been conducted for this study on HEC. The experiments are connected to the theme of this research when perceived as permutations of the 3 broad aspects of HEC: vision, haptics and cognition as described in Chapter 1. The first experiment in Chapter 4 can be generalized as the investigation of visual cues affecting HEC ability. In the second experiment in Chapter 5, the focus is on visual cues with cognition through task mastery and its associated changes in neural activity. In Chapter 6, the robotic platform provides substantive haptic cues, subjects' motor performance and its associative neural activity were compared. And finally the last experiment in Chapter 7 validates and builds on the knowledge of implementing direct and indirect visual cues and neural analysis trends that have been founded in

the previous chapters. The experiment in Chapter 7 also brings in new intra-task modality of analysis such as event-related potentials which have been lacking in the previous experiments. All these experiments contributed to proving of the hypotheses.

1.2 Objectives and Scope

Different aspects of HEC have been studied but there are still underlying voids that should be addressed:

- The significance of visual cues in affecting performance and mastery with a HEC task;
- The significance of haptic cues in affecting performance and mastery with a HEC task; and
- The changes in brain activity in relation to the mastery of a HEC task.

Specifically, the objectives of this research are to address these three main voids by:

(1) Investigating the effect of augmenting and attenuating visual cues such as depth and colour in affecting motor performance with a series of HEC tasks;
(2) Applying signal processing methodologies for EEG analysis to identify neural markers in the EEG pertinent to the motor skill mastery of HEC tasks;
(3) Investigating the efficacy of using EEG as an augmentation to conventional physical motor task performance metrics; and
(4) Investigating the effect of haptic cues in the form of robotic guidance in training two HEC tasks through motor performance analysis and EEG neural activity.

In Chapter 4, the experiment investigated Objective (1) by examining the hypothesis that HEC performance can be improved through the augmentation of visual cues. Different permutations of depth, colour and binocular cues were augmented and attenuated to investigate the effect of visual cues on HEC performance.

In Chapter 5, the experiment explored Objectives (2) and (3) by considering the hypothesis that trends in neural activity can correlate with the subjects' mastery of HEC tasks. Subjects performed on a simple cue-driven box folding task until the task was mastered. EEG analysis was performed through the computation of spectral power and LZC. Physical performance was correlated with EEG activity and pertinent EEG markers relevant to the mastery of simple HEC tasks were identified.

In Chapter 6, the experiment explored Objectives (2), (3) and (4) by studying the hypothesis that training with haptic guidance will be better than unaided practice and the difference in mastery can be contrasted through physical performance and neural analysis. Building on the findings of Chapter 4 and 5, Haptic-guidance was implemented and the neural markers identified in Chapter 5 were validated. The effect of haptic guidance on task mastery, motor performance and neural activity was also tabulated.

In Chapter 7, the experiment investigated Objectives (1), (2) and (3) by studying the hypothesis that spatio-temporal changes between epoched windows of visual-cued neural activity can potentially differentiate successful pointing events against failed events and differentiate the level of task mastery. Sequential visual cues generated by the system were correlated with neural activity in order to determine the effect of visual cues on cognitive activity, identifying the spatio-temporal pattern differences between successfully completed tasks and failed tasks.

Appropriate platforms for the training and assessment of HEC tasks were designed, developed and used to conduct experiments such that the targeted aspects of HEC can be studied upon.

1.3 Contributions

The results of this study contribute to the understanding of neural activity changes with respect to the mastery of HEC tasks and the effect of external cues such as visual and haptic cues on neural activity and performance of human subjects. Specifically, the contributions of this thesis are summarized as follows:

- In Chapter 4, the effect of visual cues on HEC was investigated. The significance of visual cues on HEC ability was quantified. A novel way of augmenting depth perception was developed and the significance of this method was proven. Different permutations of visual cues such as colour and shadows were also investigated. It was found that over-augmentation of visual cues of similar nature (shadows and binocular visuals) could inadvertently induce interference that reduced the subjects' performance.
- In Chapter 5, the neural activity of subjects performing a box folding task was investigated. Several neural analysis methods were evaluated and multiple neural markers that were pertinent to the mastery of HEC tasks were identified. The spatio-temporal nature of these neural markers have been verified through subsequent experiments to consistently exhibit correspondence with task performance and mastery. LZC was shown to reflect tonic changes in the neural activity that correlated well with subject task mastery.
- In Chapter 6, a robotic haptic guidance platform was used to train subjects in HEC tasks. In addition to verifying the neural markers introduced in Chapter 5, the experiment objectively identified that computer-generated haptic cues could

significantly aid HEC training and contrasted how neural activity and physical task mastery was different between the two groups.

- In Chapter 7, a platform that implemented a sequential planar pointing task simulation was developed, enabling the analysis of tonic and phasic traits of neural activity. Task mastery was found to correlate with tonic traits like LZC values and task performance was found to correlate with phasic traits like ERP patterns. This discovery showed that varying the timescale of EEG analysis can reveal different facets of HEC performance.

2 Literature Review

Existing literature for the three main aspects of HEC was reviewed. The literature can be categorized into the methods of monitoring vision, haptics and cognition, the tests and platforms for assessing HEC ability and the methods for the modelling and analysis of HEC, in particular, eye-guided arm motions. Neural tracking through EEG was also introduced and various EEG analysis methods have also been detailed.

2.1 Monitoring

HEC monitoring can broadly be classified under eye and gaze tracking, motion tracking and neural tracking. Much of the earlier work into HEC research has been focused on eye motion analysis such as saccadic motions and smooth-pursuit eye motion together with different forms of task-related motion tracking [5]–[7] whereas the use of neural tracking for HEC measurement is a relatively novel aspect. Eye movements and its saccadic gaze control is a key factor in coordinating precise motor control and has been a large part of HEC research [8]–[10]. Strategic saccadic control is inferred as an important aspect of HEC mastery as cognitive neuroscience research shows that goal-directed motion is optimized when both eye and hand motion are harmonized [11]. Optimal performance is achieved when eye motion precedes motor action and operates to acquire the most visually pertinent cues related to the task [12].

2.1.1 Eye tracking

Eye tracking refers to the recording of eye orientations relative to the head. In addition, when the head position and orientation relative to the task space is known, the person's gaze can be derived. This information is useful in many applications such as human-computer interfaces, cognitive psychological research of attention and perception and surgical HEC. Half of the human cortex is dedicated to visual processing. Visual scanning patterns have been shown to couple with changes of

attention focus [13]. Visual cues can significantly affect our cognition and sensorimotor behaviour. The most commonly used eye tracking method is the optical based tracking mechanisms which are popular for being non-invasive and inexpensive.

2.1.1.1 Optical based eye tracking

The optical based method of eye tracking typically uses infrared light that is shone onto the eyes to create a corneal reflection. Subsequently, when the reflected infrared light is picked up by an infrared-sensitive camera, various traits in that captured image can be processed. This technique of determining the point-of-gaze (POG) is commonly called the Pupil Centre Corneal Reflection (PCCR) method [14]. The angular difference of the reflections off the cornea and pupil, along with other geometrical information, can be used to derive the direction of gaze.

A variation in the infrared illumination of the eye is the use of Bright and Dark Pupil tracking. The difference is in the position of the infrared illumination with respect to the optical axis of the infrared camera. When the illumination is on the optical axis of the camera, light shone onto the pupil gets largely reflected into the camera hence the pupil becomes bright. When the illumination is away from the optical axis of the camera, the pupil will appear darker than the iris.

There are several factors in the choice of bright and dark pupil illumination but the fundamental aim of choosing bright/dark pupil illumination is to maximize the iris/pupil contrast for better image segmentation and tracking. For example, ethnicity plays a large factor with Hispanics and Caucasians more suitable for bright pupil illumination and Asians being more suitable for dark pupil illumination. There are robust commercially available optical eye tracking systems that can automate between using bright/dark pupil illumination.

Eye tracking information is commonly used to follow the visual attention fixations and saccades of the subject. Fixations are defined as pauses in eye motion where the foveal gaze is focused on a particular region of interest for the processing of visual information. Whereas saccades are defined as the eye motions in between fixations, shifting the foveal region to a new point of interest. Researchers have been using the fixture and saccade patterns from eye tracking information in order to explore the visual attention behaviour of subjects in response to visual stimulations.

2.1.1.2 Electrooculography

The other common eye tracking method is electrooculography. Electrooculography (EOG) is the measurement of the resting potential between the front and back of the eye, commonly called the corneo-fundal potential [15]. This potential is generated from the retinal pigment epithelium resulting in the cornea of the eye (front) being positively charged with respect to the posterior part of the sclera (back), creating a dipole electric field.

When electrodes are placed in pairs across the eyes vertically or horizontally, the change in electrode potential reflects the rotation in orientation of the eyes. The amplitude of the EOG signal depends on the range of motion of the eye and varies from person to person but it is generally considered to be linear and constant. A 30 degree saccade will produce typical amplitude of about 250 to 1000 μV. Due to the linear and constant relation between EOG signals and eye motion, EOG signals can be used to track eye motion.

The advantage of using an EOG over optical method is that EOG signals can be easily achieved as an extension of an existing electroencephalography (EEG) setup and the electrodes do not obstruct the subject's field of vision. EOG systems are also comparably inexpensive compared to optical based infrared systems for eye motion capturing. Eye motion can also be recorded when the eyelids are closed. This

advantage is used in clinical applications for sleep disorder tests where the rapid eye movement stage of sleep needs to be determined.

2.1.2 Motion tracking

Motion tracking is the process of recording the movement of human subjects. This information could be used in applications such as gait analysis, animation, virtual reality interface and rehabilitation. There are many ways to capture motion and they are primarily divided into the vision based and sensor based approaches.

2.1.2.1 Vision based marker tracking

Vision based approaches to motion capturing can be classified into two general forms: marker based and marker-less systems. Markers refer to arbitrarily inserted visually identifiable points that can be used for tracking. Conventional commercial motion tracking systems utilize marker based motion capturing although the current trend is for more convenient marker-less motion tracking such as the Microsoft Kinect which processes a stereoscopic view of the user as a controller-less interface to their Xbox 360 gaming console.

Vision based motion tracking utilize multiple known camera positions that have overlapping viewpoints of the target to be tracked within a volumetric workspace. This enables the 3D coordinates of the target to be triangulated. Overlapping of the cameras also enables some degree of redundancy such that the markers can be tracked even if they may be obstructed within a particular viewpoint.

Commercial systems commonly use infrared-sensitive systems of markers and cameras so as to easily distinguish the markers from the background. The markers can be of the passive retro-reflective type or active blinking type. Active markers can be individually programmed for its own unique flashing signature that greatly aids in marker identification at the cost of more expensive and complicated implementation over passive markers.

Marker placement positions are usually defined together with the associated system software that will link the marker identities with an internal musculoskeletal model. The markers are usually placed non-invasively on the skin, approximately at joint centres where the skin is closest to the bone and at anatomical landmarks of interest. The rationale is for the markers to not shift locally from underlying muscle flexion. The number of markers is usually chosen to adequately define the motion so as to reduce the amount of post processing. The problems with skin markers are that accuracy and repeatability of placements are not as high as invasive measures since the markers are only connected to soft tissue. Since it is impossible to place the markers right at the joint centres, there are unavoidable translational errors with each marker, even with prior calibration and subject measurement.

2.1.2.2 Vision based marker-less tracking

Aside from conventional methods of using visual markers or physical sensors, recent trends are toward the popularization of marker-less methods that make use of machine vision and image processing techniques to capture motion. The most well-known example is the Microsoft Kinect which is actually a hybrid system consisting of an RGB camera, an infrared laser system for depth sensing and an array of microphones for noise cancellation and voice localization. The infrared laser projector shines a grid array of points for an infrared CMOS camera to pick up, essentially mapping the depth of the whole scene. Coupled with the standard RGB video feed, the system is able to automatically pick out probable regions of interest from the background. Alternatively, regions of interest can also be identified through other means such as feature-based profiling and optical flow methods. Once the regions of interest are identified from the background, segmentation of the image can take place to identify the boundaries of the target. By resolving the change in boundaries over a time sequence, motion vectors can be identified.

Marker-less motion tracking is the cheapest and easiest to implement since it only requires a video feed and depth perception such as the infrared laser system in the Kinect or a pair of cameras to form a stereoscopic view. However, its accuracy is heavily dependent on the post processing algorithms and it is more susceptible to errors from overlapping planes of motions within the perspective of the camera as the targets are tracked by their boundaries instead of marker points. In the experiments conducted for this research, a multimodal system of human performance tracking was developed that included two modes of marker-less motion tracking, differentiating between macro torso and arm motions and localized finger and wrist motions (see Figure 2.1- Figure 2.2).

2.1.2.3 Sensors

Sensor based approaches to motion tracking involves the use of physical sensors such as accelerometers and gyroscopes that are attached to the regions of interest on the body. Human motion is then broken down into relevant forces and angles for interpretation. Typically, sensors work in tandem within a system, sharing a common infrastructure for the collection and transmission of the sensor data. Hence, it is common to have sensors and infrastructure integrally woven into a body suit for better management.

In addition to full body suits, there are also data gloves for the capture of fine motor control in hand motion. Depending on the cost and complexity of the system, data gloves can be used to capture hand motion as basic whole finger curls or up to every individual knuckle joint angles with the abduction between fingers. Hand motion is particularly useful for its characteristics such as hand posture, hand gestures and range of motion.

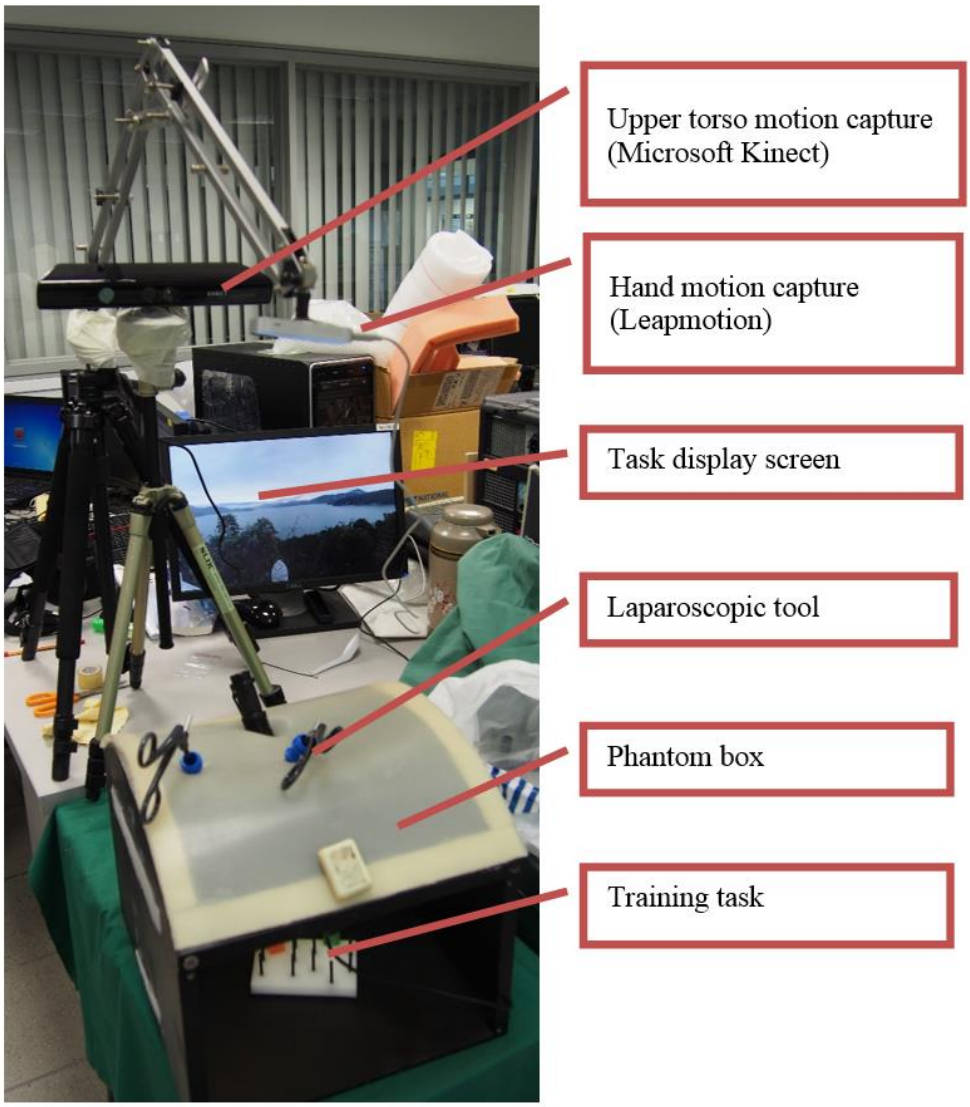

Figure 2.1: Multimodal HEC measurement system.

Multimodal HEC measurement system including dual marker-less motion tracking using a Microsoft Kinect sensor for macro motion tracking (upper body torso and arms) and a Leap Motion sensor for localized motion tracking (fingers and wrist).

Figure 2.2: Photographs of a medical student performing a Pick and Place task

Medical student performing a Pick and Place task with the Multimodal HEC measurement system tracking her physical and neural performance. System operators are in the background observing the subject's performance so that any erroneous actions can be identified.

Typically, goniometers are attached to measure joint flexion and extension angles and inertial sensors such as accelerometers and gyroscopes are used to measure acceleration and orientation respectively. However, the disadvantage with inertial sensors is that by relying on indirect higher order measurements, it leads to bias and drift upon integration. Many human joints are also multi-planar in nature so there may be a need for multiple sensors to measure the joint motion adequately. As human motion is highly non-linear, the sensors too have to be capable of capturing up to an adequate order of sensitivity.

2.1.2.4 Electromyography

Electromyography (EMG) refers to the recording of muscle activation through the electrical membrane potential signals that the muscles emit when the muscles are electrically or neurologically activated. Hence, EMG amplitudes generally correlate

with the amount of force generated by the muscles. EMG is useful for situations where muscle activation is not significantly visible. There are two types of electrodes used for EMG.

Firstly, there are the non-invasive surface electrodes that are usually made of silver/silver chloride and applied on the skin with conductive electrolyte gel. Surface electrodes are effective for superficial muscles but they have limited sensitivity due to the indirect conductivity and "cross-talk" from neighbouring muscles. Hence, they are only sensitive up to a gross muscle group [16].

The invasive approach uses needle electrodes to directly tap on the electrical signal of individual muscle units. These needle electrodes can be inserted into the deeper muscles groups that surface electrodes are unable to reach. However, needle electrodes are less reliable than surface electrodes and are susceptible to displacement by muscle motion. Typically, for HEC measurement, only surface electrodes are used since they are easier to implement and the muscle unit specificity of needle electrodes is not needed.

EMG recordings are influenced by many factors such as electrode reliability, electrode configuration, type of muscle tissue being recorded, electrode specificity and electrode placement. In order to reduce "cross-talk", the electrode locations, size and distribution over the muscle area have to be investigated [17]. Beyond electrodes, EMG signals have to be processed by band-pass filtering, amplification, rectification and smoothening [18].

2.1.3 Neural tracking

Neural tracking refers to the recording of electrical voltages and/or magnetic fields that are generated by neural activity in the brain. While there is a spectrum of invasive and non-invasive methods used to record neural activity, invasive measures such as electrocorticography (ECoG) are mainly used in clinical epilepsy treatment,

whereas non-invasive methods such as Electroencephalography (EEG) and Magnetoencephalography (MEG) are more commonly used. However, MEG requires the use of very sensitive magnetic sensors such as the superconducting quantum interference device (SQUID) along with specially built magnetically shielded rooms. Due to its expensive infrastructure costs and need for low temperature superconductivity, MEG setups are uncommon whereas EEG equipment are the cheapest and easiest to implement.

In addition, there are other methods of indirectly measuring brain activity such as the functional Magnetic Resonance Imaging (fMRI) and near-infrared spectroscopy that operate on the basis of recording the oxygenation levels of haemoglobins in the brain, where it is postulated that brain activity corresponds to the reduction in oxygenation. fMRI scans are able to achieve very high spatial resolution slices but fall short in temporal resolution. As brain activities are highly dynamic spatially and temporally, there is no perfect neural tracking solution available yet.

The main advantage of using intracranial methods is the ability to bypass the poor conductance of the skull and scalp so as to record the neural activity at much lower noise levels and with higher specificity. As the electrodes get finer and more intrusive, smaller units of neuronal signalling can be recorded. However, there has always been a debate over the use of invasive and non-invasive methods for neural tracking [19].

For EEG and MEG methods, the neural signal is recorded off the scalp of the head. Due to the amplitude and temporal aspects of the EEG and MEG recordings, it is assumed that scalp EEG and MEG readings do not directly measure the firing of individual neurons but rather the culmination of the brain acting as a volume conductor, along with volumetric representation of parallel dendrites alignment in cortical columns by excitatory postsynaptic potential (EPSP) and inhibitory

postsynaptic potential (IPSP) networks that occur in temporal synchrony after neuronal action potential firing.

EEG signals can be classified as spontaneously occurring brain activity and event evoked potentials that occur in reaction to external stimuli. Spontaneous EEG readings typically occur around the 100 μV range (see Figure 2.3) and evoked potentials typically are in the tens of micro volts range, which is why event evoked potentials have to be averaged over several epochs in order to be differentiated from the spontaneous potential.

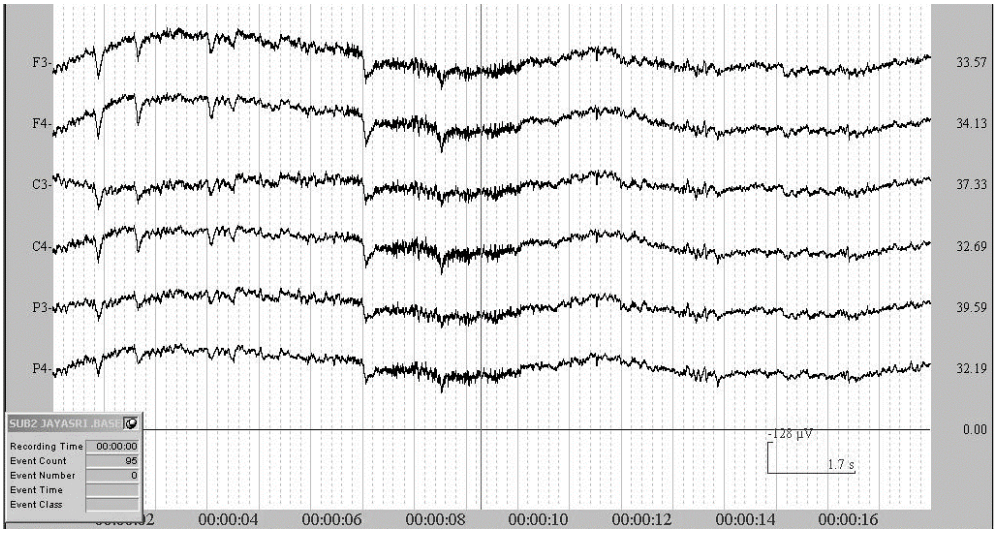

Figure 2.3: Sample snapshot showing 6 channels of raw EEG reading

EEG electrodes are attached in the standardized 10-20 system of labelling and locating electrodes [20]. EEG electrodes are typically arranged in the 10-20 system and woven into an elastic nylon cap for easy application. Electrolyte gel is injected between the interfaces of the electrode with the scalp so as to reduce the interfacial impedance. Scalp EEG readings based on the 10-20 system of electrode placements correlate with brain activity based on evidence that the cerebral hemispheres are anatomically segregated into general zones of separate functionality such as vision, perception, motor and cognitive functions. By mapping the activity in the zones, EEG readings provide a means to measure neural function.

As discussed in the section on eye tracking and motion tracking, EOG signals and EMG signals are typically of much higher magnitude than the spontaneous neural EEG signals. This shows that in order to measure EEG signals cleanly, EOG and EMG signals have to be treated as unwanted artifacts and minimized during the capture of EEG signals. For example, EOG blinking artifacts can be reduced from the recorded EEG signal through techniques such as independent component analysis (ICA) [21].

2.2 Assessment

Hand eye coordination testing methodologies can generally be grouped under two different forms. First, there are the commercialized forms of standardized motor skill testing. Alternatively, there are the arbitrary task-specific testing procedures which are more common with researchers who need to define their own set of methodologies for the novel and unique tasks and scenarios.

2.2.1 Standard motor skill tests

A popular example of a standardized motor skill test is the Movement Assessment Battery for Children (MABC) [22], [23]. HEC is part of the battery of tests of motor skills such as manual dexterity, ball skills and static and dynamic balance. The advantage of these commercial packages is that they have extensive statistical foundations as evidence for the reliability and validity of their testing methods [24]. Many researchers and clinicians alike, rely on such commercially packaged battery of testing methods as a common means of comparison. MABC has been used in a wide variety of experiments such as the effects of visual impairment on motor skill performance [25] and the correlation between sensorimotor white matter with upper-limb visuomotor tracking performance of young subjects with traumatic brain injury [26].

2.2.2 Arbitrary testing

Investigation on HEC of human subjects often involves unique scenarios that cannot make use of standardized packages since these tests might only be valid within certain conditions such as age, experience and type of task. Researchers have adapted or defined the tasks and testing metrics to suit their testing scenario. For example, in order to test HEC for laparoscopic surgery, instead of actual patients, subjects' performances are evaluated using computer simulation or animal models. In order to reduce the complexity of the task, instead of testing the entire surgical procedure, the tasks are objectively abstracted into primary technical components such as picking and placing, pattern cutting and knot tying [27]. Multiple medical simulation systems focusing on HEC training have also been developed for various surgical procedures such as percutaneous verteboplasty, Percutaneous Transluminal Coronary Angioplasty and interventional radiology [28]–[31].

2.2.3 Integrated measurement system

As described earlier, HEC comprises of a complex dynamic system of sensory inputs and motor outputs. In order to assess all aspects of HEC, an integrated measurement system is required for monitoring the human subject. The integrated measurement system primarily comprises of sensing mechanisms for concurrent eye tracking, motion tracking and neural tracking (see Figure 2.4).

Depending on the nature of the task, ease of implementation and level of accuracy required, different combinations of tracking methods can be used. For example, in Figure 2.4, motion tracking is achieved with both the pair of stereoscopic cameras and motion capture glove. The reason for using both methods simultaneously is that motion capture gloves can track the localized fine motor control of the fingers much more accurately than the cameras, especially if the hands are obstructed or skewed in the cameras' perspectives. Whereas the stereoscopic cameras are more suited for recording macro level motions of the body and arms within a larger

workspace as compared to the motion capture gloves. More recently, high resolution compact depth sensing infrared cameras (such as the Leap Motion sensor) have become commercially available that serves as an alternative to motion capture gloves for very fine (~1mm accuracy) motor tracking.

Chapters 4 to 7 document the series of HEC experiments conducted for this research, highlighting the various different combinations of measurement devices and interfaces that have been successfully implemented to achieve the experimental objectives.

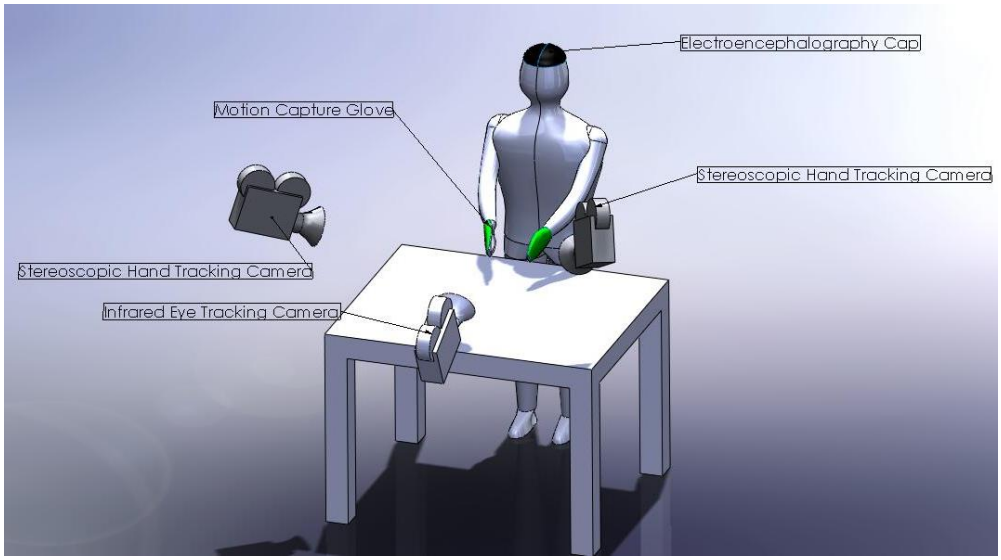

Figure 2.4: Integrated system of sensors for HEC measurement.

2.3 Modelling and analysis

The study of human motion can be divided into two forms: Kinematics – which is the study of displacement, velocity and acceleration with respect to time; and Kinetics which is the study of joint forces and moments. Depending on the type of information required, one or both forms of study are used. With regards to HEC, kinematics describes arm and hand motion through joint angles, position and orientation while kinetics resolves the motion into sequential link-segment joint forces that correlates

external known forces with patterns of muscle activation. As human muscle activation happens through a highly complex network of tendons that act indirectly over the skeletal joints, hence resolving joint forces to individual muscle activations is in itself a difficult task. Furthermore, internal joint forces are resolved from known external forces hence they are prerequisite limited to scenarios in which testing setups have been planned for force recording, through force plates or EMG signals.

In addition to subject oriented motion analysis, information about HEC can be inferred from the task performance. For example, in the computer-enhanced laparoscopic training system (CELTS) [32] recorded motion is resolved into kinematic information and presented as relevant metrics such as the time taken to perform the task, path length, smoothness of motion, depth perception and response orientation.

Path length is defined as the trajectory of the end effector of the instrument. In addition, the montage of instrument positions and orientations over time represents the spatial distribution of the motion in the workspace. The size of the spatial distribution montage represents the efficacy of the motion. The smoothness of motion,

$$\mathrm{J} = \sqrt{\frac{1}{2}\int_0^{\mathrm{T}} \mathrm{j}^2 \mathrm{dt}}\,, \qquad [1]$$

is based on the cumulative amount of instantaneous jerk which is defined by the derivative of acceleration,

$$j = \frac{d^3x}{dx^3}\,. \qquad [2]$$

Depth perception is defined as the sum of motion in the axial direction. Response orientation refers to the cumulative range of angular motion of the instrument which signifies the amount of rotation used to correct the orientation of the motion. Each

performance metric is weighted and compared against the corresponding score of the expert group in order to obtain an overall score of the motor performance of the subject.

A problem with human motion planning is the redundancy in the 7 degree of freedom kinematic structure of our human arm. This redundancy is further compounded when taking into account that both path planning and muscle action have in themselves redundantly large combinations of possible solutions to a desired outcome. In describing human arm motion, several models have been proposed over the past few decades [33]. They are further classified as descriptive or complete models. Descriptive models involve the precipitation of observed behaviour into models that can mathematically account for human motion trajectories. However, these descriptive models ignore the biologic nature of the human musculoskeletal system and the central nervous system that controls it. In contrast, complete models take into account for the lack of biologic principles void in the descriptive models.

2.3.1 Descriptive models

The main aim of descriptive models is to derive the empirical mathematic representation of human motion and they are useful as computational tools to model trajectories in experimental human motion. Some well-known descriptive models are the Fitts Law, the 2/3 power law and the bell shaped velocity profiles in straight motion.

2.3.1.1 Fitts Law

Fitts Law relates the rapid, goal orientated motion time with the size and distance of the object. It is represented mathematically by:

$$MT = a + b\left[log_2\left(\frac{2A}{w}\right)\right], \qquad [3]$$

where MT= motion time, a and b are regression coefficients, A= movement distance and w relates to the size of the object [34]. This intuitive relationship describes how when the goal distance is large and the size of the object is small, it takes a longer time for a person to approach the target.

2.3.1.2 2/3 Power Law

The 2/3 power law in general is descriptive of curved motion where the velocity (V) is proposed to be related to the inverse of the radius of curvature (k) with the equation:

$$V(t) = \gamma k(t)^{-\frac{1}{3}}, \quad [4]$$

where γ is an empirically derived constant of 0.33. This simple relation describes the relation that in curved motion, the velocity increases with decreasing radius of curvature. However, this simple equation breaks down when describing straight motion (or rather curvature at a radius of infinity), inflection points and motion with very small radius of curvature where the velocity will show to reach infinity.

2.3.1.3 Bell shaped velocity profile

The bell shaped velocity profile [35] of straight motion is one of the most prominent and consistent behaviour in human arm motion and that has led to the assumption of the underlying principle of smoothness of motion. When it is applied to the redundancy of kinematic musculoskeletal system, this enables an optimization protocol that can produce the most efficient and "natural" way of motion.

This smoothness prioritization can be manifested in several ways such as the minimum jerk model [35]. This model defines jerk as the derivative of acceleration and in planar motion, overall jerk (J) can be defined as:

$$J = \sqrt{\left(\frac{d^3x}{dt^3}\right)^2 + \left(\frac{d^3y}{dt^3}\right)^2}. \quad [5]$$

The corresponding cost function relative to this jerk in motion can be defined as the integral of the squared quantity of jerk:

$$C = \frac{1}{2}\int_0^{t_f}\left(\left(\frac{d^3x}{dt^3}\right)^2 + \left(\frac{d^3y}{dt^3}\right)^2\right)dt\,, \qquad [6]$$

where x and y are the planar coordinates and t is time.

When this cost function is applied to differential equations of motion and trajectory constraints, such as initial and final positions, velocity, acceleration, time duration and via-points, it is found that a 5th order polynomial is necessary for point to point motion that can specify a straight line trajectory with 4th order polynomial velocity profile [36]. However, the downfall of this appealingly simple model is that in curved motion and via-point motion, the velocity profile may be accurate but the actual movement path may not fulfil the trajectory requirements.

The constrained minimum jerk model is proposed by Todorov and Jordan [37] to overcome the weakness of the minimum jerk model. Given that the path trajectory is chosen and fixed, the model suggests that its velocity profile will be determined by a new cost function:

$$J = \int_0^{t_f}\left\|\frac{d^3}{dt^3}r[s(t)]\right\|^2 dt\,, \qquad [7]$$

where $r(s)$ is the vector coordinate of the path points and $s(t)$ is the distance along the path. Therefore the third order differential of the vector function with relation to the predetermined path will also lead to a minimum jerk cost function.

2.3.2 Complete models

In the descriptive minimum jerk model, the objective is for an optimal trajectory path in Cartesian space but that does not take into account the redundant joint kinematics of the human musculoskeletal system. Dynamic models will include these

arm dynamics into the cost function while stochastic models will take into account the presence of noise in the muscular signals.

2.3.2.1 Dynamic models

Dynamic models are classified as dynamic because their cost functions carry variables that are dependent on the dynamics of the arm and task. Where the traditional kinematic minimum jerk model only depended on the initial and final states, ignoring the physical forces involved in producing the motion, the dynamic minimum torque change model [38] addresses this problem and its corresponding cost function is defined as:

$$C = \frac{1}{2}\int_0^{t_f}\left(\frac{dz_i}{dt}\right)^2 dt, \qquad [8]$$

where Z_i is the torque at joint i. However, due to the nonlinear properties of arm dynamics, the result of this implementation is that individual joint torques cannot be calculated independently and they must all be reiteratively processed in order to derive an optimal solution for each joint torque and trajectory.

2.3.2.2 Stochastic models

In general, the minimum jerk and minimum torque models are able to be applied to different aspects of human arm motion but other than being able to correlate with certain experimental data, they lack premise when assuming that the central nervous system (CNS) has to optimize through such priorities.

In an attempt to solve this divide, Harris and Wolpert [39] proposed a theory of minimum final position variance which they renamed as task optimization in the presence of signal dependent noise (TOPS). The key hypothesis put forth by this model is that neural noise is signal dependent and proportional to its amplitude. This neural noise is purported to cause the stochastic results of natural motion. This model hypothesizes that even though neural noise is cumulative over the trajectory, trying to

avoid it by using rapid motion will also increase the amplitude of noise. Interestingly, when applied to saccades and arm motions, this relation correlates with the well-established Fitt's Law.

In the minimum variance model, the hypothesis is that the neural commands are selected in a feedforward sequence of commands that minimize end point variance with the target while keeping to the time constraints of the task. As a result, the velocity profile reduces into a bell curve where the end phase of the motion has slower velocity in order to minimize variance in the neural signal. The advantage of this model is that it has a better biologic standpoint as compared to the earlier assumptions of the CNS having to compute with third order differentials in the minimum jerk and minimum torque models.

More recently, Todorov and Jordan [40] proposed a modification with respect to the TOPS model. The key notion that is different in their model is the inclusion of feedback control which is lacking from all models so far, including that of the TOPS model. The previous models described all worked under the assumption that the CNS performed motor planning before all motor commands in a feedforward manner.

2.3.3 Biological model

As described in the earlier section on complete models, there is a need for a biologic correlation between conceptual control models and the neural CNS of our brains. Until recently, the internal workings of the brain have been largely inaccessible unless volunteers were willing to undergo invasive electrode placements. Pioneering work into the mapping of sensorimotor function within the primary motor cortex was done by the neurosurgeon Wilder Penfield in 1949. A popular depiction of his ground-breaking work is the motor and sensor homunculus where the difference in size of representation of different parts of the body signifies the associated level of complexity. With the development of non-invasive neuronal technologies such as

functional magnetic resonance imaging (fMRI), electroencephalography (EEG) and near infra-red spectroscopy (NIRS), comes with advancement in the experimentation and observation into how parts of the brain works.

The cerebral cortex is roughly divided in function into several local areas [41]. Right after the generation of intent of motion in the posterior parietal cortex and cerebral limbic system, it is relayed through the basal ganglion into the corresponding area of the frontal cortex, where sensory information are collated and processed, which includes the premotor cortex (PMC) and supplementary motor area (SMA). After which, the information is fed to the cerebellum, brain stem and pyramidal tracts within the primary somatosensory cortex (SmI).

The cerebellum is responsible for integrating signals from the frontal cortex, proprioceptive feedback from the spinal cord and positional information from the vestibular system. Within the cerebellum, all these sources of information are processed for complex coordinated control and fed back to the PMC and primary motor cortex (MsI) as well as output into the brainstem for motor neuron activation. In cases where patients' cerebellum is damaged, refined motor control is lost and the motion degenerates into short jerky motions.

2.3.4 Internal models

Descriptive models do not include control of motor execution but in dynamic and stochastic models, the optimization control implicitly creates all levels of motor control which includes motor execution. However, for models such as TOPS, they operate in a feedforward manner that is not sufficient for motor execution as there is no implicit conversion into motor commands. This leads to the introduction of internal models that help map out the neural commands necessary for motor control. Internal models are divided into the forward model and the inverse model.

2.3.4.1 Forward model

The forward model signifies the causal relationship between the inputs of the system to the estimated output. Hence, when looking at arm motion, inputting an efference copy (copy of the motor command) of variables such as arm position and velocities will produce an output of the estimated behaviour of that motion and the sensory effects of that motion (reafference). In effect, because our proprioceptive feedback includes both the actual feedback from interaction with the environment as well as the effects of sensation induced by self-motion, the forward model will serve to negate that self-motion sensation so as to only contemplate with external feedback.

Another evidence of argument for the validity of forward modelling is the fact that forward models are able to provide balance and stability to a system if it were assumed to only be based on feedback control. That is because the feedback mechanisms in our neuronal pathways are comparatively significantly delayed when compared to the time taken in fast motion [42]. This reduces the ability of feedback control to generate a stable output. With the addition of forward model predictive motor control, it reduces the dependency on feedback to generate and correct fast motion. In addition, it is also postulated that in assuming only pure feedback control, the initial phase of the motion where there can be no proprioceptive feedback due to inherent delays in the motor and visual relays, the argument for motion breaks down due to lack of guidance at that gap of time if there were no forward mechanisms in the cerebellum.

The Smith predictor is utilized in the modelling of the cerebellum to account for the long proprioceptive and visual delays [43]. The critical concept of the Smith predictor is the utilization of an efference copy of the motor command that is fed into the forward dynamic model in order to generate a predictive estimate of the causal state of the system.

This output is fed back into the state estimate and into a forward output model that translates the information relative to the delays anticipated in enacting these corrective commands onto the sensory feedback. The key advantage of this system is the fast reiterative internal loop that enables the system to manipulate the state estimate faster.

The overall loop of the proprioception from the motor command against the corrective commands from the forward output model is fed back to the state estimate as sensory discrepancy and used in the new state error.

2.3.4.2 Inverse model

The inverse model is the opposite effect of the forward model in which the motor commands are estimated in order to achieve a desired state. This inherently suggests that inverse modelling is used as a controller of the motor system and allows for a system to generate a set of motor commands without the necessity for feedback [43].

However, the biggest problem in inverse modelling is the assumption that the CNS has good inherent mastery over the inverse model such that it can provide the good estimate of motor commands without the initial feedback error correction. In addition, motor command error is received in sensory coordinates and need to be transformed into motor errors in order to be fed back into the inverse model.

2.3.4.3 Cerebellar feedback-error-learning model (CBFELM)

In responding to the weaknesses of the inverse model, Kawato [44], [45] proposed the CBFELM in order to account for the training of the inverse model necessary for adaptation to the motor task. Trajectory error derived from the difference in desired initial trajectory and actual trajectory is fed through the feedback controller in order to convert the sensory coordinates into a motor command error that can then be used to train the inverse model.

The updated inverse model can then be used to act upon the desired and actual trajectory input to generate a feedforward motor command. This feedforward motor command is summed with the feedback motor command to generate the overall motor command that will act upon the controlled object.

2.3.4.4 Multiple paired forward-inverse models

In the previous models, we have seen the advantages and weaknesses of forward and inverse models in the construction of motor control modelling. In the next example, Wolpert and Kawato [46] have proposed a unifying model that seeks to incorporate paired forward and inverse modelling as a single controller that is set in a framework of multiple parallel controllers selected off a responsibility predictor. By pairing forward and inverse models, they seek to couple the advantages of both models and unify their application. This model was then further updated and renamed as the MOSIAC model [47].

Firstly, the forward model is used both as the predictive initial motor command through the forward dynamic model and forward output model as well as part of the prediction error used in weighing the likelihood of this controller as the correct controller to be used. Overall, the efference copy, sensory feedback and contextual signals influence the overall determination of the most appropriate controller to be used for the task.

With each forward model within each controller, a corresponding inverse model is paired to learn off the motor error from the feedback motor command and generate a feedforward motor command that will act with the feedback motor command to yield an overall motor command onto the controlled object.

The advantage of a modular model is that human motor tasks are inherently modular and rather than relying on relearning a single controller, it is more practical to assume the brain divides up the modular task into appropriate efficiently learned

forward-inverse controllers. This behaviour also provides proof that when we learn similar tasks faster as common modular tasks can be applied without learning the inverse model again.

2.3.4.5 Bayesian model

Bayesian modelling of motor control is essentially based on the premise that humans modify behaviour based on a sense of probability. Therefore, the rules of probability apply to influence our behaviour [48], [49].

The mathematical notation for the probability of an event A is given by $P(A)$ and $P(A|B)$ refers to the probability of event A given that event B is true. Mathematically, $P(A|B)$ can also be expressed as:

$$P(A|B) = \frac{P(B|A)P(A)}{P(B)}. \quad \textbf{[9]}$$

When this identity is applied to the brain, event A can be interpreted as the state of the system and event B as the sensory input. Therefore, the identity becomes:

$$P(state|sensory\ input) = \frac{P(sensory\ input|state)P(state)}{P(sensory\ input)}. \quad [10]$$

This shows that an updated probability of the state is given by incorporating probabilities from the new sensory input and the prior state of the system.

Cue assimilation: The Bayesian model also provides with a useful mathematical proof that humans are able to incorporate multimodal sensory cues in order to reduce the individually inherent noise from each source [48]. By looking at cues as a probabilistic framework, we can associate noise ε with each signal θ as one with Gaussian distribution set at zero mean and having a variance of σ^2. Hence for a sensory input:

$$S = \theta + \varepsilon. \quad [11]$$

When we consider two independent sensory inputs, the optimal estimate of θ will be based on a weighted average of the two sensory inputs based on the ratio of their variances given by:

$$\theta = ws_1 + (1 - w)s_2 \,, \qquad [12]$$

where

$$w = \sigma_2^2/(\sigma_1^2 + \sigma_2^2) \,, \qquad [13]$$

and their variance σ^2 can be calculated by:

$$\sigma^2 = \sigma_1^2\sigma_2^2/(\sigma_1^2 + \sigma_2^2) \,. \qquad [14]$$

This equation from [50] shows that the variance of two sensory inputs together is always lower than either of each input independently. The mathematical proof from this equation reflects in the real life experimental results that show improved motor performance when subjects are able to incorporate more independent sensory inputs.

In reality, we can look at sensory inputs and motor output in terms of a probabilistic distribution. For example, we can continuously throw darts at the centre of the board and the cumulative outcome will show a probabilistic output distribution of the mean dart position and its associated variances. By accounting for this distribution, we correct the aiming target to coincide with the mean dart position in order to achieve the optimal motor control hence incorporated motor learning based on a Bayesian probability model.

2.4 HEC measurement and monitoring

HEC is the ability to coordinate between the person's visual system and motor actions in order to fulfil a task. Although there is no definitive test for measuring

HEC ability, conventionally, HEC ability is inferred through measurable aspects such as eye movements and motor performance in reaction to a controlled stimulus or task. Such aspects can then be tabulated and ranked in order to gain a measure of the inferred HEC ability. For example, in the Fundamentals of Laparoscopic Surgery, their technical skills curriculum[1,2] details the performance level adequate for each simulated task that signifies a proficient level of surgical skill. The required proficiency level was determined by benchmarking against expert surgeons who performed on the same tasks.

The pick and place experiment tasks performed in Chapters 4 and 6 and the circle tracing task in Chapter 6 have been modelled after tasks performed in the Fundamentals of Laparoscopic Surgery. However, the benchmarks from the Fundamentals of Laparoscopic Surgery are not directly applicable as the task protocols are not identical as they have been modified to suit our experimental objectives. In addition, the participants in the experiments conducted have no surgical or medical background hence it would be naturally biased to use the same benchmarks for the appraisal of HEC ability in laypersons.

2.5 Methods and Materials of EEG Analysis

EEG signals have been used for decades to map brain activity. Their first clinical therapeutic implementation was on the use of neurofeedback brain wave conditioning by patients with epileptic seizures [51], [52]. It was found that the sensorimotor rhythm (SMR), which is found in the 12-20Hz range, is able to suppress the depolarization of low frequency brain signals that led to seizures. Hence, with

[1] http://www.flsprogram.org/wp-content/uploads/2014/03/Revised-Manual-Skills-Guidelines-February-2014.pdf

[2] http://www.flsprogram.org/wp-content/uploads/2014/02/Proficiency-Based-Curriculum-Word-File-updated-February-2014.pdf

reinforced training to voluntarily induce high frequency brain waves, like the SMR, the likelihood of full blown seizures in epileptic patients can be reduced.

Another way of utilizing EEG signals is in mapping the brain's attention level. It was shown that when the quantitative EEG was categorized into the different frequency bands, there was correlation between the bands with different aspects of behaviour in the patients (see Table 2.1) [53]. In patients with Attention deficit/hyperactivity disorder (ADHD), it was observed that their theta band is excessively activated while the beta band activity is low [54]. And in response, clinicians have been able to use neurofeedback brain wave conditioning by training subjects with abstract tasks to focus their attention and inducing higher beta band activity.

One commercial example is the attention training toy by Uncle Milton Industries, Inc: The Star Wars Force Trainer[3] is a toy in which players are instructed to concentrate their thoughts on levitating a ball, which is picked up by a dry sensor wireless EEG headset and relayed to a controller that adjusts the speed of a fan under the ball which is blowing air upwards in order to make the ball levitate with respect to the EEG signals recorded. In a similar example, Necomimi[4] by Neurowear is a dry sensor EEG headset that is attached with articulating mechanisms in the shape of cat ears. Depending on the level of concentration, the ears are rotated upwards when the subject shows high levels of concentration in the EEG signals and rotated downwards when the subject is relaxed.

Fundamentals of EEG processing such as data pre-processing, EEG frequency bands, topographical spatial contour mapping and Lempel-Ziv Complexity are

[3] http://www.starwars.com/vault/collecting/20090209b.html
[4] http://neurowear.net

detailed in Section 2.5. Additional EEG analysis methods such as Event-Related Potentials (ERP) are detailed in Chapter 7.

2.5.1 EEG fundamentals

Raw EEG signals that have been recorded from electrodes placed in the 10-20 system are first processed for the removal of line noise (notch filter at 50Hz or 60 Hz depending on the country), band pass filtering for the removal of low frequency noise (typically with a high-pass filter set at 0.1 to 1Hz and used to remove slow artifacts such as movement) and high frequency noise (typically with a low-pass filter set at around 50Hz, depending on focus of study. High frequency artifacts such as EMG signals are removed.)

In addition, Independent Component Analysis (ICA) methods can be used to remove eye blinking artifacts and movement artifacts (see Figure 2.5 and 2.6). ICA is a digital signal processing method for signal-noise decomposition which assumes that there are N number of statistically independent inputs (S_1,...., S_N) that are mixed linearly channels into N number of outputs (X_1,....., X_N).

$$X = AS, \qquad [15]$$

where A is the mixing matrix.

ICA is used to find an equivalent solution to the matrix X through a decomposition matrix W and a matrix of estimated source vectors $\hat{S}$,

$$\hat{\mathrm{S}} = \mathrm{WX}\,. \qquad [16]$$

Matrix W is defined in a way such that the components of matrix $\hat{S}$ are as independent as possible.

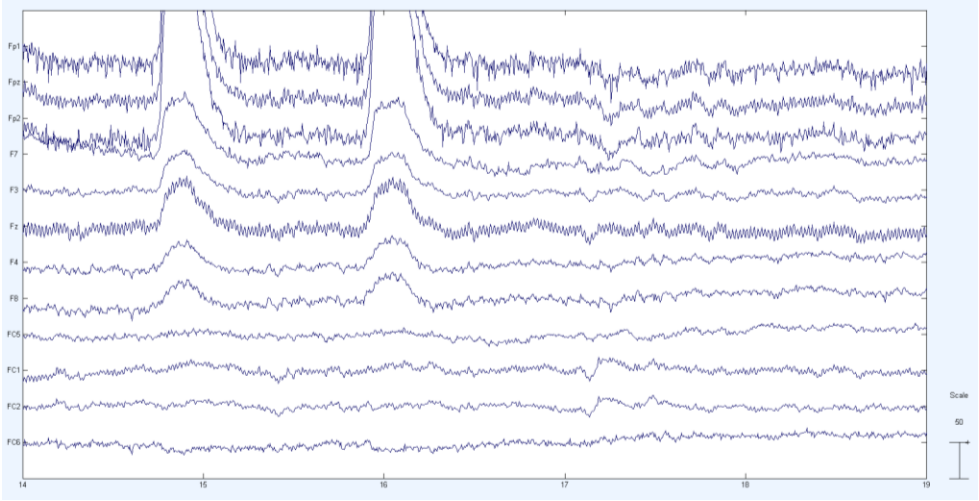

Figure 2.5: Sample snapshot of a raw EEG reading with eye blinking artefact.

The readings are scaled to 50µV/unit length in amplitude and the horizontal axis is scaled to 1 second intervals.

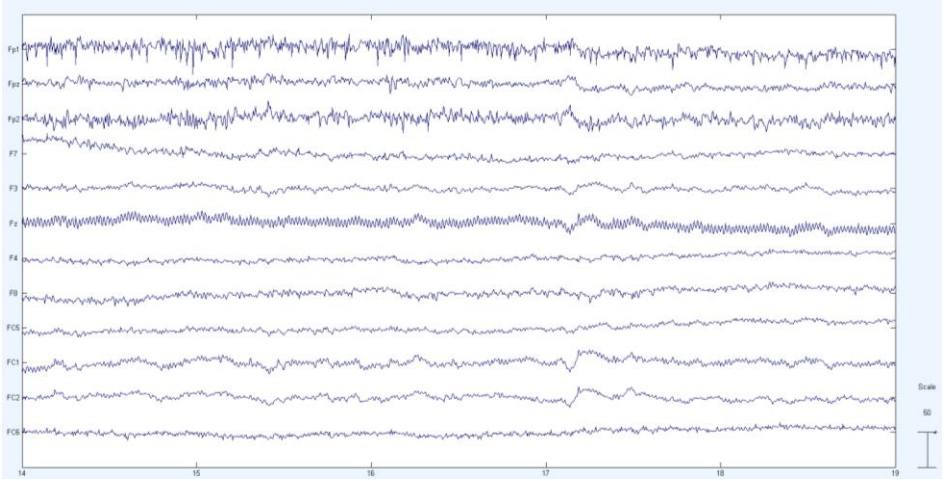

Figure 2.6: Sample snapshot of a raw EEG reading.

The eye blinking artifact removed by ICA. The readings are scaled to 50µV/unit length in amplitude and the horizontal axis is scaled to 1 second intervals.

Spatial Potential Mapping

Spatial potential mapping is a form of graphical representation of the EEG signals recorded. EEG electrodes allocated according to the 10-20 system have been proportionally defined to be independent of anatomical variance. By assuming that the electrodes act as node sources on a spherical grid system, the potential

distribution at any point on the grid is interpolated from neighbouring electrode nodes. In addition, the derived potential distribution can be graphically coded by isopotential contour lines (as shown in Figure 2.7)

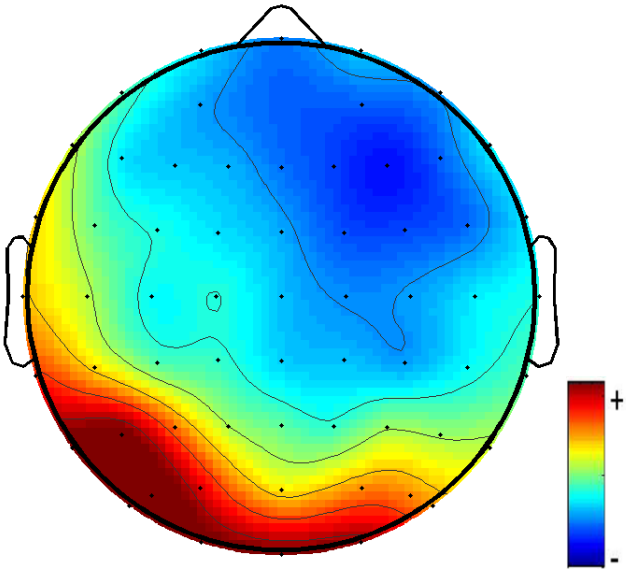

Figure 2.7: Spatial potential mapping of EEG signals with isopotential contour lines.

The potentials can be colour-scaled with respect to an overall range of electrode potentials present in the recordings. As each spatial potential mapping corresponds to a single snapshot in time, we can also collate a series of such spatial potential maps into a dynamic representation of changes in scalp potential over time.

EEG frequency band classification

Fourier transform is used to convert the time-based EEG signals into the frequency domain. Mathematically, any signal for a given interval, can be decomposed into a sum of mutually orthogonal sinusoidal waves of different amplitudes, phases and frequencies. The power of the signal hence refers to the square of the amplitude of the sinusoidal signal of a specific frequency. The larger the time window interval for sampling, the better is the accuracy of transformation but more artifacts get included and the temporal resolution drops as well.

It is experimentally shown that EEG waves can be pathologically correlated with activity of different frequency bands (see Table 2.1) [53] and there is spatial prevalence associated with each frequency band activity.

Table 2.1: EEG Frequency Bands

Frequency band	**Traits**	**Prevalence**
Delta (δ) 0.5-4Hz	• Predominant in infants • Associated with deep sleep in adults • Disruptions to delta wave activity correlated to neurological disorders such as schizophrenia and dementia	• Posteriorly in children • Frontally in adults
Theta (θ) 4-8Hz	• Linked with drowsiness and meditation	• Found in areas that are idling
Alpha (α) 8-13Hz	• Attenuation with mental action or eye opening	• Occipitally when mind is relaxed and/or eyes are closed • Related mu rhythm that egresses in the contralateral sensorimotor areas on the cortex when arms and hands idle
Beta (β) 13-30Hz	• Attenuation with action • Linked with active thinking and concentration	• Frontally

Lempel-Ziv Complexity

Lempel-Ziv Complexity is a means of characterizing the distinct dynamic and nonlinear patterns of biomedical signals [55], [56], including EEG [57]–[61]. When used on EEG signals, the Lempel-Ziv Complexity value represents the rate of emergence of new neural spike patterns in a time series. Hence, a higher LZC value indicates that the signal is more complex. The advantage of the LZC computational method on EEG analysis is it is a direct single-pass processing step that reduces the dimensionality of the EEG signal into a single value. The binary conversion of the

analog EEG signal also inherently negates the effect of high amplitude noise that is typical in motion related artifacts in the EEG signal.

The first step in LZC is the conversion of the analog EEG signal into a binary signal. Conventionally, the median or mean of the signal is used as the binary thresholding value [62]. Data points above the thresholding value are converted into ones and data points below that value are converted into zeroes. The binary string is then read from left to right while each character is compared against a concatenating 'vocabulary of unique words'. As the string is read, the vocabulary increases and the rate of unique word entry into the vocabulary represents the emergence of new patterns in the string. Normalized over a function based on the length of the entire string, this value represents the complexity of the string.

2.5.2 EEG for motor learning of HEC tasks

Motor learning is the process of acquisition and optimization of a motor skill through practice or experience, leading to relatively plastic changes in the motor skill capability. The progression of mastery is typified by a power law relationship where there is a steep rise in skill in the beginning and the improvement asymptotically tapers over time. Several EEG analysis methods such as spectral power [63], electrode coherence [64] and event-related potentials [65] have been used to quantify the changes in neural activity associated with motor learning [66].

However, EEG studies of motor skill performance have typically been cross-sectional studies between groups of varying skill levels [63], [67], [68]. For example, Haufler et al. [63] discovered that experts at marksmanship possessed higher alpha power in the left temporal region on the cerebral cortex as compared to novice shooters. Baumeister et al. [67] found a difference in the theta band at the frontal midline region between novice golfers and expert golfers. This increase in theta band activity is associated with higher focused attention in other studies as well [66].

The severe limitation with such cross-sectional studies is that the study assumes differences in neural activity patterns between the groups of subjects, arise only from the different levels of skill mastery. In reality, even under tightly controlled experimental conditions, EEG is found to be highly variable from person to person and susceptible to external noise. Therefore cross-sectional comparisons have to be highly scrutinized and their findings are limited and unlikely to be reproducible. In order not to be limited by such pitfalls, the experiments conducted in this study have been designed for inter-sectional comparisons such that the comparison is on the same individuals who trains on a single task from novice to master.

The reported trends in neural activities for various tasks such as shooting [64], archery [69], table tennis [65], video games [70] also appear to be highly task-specific. Unless the tasks are comparable or the trends, such as high theta band activity for focused attention [66], have been corroborated in several studies with unrelated tasks, the reported trends cannot be assumed to be generalizable. Hatfield et al. [66] is a good review article that reported that trends in spectral power for marksmanship-related tasks are very different from that of other sports like karate or golf. These reports in literature highlight the limitations of the current body of literature with respect to HEC tasks as well as the inherent limitations to EEG analysis methods.

Experiments are highly customized for specific studies. Experimental findings and neural analysis are also typically limited to the specific experimental scope and are not readily translatable [66]. There are few research on the neural or cognition aspect of the mastery of HEC tasks [63], [64], [66]. To the best of our knowledge, trends of neural activity for the mastery of HEC tasks have not been investigated. An important aim of this study is the verification of neural markers over a series of experiments with HEC tasks such that the groundwork for further benchmarking of HEC-related neural activity can be investigated upon. Although LZC is a common

method for biosignal analysis, very little is known on the use of LZC with EEG signals [57]–[61]. Consequently, the consistency of the LZC neural trends for HEC-related tasks has been established by utilizing the same processing algorithms and parameters with varied experimental setups.

3 Integrated Framework for Hand-Eye Coordination Training

In this chapter, we conceptualized a hypothetical integrated framework for HEC. The conceptual framework represents the interconnection of various aspects of HEC described in Chapter 2, such as neural tracking and analysis, motion analysis and control modelling, which will serve as a map for the development of a holistic and autonomous system to train and assess HEC-related ability of a subject. Various aspects of this framework have been developed through the course of this study.

3.1 Conceptual framework

The foundation of the framework is created using the biological brain's sensorimotor model with sensory feedback (see Figure 3.1). By adapting the biological motor control system, as discussed in Section 2.3.3, to include the mechanisms of sensorimotor feedback, we can get a closed loop representation of the biological model.

In HEC, sensory feedback is achieved primarily through two modalities: haptics and visual information. Haptic information can be seen as physical cues and proprioceptive sensing of the physical orientation and motion of the subject's limbs and eyes. Such haptic information is processed at the primary sensorimotor cortex [41]. Visual information can be seen as visual cues such as colour and depth and the processing of such cues into information such as objectification and spatial orientation. Such visual information is processed at the primary visual cortex [41].

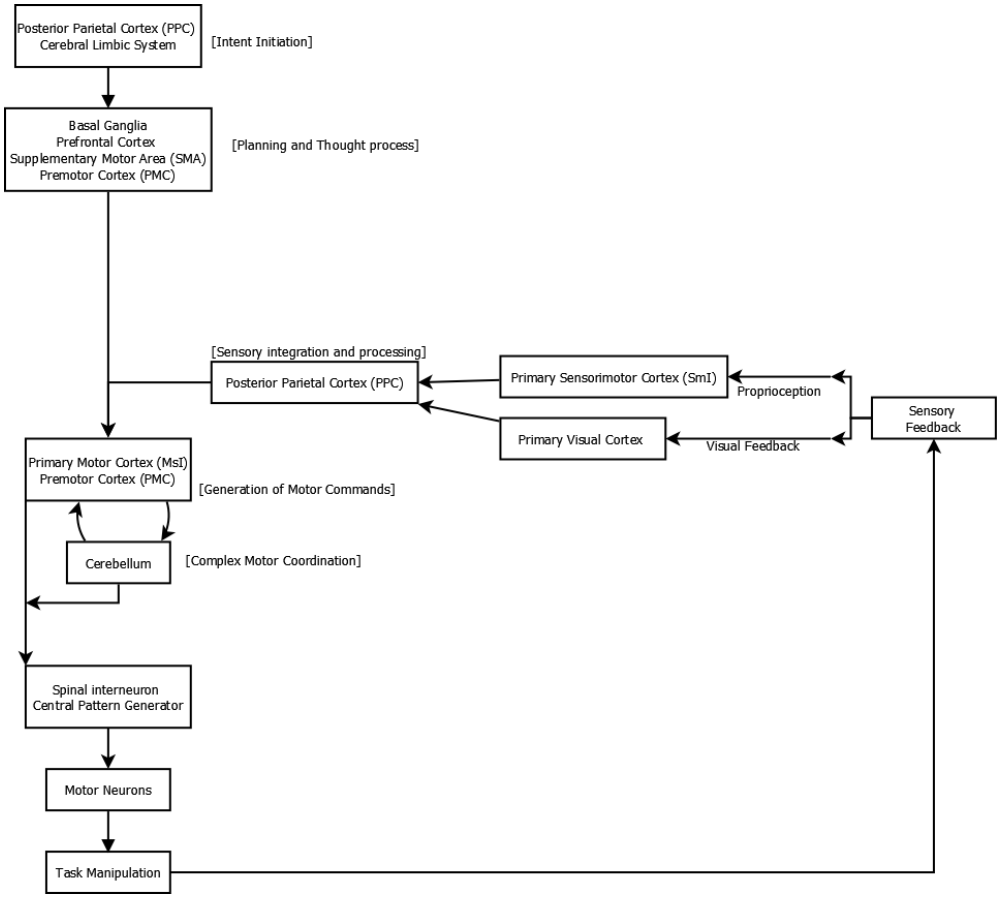

Figure 3.1: Biological Model with Sensory Feedback.

In addition to the biological model, we introduce forward and inverse control models incorporated into the different levels of motor planning and execution (see Figure 3.2). The forward model draws on an efference copy of the motor commands and is fed back into the thought and planning process of the brain in order to reiteratively plot a causal prediction of the motor execution. In addition, the forward output model is used as an offsetting re-afference signal to filter the proprioceptive feedback of sensation caused by self-motion. This forward model concept has been shown to be useful in characterizing the effects of schizophrenia [71].

The inverse control model is applied in this framework to formulate an approximation of motor learning skill into control theory. That is because, when an inverse control model is improved by motor learning, it is reflected in the parametric characteristics of the controller. A “black box” strategy can be implemented by

assuming a simplified and generalized transfer function. The regressive comparison of the generalized transfer function with empirical data will generate the transfer function parameters [72]. This effectively maps motor execution performance into the domain of control modelling. The forward and inverse models complement the biological model because they serve as an idealistic mathematical rationalization of HEC behaviour which can be more easily modelled as compared to neuronal mechanisms of the biological model.

The final step of the integrated framework is the inclusion of EEG derived neurofeedback into the previous model (see Figure 3.3). EEG signals will be recorded on all relevant locations pertinent to motor control as defined by the biological model. The EEG signals can be used either in an online manner or as offline analysis.

Offline analysis of EEG signals is mostly used for data that requires complete recordings such as LZC analysis, as discussed in Section 2.5. In the spatial mapping of the electrical activity of electrodes, we can gain a mean overview of the activity of the different parts of the brain. This overview is beneficial in the classification of the stage of motor skill learning due to the known segregation of brain function into different locations of the brain.

In the online utilization of EEG signals for neurofeedback, we can perform live transformation of the EEG signals in order to separate the EEG activity into its bands of brain wave frequencies as described in Section 2.5. This allows us to monitor and utilize live information of the subject's neural behaviour such as the attention level by inference on the degree of Alpha band brain wave activation [73]. This, in effect, helps us to quantify the cognitive state of the subject and we can incorporate the performance of the subject's cognitive state into supervised/ reinforcement learning protocols. These protocols map the deviation in the desired cognitive state and the current cognitive state and level of motor and task performance, so as to decide upon

an appropriate feedback that is directed to the subject through different visual, aural and haptic cues.

The evolution of the hypothetical framework from Figure 3.1 to Figure 3.3 represents the author's overall interpretation of the various interdisciplinary aspects of literature in HEC as detailed in Chapter 2. The framework serves as an abstract model of what HEC would look like when intra-cortical neurobiological mechanisms, physical control modelling and neurofeedback are integrated as a single concept. Such a framework could eventually be substantiated with new knowledge which is yet to be discovered. The experimental findings from Chapters 4 to 7 serve as preliminary steps towards the realization of some aspects of this framework.

3.2 Motor performance analysis

The primary function of motor performance analysis is the classification of different aspects of motor execution such as path length, efficacy of path planning, trajectory smoothness, time taken and errors incurred. Our initial implementation of motion capture was through computer vision based marker motion tracking of the subject performing HEC tasks as it is the easiest to implement and the subjects are minimally hindered in motion by any sort of equipment. Progressively, we acquired marker-less computer vision based motion capturing solutions (Microsoft Kinect and Leap Motion) for completely unhampered motion capture.

The other aspect of motor execution is the tracking of eye saccades. Eye saccades have been shown to predate and guide goal oriented hand movement. Studies in cognitive neuroscience show that task oriented HEC requires the synergy of both hand and eye movement [74]. Additionally, the eye movement is leading and naturally acquires a gaze strategy in order to achieve the most advantageous view that can reveal the best spatio-temporal information significant to the task [9].

It has been suggested that gaze strategy itself can be trained in order to improve HEC in novice laparoscopic surgeons [75]. That is because visual attention is a limited resource that directly affects motor planning. Hence, when the strategy for visual attention in a laparoscopic environment is trained to be efficient, the advantages manifold into better hand eye coordination and laparoscopic skills. Hence, by incorporating the physical motor performance analysis and neuronal analysis of cognitive activity, we can achieve an objective scoring of a subject's hand eye coordination.

Another aspect of motor performance is the development of motor skill learning. Motor skill learning involves the acquisition of complex sequential motor tasks. Motor skill learning can be divided into segmental tasks that are learned through repetition over time and the rate of acquisition (learning curve) is regulated by the cognitive process. What we see in the cellular level as synaptic plasticity where the connection between neurons grow stronger in response to repeated activity, it is represented in the common layman phrase "practice makes perfect".

The alternative way to improve HEC would be to investigate on the mental process within cognition. What we learn from cognitive psychology is that attention, learning and memory are all part of the cognitive process [76]. Through the use of EEG, we are able to map the brain activity of the subject and approximate the level of attention [77] that the subject is giving to perform a task. Research has shown that attention levels peak at the start when the brain is processing new visuospatial data and reduce slowly over time just as motor skill improves for the task [78].

3.3 Cognitive cost and cognitive capacity modelling

Conventionally, cognitive workload for a human-machine interface task is determined with self-report scales such as the NASA Task Load Index [79] but they

are subjective in nature. More recently, there have been studies that involve the use of EEG/ERP-based methods [80] to determine the cognitive workload on a subject.

The general approach is to implement a dual-task paradigm and the user's ERP response to the secondary task cue is used to infer the level of workload that the subject is under due to the primary task [81]. The use of EEG to determine workload is based on the rationale that due to the allocation of limited neural resources to a primary task, the remaining neural resources illicit changes to ERP related to the secondary task. Hence by looking at the change in ERP related to a secondary task, the workload of the primary task can be inferred.

In our approach, we propose to directly track and label the ERP changes associated with successful and unsuccessful tasks and hypothesize that there is a correlation for a task-related cognitive workload cost with a parameter from its corresponding ERP profile. In this manner, each ERP epoch will be able to contribute a sense of the cognitive cost of a repeated task.

Another notion is that once the cognitive cost of the task reduces the person's cognitive capacity down to a certain threshold, there will not be enough neural resources to properly complete the task hence the subject fails in that task instance. Hence by collaboratively analysing these concatenations of ERP trends in a single subject repeatedly performing a single we can estimate the cognitive cost of the task to the person and estimate the cognitive capacity of the person.

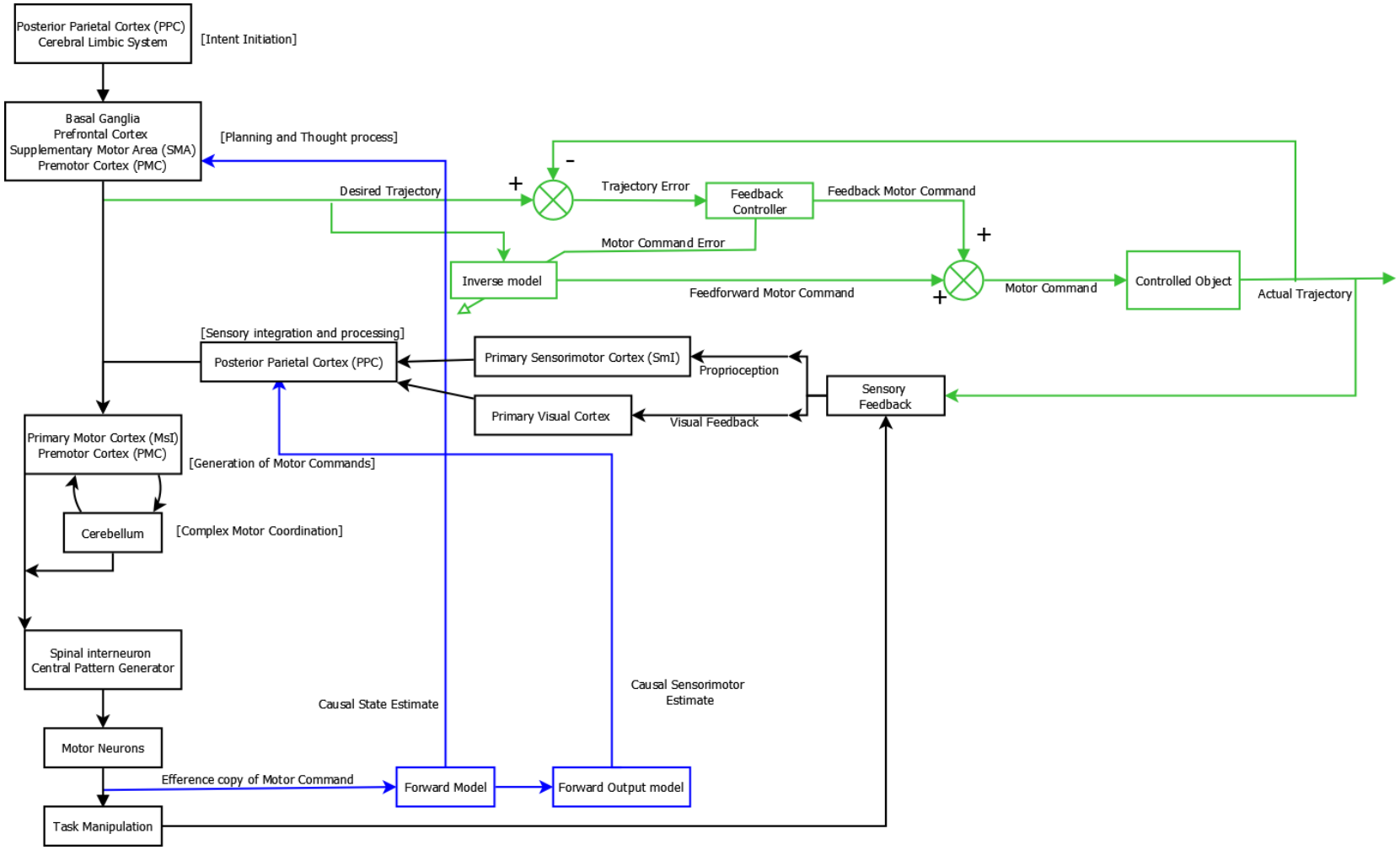

Figure 3.2: Biological model with integrated forward and inverse models.

The forward model is coloured blue and the inverse model is coloured green.

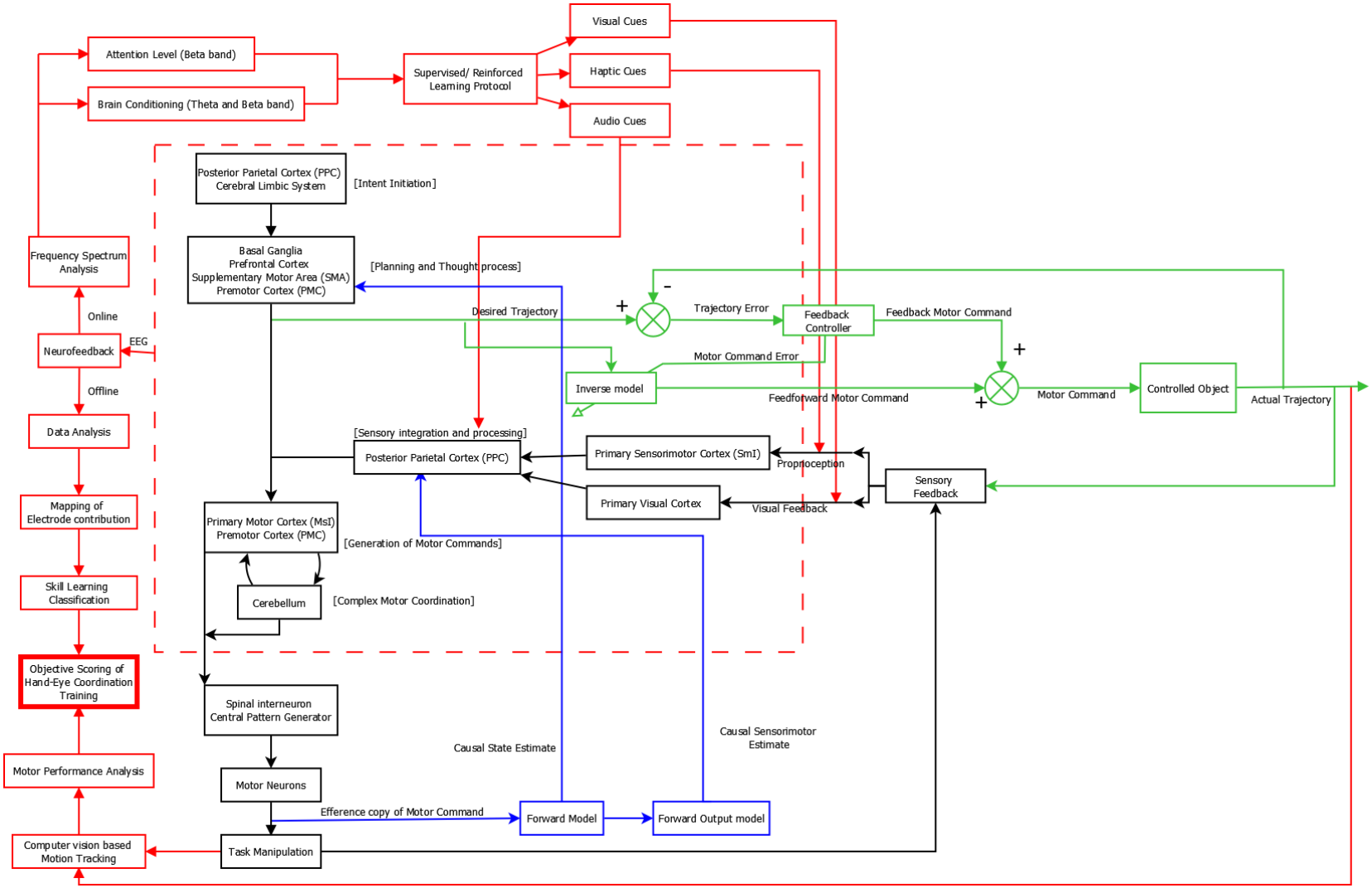

Figure 3.3: Biological model with integrated forward and inverse models and neurofeedback.

The neurofeedback aspect is coloured red.

4 Experiment - Depth Perception and Colour Cues

Four experiments were conducted exploring the various aspects of HEC. In Chapter 4, the aspect of visual cues in the form of depth perception and colour cues for endoscopic visualization was investigated. In Chapter 5, a visual cue guided box folding experiment was conducted to identify pertinent neural markers related to simple task mastery. In Chapter 6, an experiment was conducted to investigate the effects of haptic guidance from a robotic trainer on tracing and pointing tasks. In Chapter 7, a touchscreen based sequential pointing simulation game was created and used to explore the effects of visual cues with sequential planar arm motion through epochal EEG responses.

In Chapter 4, the effect of visual cues on HEC was investigated. The motivation for this experiment is that visual cue is the singularly most important cue for HEC [82]. Understanding how visual cues can affect HEC performance will be fundamental to any subsequent implementation of visual cues for HEC research. The subjects' visual cues were affected by the augmentation of depth cues and colour. The corresponding effects on the subjects' HEC ability were measured through the performance of a series of basic abstract surgical tasks.

4.1 Background

Minimally invasive surgery (MIS), also called laparoscopic surgery, has evolved into a common preference as the main treatment approach for many types of surgeries such as laparoscopic cholecystectomy. There are many advantages in laparoscopic surgery for the patient such as reduced recovery time, lesser analgesic use and less post-operative pain [83]. However, laparoscopic surgery has its disadvantages as well. Compared to open surgery, surgeons have to work with harder visual and

physical conditions [84], [85]. Because of the skewed hand-eye-instrument axis, the dexterity of the surgeon is reduced. The stationary positioning of the laparoscopic trocar ports imposes a counter-intuitive fulcrum effect on the mapping between the surgeon and the instrument's movement. The long and thin laparoscopic instruments amplifies hand tremor and, along with frictional effects of the trocar, reduces haptic feedback to the surgeon. As most conventional endoscopic systems can only display a two-dimensional (2D) representation of the three-dimensional (3D) operating workspace, it leads to a reduced perception of depth. This is due to the removal of 3D depth cues such as binocular stereopsis that is derived from binocular disparity that occurs due to the slight difference of vision experienced in both eyes. For a 2D display, both eyes view the same image; hence there can be no binocular disparity.

While there are many aspects to HEC in laparoscopic surgery, this study focuses on laparoscopic visualization, in particularly, on depth perception. In a previous study that explored laparoscopic training methodologies with a customized laparoscopic box trainer, it took about twice as long for subjects to perform abstract laparoscopic tasks with laparoscopic visualization as compared to open visualization [86]. Similarly, even the hybrid hand-assisted laparoscopic surgery (HALS) method, with better depth perception from the inclusion of an intracorporeal hand, was reported to be significantly faster than conventional laparoscopy [87]. Improving depth perception is necessary as surgeons, especially inexperienced ones, tend to compensate for the reduction in depth perception by "crashing" onto the tissue surface when trying to probe for the relative depth of the surfaces that results in past-pointing tissue damage [88].

Depth perception is a crucial part of HEC as it affects the accuracy of the brain's internal representation of the physical scene. Depth perception is based on binocular and monocular depth cues such as stereopsis, motion parallax, accommodation, convergence, occlusion and shadows. Literature shows that the most dominant cue,

especially for close proximity sight, is binocular stereopsis [89] which led to the development of 3D stereoscopic endoscopes that try to recover that cue. However, 3D laparoscopic visualization products are still in its infancy and prohibitively expensive. Furthermore, earlier studies have shown that initial 3D products had mixed results and tend to induce mental fatigue as well as look unnatural [90], [91]. Although recent studies have shown that using state of the art 3D HD systems increased task efficiency while performing abstract tasks in a physical phantom [92], [93].

One way to improve depth perception within conventional 2D displays is to reinforce monocular cues. In an endoscopic environment, some of the more significant monocular depth cues are motion parallax, occlusions and shadows [89]. Shadows are typically absent in the endoscopic view due to the coaxial arrangement of the illumination and camera. Recent research has gone into the restoration of absent cues such as shadows, through optimal secondary illumination positioning [94], shadow contrast ratio [94], enhanced shadowing from image processing [95] and colour contrasting shadows [96]. However, to our knowledge, no work is done on enhancing motion parallax for laparoscopic visualization. This is not surprising as the nature of motion parallax requires a translating viewpoint to be effective. In the small laparoscopic environment, fixed trocar positioning makes it hard to achieve a manual, steady and translating endoscopic viewpoint. In addition, the endoscopic field of vision is very narrow hence excessive and unstable movement of the viewpoint will induce mental fatigue to the observer [97].

This leads to the first aim of our study which is to integrate motion parallax and shadows by introducing dynamic shadowing. Conventionally, in order to achieve the motion parallax depth cue, a translating viewpoint is needed. However, in our experiment, it is the light source and shadows that are moving instead of a translating viewpoint. This is achieved by mounting a secondary light-emitting diode (LED) light source onto the laparoscopic grasper that shines onto the tip of the instrument

itself, producing a dynamic silhouette of the instrument against the surface that the tip is pointing at. The background illumination from the moving LED casts dynamic shadows against objects in the workspace as well. Indirectly, motion parallax can be inferred as shadows of objects nearer to the moving light source have a higher shadow contrast and move faster than the shadows of objects farther away. In addition, moving cast shadows have also been found to be such an effective depth cue that it can override [98] other depth cues such as object size changes and movement in light sources [99].

The second part of this study involves the evaluation of infrared light (IRL) as the illumination for the application of dynamic shadowing and laparoscopic visualization. Aside from thermal imaging18, IRL has long been attempted for use in medical purposes such as classification of tissue type based on IRL, which is capable of penetrating into tissue and is absorbed and reemitted differently by different tissue types [100], [101]. The second useful property of IRL is the strong optical absorption by haemoglobin. Coupled with its penetrative nature, IRL is capable of enhancing and revealing near surface vasculature [102] which is very useful to help surgeons avoid unnecessary haemorrhages. However, one major drawback of using IRL is the loss of colour which is an important source of visual information for the surgeon to differentiate between tissue types. In this study, we replaced visible light with IRL and examined whether dynamic shadowing translates well into a monochrome environment where shadows are less distinguishable from the environment.

The scope of this study is to investigate two hypotheses put forward by the authors. In the first experiment, we investigate the first hypothesis which is that the implementation of a dynamic light source to produce dynamic shadowing will improve depth perception and enhance the performance of three abstract laparoscopic tasks under a conventional 2D view and an autostereoscopic 3D view. In the second experiment, we investigate the second hypothesis which is that IRL can be used as an

alternative invisible light source for the implementation of dynamic shadowing as well as general illumination in laparoscopic surgery.

4.2 Materials and Methods

4.2.1 Experiment 1

Participants**:** Ethics approval for both experiments was granted by the local institutional review board. Twelve volunteers from non-medical backgrounds were recruited for the first experiment. Their age varied from 22 to 26 years. None of them had any prior laparoscopic training. All of the subjects had good (or corrected) eyesight and no colour impairment. Subject demographics are listed in Table 4.1.

Apparatus: A 300mm by 300mm by 270mm laparoscopic box trainer made of acrylonitrile butadiene styrene (ABS) was designed and fabricated (see Figure 4.1). The box trainer had a 3mm thick silicon rubber that was stretched over the curved top cover of the box and fastened with Velcro. It was designed with detachable side panels for easy access into the workspace.

Instead of a 2D endoscope, an 8.1 megapixel USB webcam was used as the primary overhead video source (model webcam 7100; Sensonic, Singapore). Conventional commercial dry-box laparoscopic trainers also utilize USB webcams as a low cost, widely available alternative to endoscopes. USB webcams are able to provide a similar image quality and field-of-vision as surgical endoscopes when used in the dry-box ex-vivo setting so they are a feasible and economical alternative. The webcam was secured in place through the use of an adjustable mechanical arm. The 2D output was displayed onto a 17” LCD monitor (model 1708FP; Dell) and the 3D output was displayed onto a 20” lenticular autostereoscopic 3D monitor (model AD2; Newsight, Jena, Germany).

The laparoscopic instruments used are a 5mm diameter 310mm length bullet nose grasper (BBraun, Tuttlingen, Germany) and a straight tip needle holder (model E705R; Ethicon). Primary static overhead illumination is from six white LED bulbs built into the webcam or by a separate overhead LED probe (see Figure 4.2) that houses five 3 mm Clear 3.6 V Visible LEDs (Nichia, Tokyo, Japan) and is secured through the silicone sheet with an external magnet. Secondary dynamic grasper illumination (see Figure 4.3) is provided by two 3mm diameter white LED bulbs powered by an external DC source (model E3616A, Hewlett Packard). All probes were designed to be implantable and conform to 15mm laparoscopic trocar size restrictions. In addition to the size advantage, compared to arc-lamp light sources, LED light was reported to produce sharper shadows, uniform lighting and less flickering [103].

Table 4.1: Subject demographics for the first experiment

Mean Age	23.8 years
Gender	9 Males, 3 Females
Master hand	10 Right, 2 Left
Hand eye coordination games experience and frequency	67% have experience/ About twice monthly
Racquet games experience and frequency	100% have experience/ Seldom

Figure 4.1: Overview of the laparoscopic box trainer.

Procedure: We have come up with three abstract laparoscopic tasks in order to test the depth perception of our subjects. The tasks comprised of threading, pushing and pick & place. The first was a threading task (see Figure 4.4). It involved the subject withdrawing and inserting a thin stick held onto the end of the needle holder into a perforated vertical surface. The perforated surface is split into 4 separate rows of holes and the subject was tasked to insert the stick into a randomly generated sequence of targets. Because of the nearly top-down orientation of the view, the rows of holes are perceived as targets at different depths.

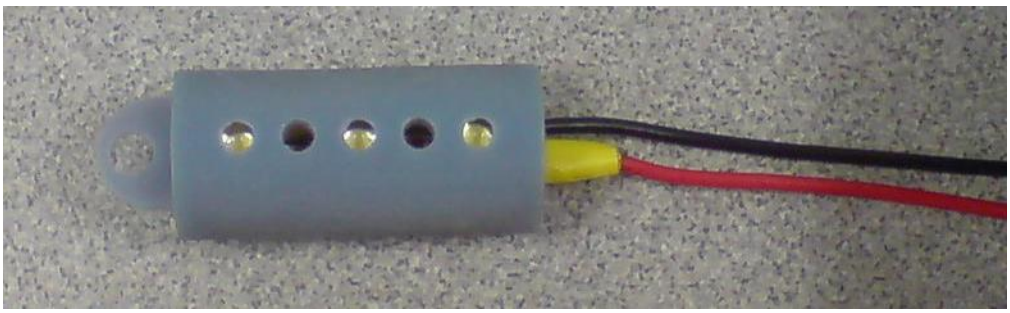

Figure 4.2: Overhead light-emitting diode probe.

Figure 4.3: Light-emitting diode probe mounted on a laparoscopic grasper.

The subjects were assessed based on their execution time only as the majority of the subjects did not make any gross mistakes and were able to self-correct, at the expense of slightly additional time incurred. Each run consists of 8 holes and each run was carried out twice, once with the perforated surface located frontally to the camera's orientation and once with the perforated surface located obliquely to the camera's orientation.

The second and third tasks involved the use of a hollow box that was interlaced with wires inserted at various depths across the box (see Figure 4.5). By linking a light and buzzer circuit with the network of wires and the electrode of the laparoscopic instrument, we created a maze to test the subject's instrument navigation performance in an intricate 3D space. We have previously used this 3D wire maze as part of training and assessing accuracy in laparoscopic motion with a robotic platform [104].

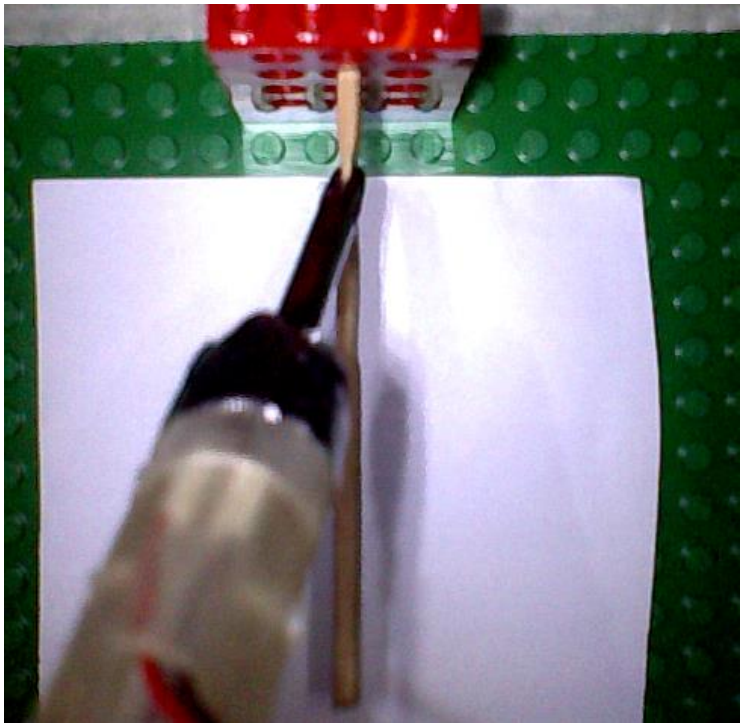

Figure 4.4: Task 1: Threading a wooden stick through the perforated Lego brick.

The second task was to drag a piece of Lego brick horizontally across the length of the box. A subject has to withdraw and insert the laparoscopic grasper at appropriate positions and orientations several times across the maze in order to avoid touching the wires and be within reach of the brick as the brick was moved. The subjects were assessed on total time taken and the number of times the instrument tip touched the wires and triggered the circuit.

The third task was to pick six sponge cubes that were randomly placed within the maze and deposit them in a designated corner of the screen (see Figure 4.6). Similarly, the subjects were assessed on time taken and the number of times the circuit was triggered.

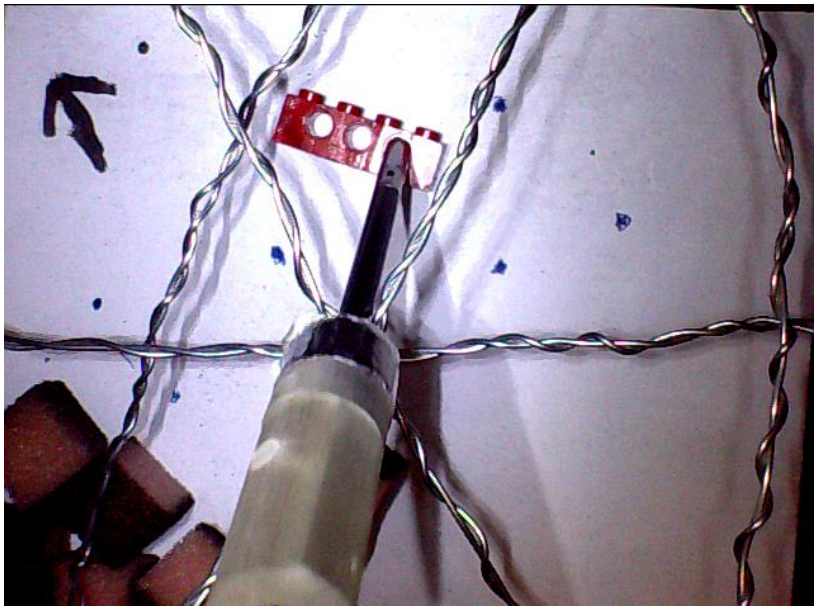

Figure 4.5: Task 2: pushing a Lego brick horizontally across the workspace.

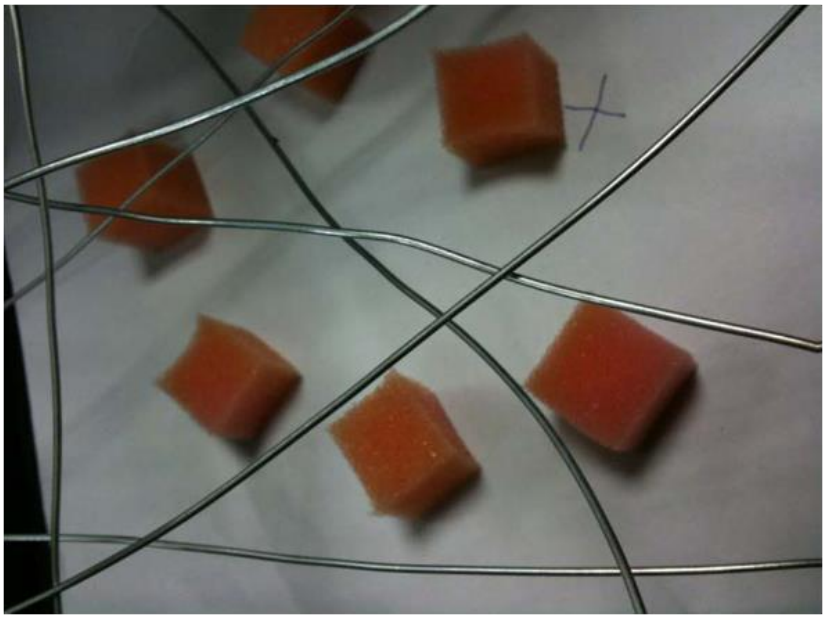

Figure 4.6: Task 3: Picking and placing the randomly positioned sponge cubes.

The sequence of the tasks and viewing conditions assigned to the participants was randomized to minimize any learning effect on the results. The result collected were evaluated using Analysis of Variance (ANOVA) to determine if there is significant difference in the mean time taken and error rates for the different viewing conditions. Significance was set at $p < 0.05$.

Each set of three tasks were carried out under the following four viewing conditions:

a) 2D view with static illumination only,

b) 2D view with dynamic grasper illumination,

c) 3D view with static illumination only,

d) 3D view with dynamic grasper illumination.

4.2.2 Experiment 2

The objective of the second experiment is to investigate the second hypothesis which is that IRL can be used as an alternative light source for the implementation of dynamic shadowing as well as for general illumination in laparoscopic surgery.

Participants: Twenty Five volunteers from non-medical backgrounds were recruited for this part of the study. Their age varied between 22 and 27 years. None of them had any prior laparoscopic training. All of the subjects had good (or corrected) eyesight and no colour impairment. Subject demographics are listed in Table 4.2.

Table 4.2: Subject demographics for the second experiment

Mean Age	23.9 years
Gender	15 Males, 10 Females
Master hand	23 Right, 1 Left, 1 Ambidextrous
Hand eye coordination games experience and frequency	60% have experience/ about twice monthly
Racquet games experience and frequency	88% have experience/ Seldom

Apparatus: The setup used for the second experiment was similar to that of the first experiment except for changes to the camera and lighting. A second webcam of the same model was modified to capture video in infrared (see Figure 4.7). The IRL filter on the second webcam was removed so as to make it sensitive to IRL. In addition, a visible light filter made from standard photography film negative was added to the lens of the camera. The filter was prepared by overexposing a strip under

visible light for a few minutes and then developed. The strip was subsequently sized and fitted onto the lens of the camera. 860nm peak wavelength Infrared LED (SFH 4350, OSRAM Opto Semiconductors) was also incorporated into the overhead lighting probe and the grasper lighting probe.

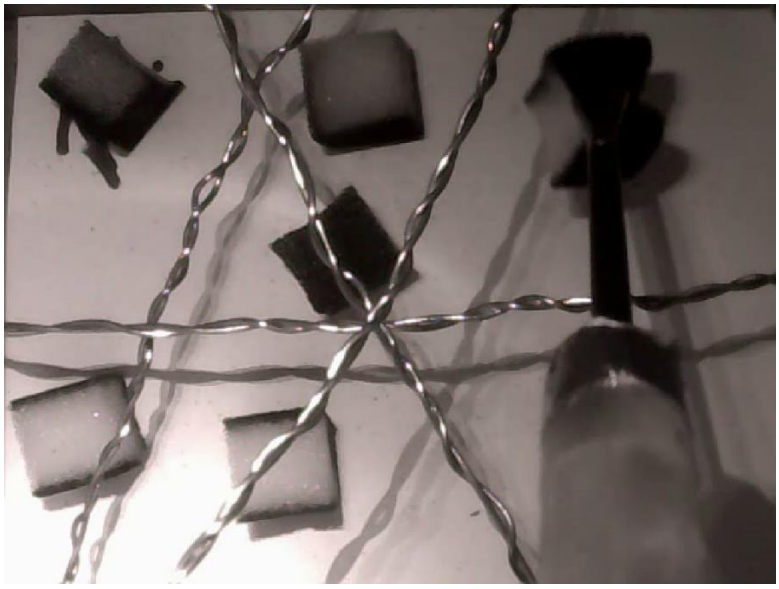

Figure 4.7: Performing task 3 under infrared illumination.

Procedure: The task evaluation methods for the second experiment were the same as those used in the first experiment. Volunteers were asked to perform the same set of laparoscopic tasks under four viewing conditions:

a) Static illumination with visible lighting
b) Dynamic illumination with visible lighting
c) Static illumination with Infrared lighting
d) Dynamic illumination with infrared lighting

4.3 Results

4.3.1 Experiment 1

For Task 1: Threading task, the viewing condition with the lowest average threading time is the 2D display condition with dynamic illumination (56.37s). Overall results also show that the 2D display conditions (60.53s) yielded significantly better results than the 3D display conditions (79.12s) (p=0.008) and dynamic shadows (68.41s) was slightly better than static illumination (71.24s) although the difference was not significant (p= 0.672).

For Task 2: Pushing task, the viewing condition with the lowest average pushing time is the 3D display with static illumination (43.91s). Overall results show that the time taken to complete the task under 3D viewing conditions (56.85s) was generally shorter than that under 2D viewing conditions (60.46 s). The difference was not statistically significant (p= 0.736). The overall mean for static illumination is 53.25 s and the overall mean for dynamic illumination is 64.06 s which is not significantly different (p= 0.315). The least amount of errors was made under 2D display conditions with dynamic shadowing (2.42). However, overall trends indicate static illumination (2.67) to be slightly better than dynamic illumination (2.92).

For Task 3: Pick and Place task, the viewing condition with the lowest average pick and place task was 2D display conditions with dynamic illumination (103.53s). Overall trends correlate with this result, with 2D display conditions (114.82s) faring better than 3D display conditions (119.65s) and dynamic illumination (111.48s) doing better than static illumination (123.00s). The least amount of errors was recorded under the 2D display condition with dynamic illumination (3.00). However, overall trends show that the 3D display condition (3.46) has a better error rate than 2D display conditions (3.88).

4.3.2 Experiment 2

For Task 1: Threading task, the viewing condition for with the lowest mean threading time is visible light with dynamic illumination (51.98s). Overall, dynamic illumination (52.02s) was better than static illumination (57.17s) but the difference was not statistically significant (p=0.24). IRL (52.74s) was found to be slightly better than conventional visible light (56.46s, p=0.39).

For Task 2: Pushing task, the viewing condition for with the lowest average time taken for this task was visible light with static illumination (40.87s). Overall, the performance under visible light (41.81s) was significantly better than under IRL (61.33s, p=0.0051) and dynamic illumination (48.21s) was found to be slightly better than static illumination (54.94s, p=0.32).

The least number of mean errors made was under visible light and static illumination (1.04). Overall, the number of errors made under visible light (1.18) was found to be significantly lesser than under IRL (2.30, p=0.019) and the number of errors made under static illumination (1.56) was lesser than dynamic illumination (1.92, p=0.44).

For Task 3: Pick and Place task, visible light with dynamic illumination was found to have the lowest mean time taken for this task (74.99s). Overall, Visible light (77.99s) was found to be better than IRL (91.55s) and dynamic illumination (81.02s) was found to be better than static illumination (88.52s).

Similar to the pushing task, the mean number of errors made was lowest under visible light and static illumination (2.44). Overall, there were fewer errors made under visible light (2.68) compared to IRL (3.30) and there were fewer errors made under static illumination (2.76) compared to dynamic illumination (3.22).

4.4 Discussion

4.4.1 Experiment 1

In general, from the tabulation of mean results (see Table 4.3), for all three tasks, using the 2D display, performance improved with the use of dynamic shadows. The experiment has shown that dynamic illumination with 2D display conditions reduces execution time and the number of errors made. The user relied on the brightness of the reflected light and the size of the shadow to gauge the distance between the instrument and the target.

However, this was not true when looking at 3D display results. Mean performance for Task 1 and Task 3 was almost the same but Task 2 took 60% longer when using dynamic shadows. We hypothesize that this was due to the Pulfrich effect that the 3D monitor utilized to simulate depth. This effect generates a decaying ghosting effect that tended to duplicate the number of shadows, hence the 3D effects served to disorientate the subject more than aiding him. Feedback from the volunteers was that the 3D images had distorted depth judgment and induced dizziness. Some of them also stated that they became mentally fatigued faster when using the 3D monitor.

Looking at the mean number of errors; as compared to the static counterpart, using dynamic shadows reduced the number of mistakes with the 2D display but the trend reversed with the 3D display. This showed that the Pulfrich effect not only increased the time taken but also increased the number of mistakes made.

When we look at the results of each task under the four viewing conditions, 2D display with dynamic illumination and 3D display with static illumination tend to perform better in terms of time taken and number of errors made as compared to the remaining two viewing conditions. This trend signifies two findings. First, implementing a dynamic illumination or 3D display improves on the conventional 2D

display with static illumination. Second, although individually, the dynamic illumination and 3D display generated an improvement in performance over the 2D display with static illumination, their joint effect produced an opposite effect, resulting in the worst performing viewing condition in most of the results.

Pre-emptively, the task order was randomized for each subject in order to minimize the learning effect. However, there were still signs of familiarization as each task was carried out four times per subject. In addition, subjects feedback that the dynamic shadowing did help them in perceiving depth but they needed to be reminded to actively use the shadows to gauge depth. This may be accounted for by the evidence that individuals have different strategies for depth cue combination [105]. As a consequence, some subjects might need to specifically train to consciously take notice and make use of the shadows.

4.4.2 Experiment 2

By comparing static illumination to dynamic illumination (see Table 4.4), dynamic illumination has reduced the overall mean time taken for all 3 tasks. This trend is also evident for all 3 tasks under IRL which shows that the benefit of dynamic shadows, as shown in experiment 1, can be applied with IRL as well.

Both the first and third tasks showed that performance under IRL yielded no significant penalty as compared to visible light. However, the performance under IRL was significantly worse in the second task. Both mean time and number of errors made were significantly higher. We hypothesize that it was due to the nature of the task coupled with the optical property of the block material under IRL. The red Lego brick used for the second task actually appeared white under IRL (See Figure 4.8 . The background also appeared white so subjects might have had difficulty trying to differentiate the brick from the background. In the first and third task, since there were no problems in recognizing the perforated surface or sponge cubes under IRL, it

explains why using IRL did not result in significantly longer execution times as compared to using visible light.

Overall, when comparing visible light to IRL, the mean performance was faster with visible light in two tasks and less number of errors was made under visible light as compared to IRL in both Task 2 and Task 3. This showed that the loss of colour under IRL did reduce the laparoscopic performance of the subjects.

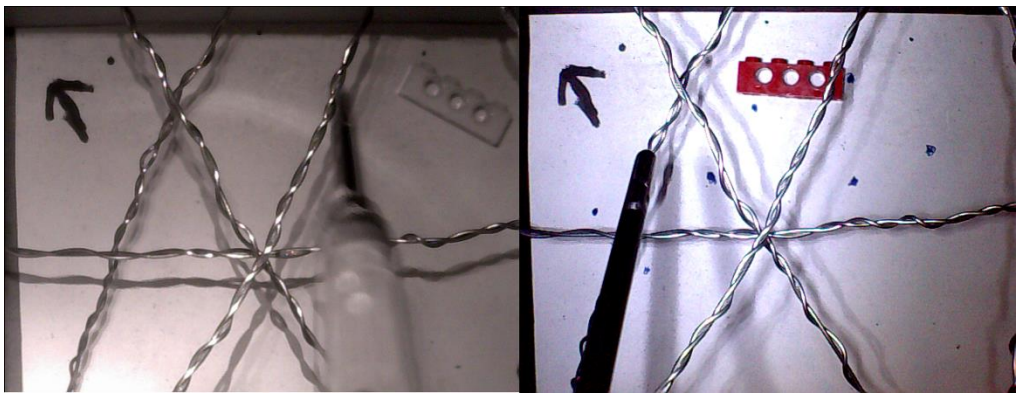

Figure 4.8: The colour differences of the same Lego brick under (left) infrared and (right) visible light.

4.5 Summary

In Experiment 1, it has been shown that the implementation of a dynamic light source in 2D visualization provides better depth information in the form of moving shadows. In Experiment 2, the results indicated that dynamic shadowing continued to show that it improved the subjects' performance and its improvement can be shown even under IRL. IRL was found to be generally inferior to visible light as general endoscopic illumination, especially if the task involved colour recognition.

The experimental results in Experiment 1 showed that dynamic shadowing with 2D display reduced execution time and number of errors. Dynamic shadowing with 3D display increased execution time for one of the tasks and increased number of errors for all three tasks. This demonstrates that dynamic shadowing could be an

inexpensive method to improve conventional 2D laparoscopic depth perception. However, familiarization is necessary to increase the dominance of shadows as depth cue. In the experiment, subjects had to be reminded to pay attention to the shadows. A possible improvement would be to enhance the delivery of shadows to the subject's view through image processing.

The general feedback from the volunteers was mixed. Some were in favour of IRL citing that the lack of colour created less confusion and gave a sharper tone contrast. However there were also those who claimed that the visible lighting allowed them to perform better as people were generally more accustomed to viewing from a full colour display.For future work, we intend to improve on mounting of the grasper illumination as the current LED setup was deemed to be too bulky and became entangled with the live wires frequently. We also aim to introduce another variant of dynamic illumination using a static and flexible array of LEDs that can be magnetically mounted onto the inner wall of the operating space.

Currently, the main performance indicator of the tasks was derived from time. We intend to improve on the assessment criteria by including image based motion tracking as well as force analysis. The author proposed that further experiment could track the path taken by the instrument and use the path length and path deviation to further assess individual performance. Secondly, the assigned game could simulate actual laparoscopic task like suturing and cutting. Thirdly, besides using near-infrared, medium and far infrared can also be considered for illumination. Last but not least, the torso case should not only mimic the human body externally but also internally. Inserting synthetic organs and vessels that have wet surface finish can make the workspace looks and feels like the actual abdomen. In this way, the user can experience the real visual and tactile restrictions encountered by laparoscopic surgeons.

Table 4.3: Averaged results for experiment 1
(corresponding standard deviation is listed in parenthesis. Best performance highlighted in bold)

Task 1: Threading time (seconds)			
	Static	Dynamic	Overall (2D/3D)
2D	64.70 (17.76)	56.37 (11.54)	**60.53 (15.25)**
3D	77.79 (30.05)	80.45 (27.93)	79.12 (28.40)
Overall (Static / Dynamic)	71.24 (25.05)	**68.41 (24.25)**	

Task 2: Pushing time (seconds)			
	Static	Dynamic	Overall (2D/3D)
2D	62.58 (28.69)	58.34 (34.54)	60.46 (31.13)
3D	43.91 (19.19)	69.79 (55.37)	**56.85 (42.63)**
Overall (Static / Dynamic)	**53.25 (25.71)**	64.06 (45.51)	

Task 3: Pick and Place time (seconds)			
	Static	Dynamic	Overall (2D/3D)
2D	126.11 (55.22)	103.53 (50.25)	**114.82 (52.91)**
3D	119.88 (66.87)	119.43 (76.23)	119.65 (70.13)
Overall (Static / Dynamic)	123.00 (60.06)	**111.48 (63.66)**	

Task 2: Pushing Errors (touches)			
	Static	Dynamic	Overall (2D/3D)
2D	2.83 (3.24)	2.42 (1.93)	**2.63 (2.62)**
3D	2.50 (2.28)	3.42 (3.26)	2.96 (2.79)
Overall (Static / Dynamic)	**2.67 (2.75)**	2.92 (2.67)	

Task 3: Pick and Place Errors (touches)			
	Static	Dynamic	Overall (2D/3D)
2D	4.75 (4.47)	3.00 (1.95)	3.88 (3.49)
3D	3.17 (1.85)	3.75 (2.77)	**3.46 (2.32)**
Overall (Static / Dynamic)	3.96 (3.44)	**3.38 (2.37)**	

Table 4.4: Averaged results for experiment 2
(corresponding standard deviation is listed in the parenthesis. Best performance highlighted in bold.)

Task 1: Threading time (seconds)				Task 2: Pushing time (seconds)				Task 3: Pick and Place time (seconds)			
	Static	Dynamic	Overall (Visible / IR)		Static	Dynamic	Overall (Visible / IR)		Static	Dynamic	Overall (Visible / IR)
Visible	60.93 (30.06)	51.98 (19.64)	56.46 (25.78)	Visible	40.87 (18.79)	42.76 (24.24)	**41.81 (21.71)**	Visible	80.99 (34.31)	74.99 (30.76)	**77.99 (32.72)**
IR	53.42 (17.40)	52.06 (14.18)	**52.74 (15.89)**	IR	69.00 (46.99)	53.66 (36.05)	61.33 (42.58)	IR	96.05 (40.85)	87.05 (40.20)	91.55 (40.77)
Overall (Static / Dynamic)	57.17 (24.84)	**52.02 (17.13)**		Overall (Static / Dynamic)	54.94 (38.45)	**48.21 (31.20)**		Overall (Static / Dynamic)	88.52 (38.47)	**81.02 (36.29)**	

Task 2: Pushing Errors (touches)				Task 3: Pick and Place Errors (touches)			
	Static	Dynamic	Overall (Visible / IR)		Static	Dynamic	Overall (Visible / IR)
Visible	1.04 (1.40)	1.32 (1.43)	**1.18 (1.42)**	Visible	2.44 (2.95)	2.92 (3.11)	**2.68 (3.04)**
IR	2.08 (2.43)	2.52 (3.32)	2.3 (2.92)	IR	3.08 (2.76)	3.52 (2.32)	3.3 (2.56)
Overall (Static / Dynamic)	**1.56 (2.05)**	1.92 (2.63)		Overall (Static / Dynamic)	**2.76 (2.87)**	3.22 (2.75)	

5 Experiment - Folding task with visual cue

In Chapter 5, the preliminary experiment with EEG recordings was carried out. The motivation for this experiment was to identify any possible EEG trends that can signify mastery of a HEC task. The target was to explore the differences in a subject's neural activity as he repetitively practices on a simple paper folding task. Through offline EEG analysis methods, the changes in neural activity was quantified and compared. Several topological neural markers that potentially corresponded with subjects' task mastery were identified.

5.1 Background

In a large scale epidemiological study conducted in 2010 by the Institution of Mental Health in Singapore, it was found that more than one in ten people will be stricken by a form of mental illness within their lifetime. Increasing prevalence of mental illness in society is a growing concern and as a result, there is a need for better management and rehabilitation of these mental patients. In order to reintegrate mental patients back to society as productive and self-reliant individuals, mental patients undergo rehabilitation and are exposed to occupational therapy that are designed to train them for suitable jobs in areas such as clerical work and food handling in food and beverage industries. Conventionally, due to the delicate nature of the interactions with mental patients, occupational therapists are required to manually train them in cognitive and motor skills crucial in the job scope. In addition, it is often hard to judge a subject's level of competence and task mastery without the professional supervision of therapists. As such, the occupational therapy sessions are limited to small groups. These factors put pressure on the already constrained manpower available. Therefore, one possible solution is to create an autonomous rehabilitative

training protocol with serious games that mental patients can train independently so as to reduce the reliance on therapists.

Conventionally, serious games involves simulations of tasks with the main notion of educating the user to master achieving certain task objectives, likely through a supervised or reinforcement learning protocol. For example, the occupational task objectives for a kitchen aide could be the proper technique for wielding and using a knife. The corresponding task performance would be the speed and accuracy of cutting the food ingredients. However, with respect to the training of mental patients, purely using conventional task performance metrics are insufficient in assessing the overall performance of the mental patients. Revisiting the example of a kitchen aide's cutting skill, an occupational therapist would focus more on the confidence in wielding the knife and mood of the mental patient in participating in the training before the product of the practice itself. Hence, the focus is on affective nurturing [106] of the mental state of the patient that further enables effective learning of tasks. This example highlights that in order to develop an effective rehabilitation solution; we should combine human performance engineering with cognitive science. Hence, to assess the rehabilitation progress of mental patients, the motor performance and mental state should ideally be assessed in conjunction with each other.

The most common way of observing a person's mental state would be through non-invasive scalp EEG readings, as described in Chapter 2.3.5. However, EEG itself is an indirect measure of mental activity through the spatial recording of spontaneous electrical fields that perpetuate a person's brain which are generated by the ionic activations of neurons in the brain. Raw EEG data can be recorded with multiple low impedance electrodes on the scalp. In order to interpret the sheer multiplicity of EEG readings, post processing of the EEG data is required.

A conventional way of post processing the EEG data is through the Fourier transformation of the signals into the frequency domain. This is because neurons are known to activate with causal synchrony resulting in neural oscillations across the brain. This synchronous activity is revealed with frequency analysis of the EEG data. The classification of brain waves into frequency bands within the frequency domain has been classically shown to correlate with certain mental states and spatial prevalence [107]. For example, the alpha frequency band in the occipital region (8-13Hz) has been associated with a more relaxed mental state [108], [109]. Hence, the relative changes in activity in the frequency domain are an indication of the mental state of the brain as the subject performs the training task. In fact, one of the earliest clinical uses for EEG was in EEG biofeedback which was fundamentally based on training individuals to alter levels of brain activity in certain frequency bands. This form of therapy was widely used with the treatment of attention deficit / hyperactivity disorder (ADHD) where ADHD patients were frequently found to have relatively elevated levels of activity in the theta frequency band (4-7Hz) and lower relative levels of activity in the alpha (8-13Hz) and beta (14-25Hz) range [110].

Another method of interpreting the EEG recordings is through the computation of the complexity of the EEG time series data. Lempel-Ziv Complexity [111] has been a popular method of characterizing several types of biological signals including classifying genomic sequences [112], [113], identifying subjects with Alzheimer's disease [114], classifying mental fatigue [57] and the depth of anaesthesia from EEG complexity [58]. It represents the rate of emergence of new patterns in a time series. Hence, a higher LZC value indicates that the signal is more complex. Before an EEG signal can be computed with LZC, it first has to be converted into a binary signal. Conventionally, the median or mean of the signal is used as the binary thresholding value [62]. Data points above the thresholding value are converted into ones and data points below that value are converted into zeroes. The binary string is then read from

left to right while each character is compared against a 'vocabulary of words'. As the string is read, the vocabulary increases and the rate of unique word entry into the vocabulary represents the emergence of new patterns in the string. After being normalized over a function based on the length of the entire string, this value indicates the complexity of the string. Thus, LZC is useful in reducing the dimensionality of an EEG data channel into a single value.

In this study, the objective is to compare a subject's task performance against the corresponding scalp EEG data recorded during the task. The comparison enables the identification of possible markers for gauging mental activity pertinent to the mastery of simple tasks such as the origami box folding used in this study. This enables a benchmark for deeper analysis of a person's performance beyond that of the conventional physical kinematic analysis.

5.2 Materials and Methods

5.2.1 Subjects and Experimental Protocol

We recruited six healthy male volunteers with ages between 21 and 30 who were all right-handed to perform the study. The experimental task chosen in this study was to fold a simple paper origami box. The folding instructions were presented in the form of 39 animated steps within a PowerPoint presentation. Each subject was required to build one box per trial with 5 trials in all. The first four trials were aided by the PowerPoint instructions while the last trial was unassisted.

5.2.2 Equipment

In order to record the scalp EEG readings, a Neuroscan NuAmps EEG amplifier was used. The amplifier is connected to a flexible lycra stretch cap where 32 sintered silver/silver chloride electrodes have been pre-positioned to the International 10-20

system of EEG electrode placements. The amplifier converts the analogue electrode signal and outputs to a PC for recording. 19 electrode channels were recorded in this study and their topographical map is shown in Figure 5.1. EEG conductive gel were applied on each electrode to reduce the impedance of the electrodes (<5KΩ) before the EEG data was recorded. On a separate PC, a series of animated origami folding instructions are shown to the subject (see Figure 5.2). A webcam was also used to record the subjects performing the task (see Figure 5.3).

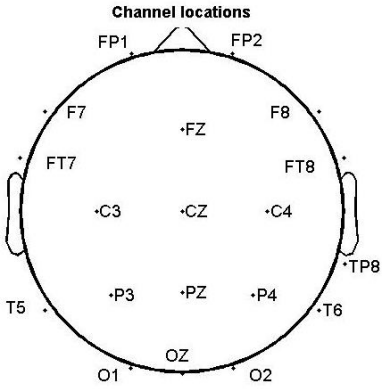

Figure 5.1: Topographic plot of the EEG electrodes recorded in accordance to the International 10-20 system of EEG electrode placement and labelling.

The electrodes are named and abbreviated according to the topological regions of the brain. FP stands for frontal polar, F stands for frontal, C stands for central, T stands for temporal, P stands for parietal and O stands for occipital.

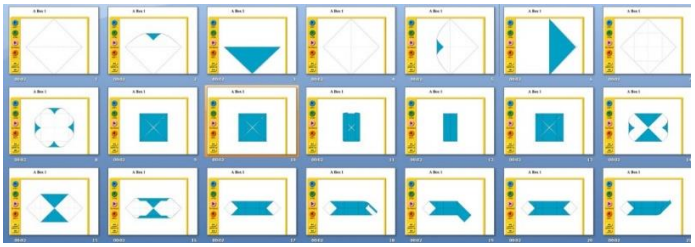

Figure 5.2: Sequential screenshots of the origami folding instructions shown to the subjects.

The cue sequence is from left to right and top to bottom.

Figure 5.3: Screenshot of Subject 1 performing the folding task.

5.2.3 EEG processing

In this study, raw EEG data was recorded from the 19 EEG channels sampled at 1000Hz and exported for further processing in the EEGLAB toolbox [115] for Matlab. Using EEGLAB, the EEG data was notch filtered at 50Hz to remove electrical line noise. Recorded EEG data tends to be very noisy due to external physiological artifacts such as ocular motion (EOG) and muscle activation (EMG). Eye blinks also induce large slow waveforms at the frontal regions of the EEG recorded. These obvious visible noise artifacts are manually cropped from the raw EEG readings before analysis. The EEG signal is then band pass filtered between 0.5Hz and 45Hz to remove low frequency noise such as slow drift found in continuous raw EEG data and high frequency noise such as muscle activations.

The Fast Fourier transform (FFT) function implemented in Matlab was used by EEGLAB to perform the spectral analysis of the EEG data. Subsequently, for LZC calculation, the EEG data after preprocessing is converted to a binary string by thresholding using the median value of the individual channel's signal. The binary string is then fed into a Matlab function to extract the LZC value.

5.3 Results

The six subjects took an average of 14 minutes to complete the five trials. The individual time taken for all six subjects to perform the 5 folding tasks is plotted in Figure 5.4. It can be seen that the subjects were able to almost plateau the time taken to fold the paper box by the 3rd trial. The timings for Trial 5 remained low, suggesting that the subjects have managed to master the folding task by the 4th iteration since there was no guidance given in Trial 5. Looking at Figure 5.4 it is evident that Subject 5 was the worst performing subject overall and Subject 6 was the fastest performer overall. Even with the relatively stabilized plateau of timings between Trials 3 to 5, Subject 5 still took approximately 3 times as long as the fastest person, Subject 6, to perform the folding task in those trials. In the subsequent spectral analysis, we shall focus mainly on the disparity between the trends in these two subjects' EEG data.

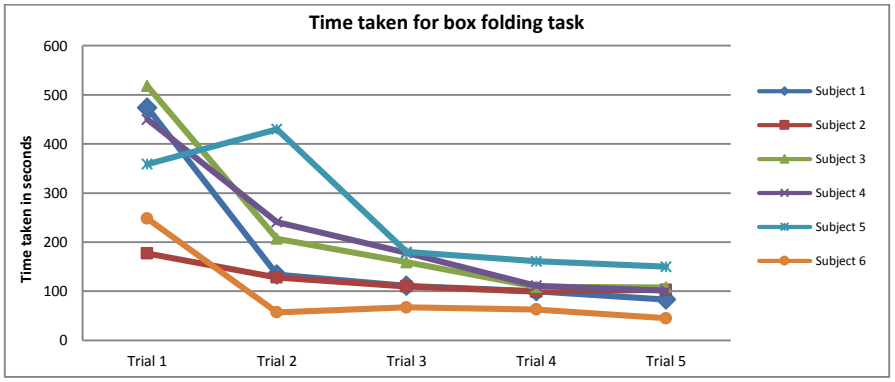

Figure 5.4: Time taken for each origami box folding trial of all 6 subjects.

The calculated LZC values for each subject are plot for the 19 EEG channels in Figure 5.5 to Figure 5.10. The LZC values averaged across the 6 subjects is shown in Figure 5.11. The LZC values are found to range between 0.10 and 0.35 for all the EEG data recorded in this study.

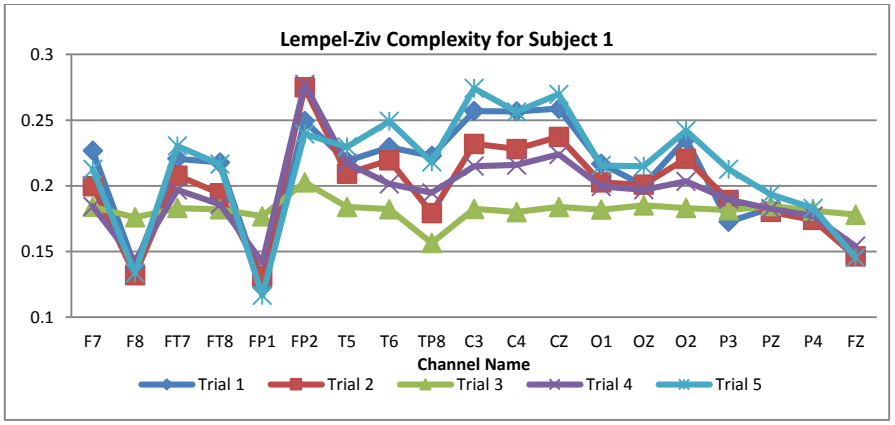

Figure 5.5: Lempel-Ziv Complexity values for all 19 EEG channels at all 5 trials of Subject 1.

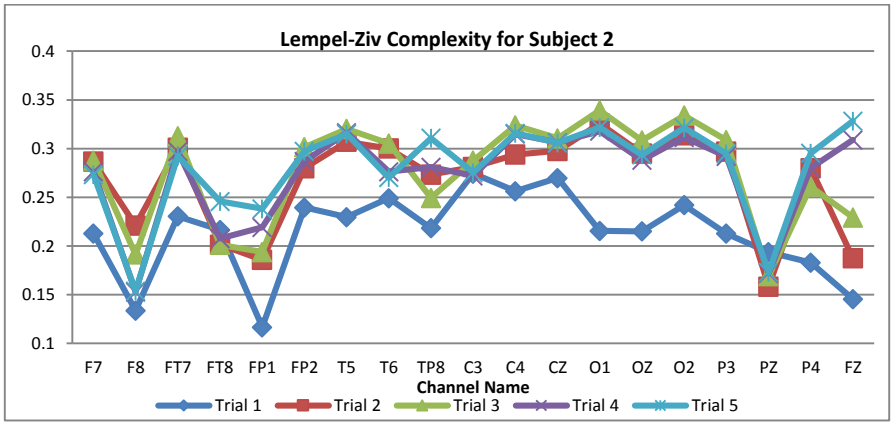

Figure 5.6: Lempel-Ziv Complexity values for all 19 EEG channels at all 5 trials of Subject 2.

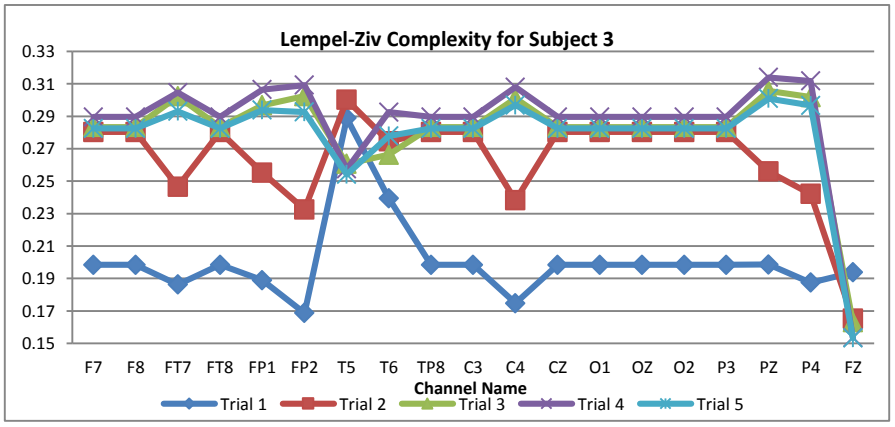

Figure 5.7: Lempel-Ziv Complexity values for all 19 EEG channels at all 5 trials of Subject 3.

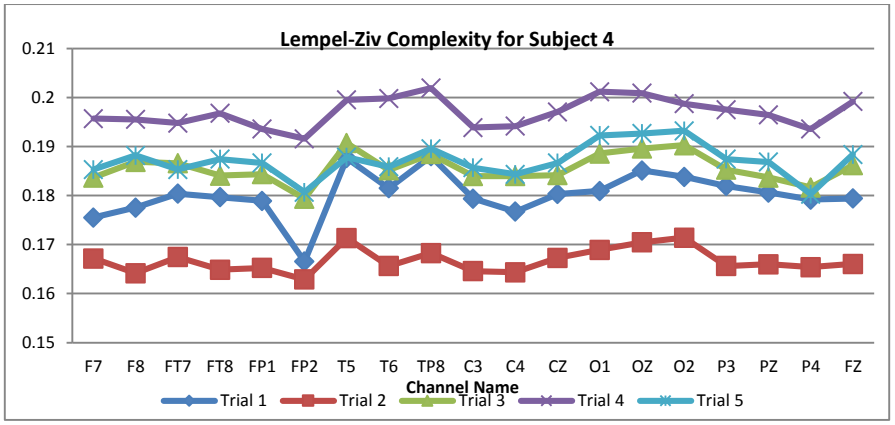

Figure 5.8: Lempel-Ziv Complexity values for all 19 EEG channels at all 5 trials of Subject 4.

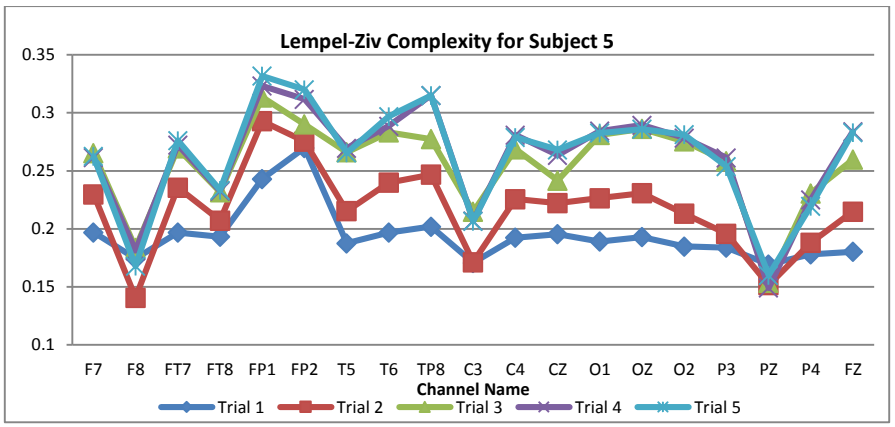

Figure 5.9: Lempel-Ziv Complexity values for all 19 EEG channels at all 5 trials of Subject 5.

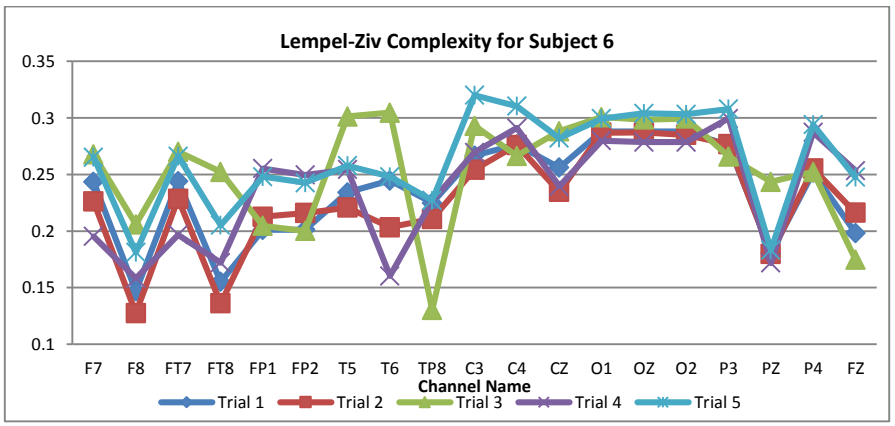

Figure 5.10: Lempel-Ziv Complexity values for all 19 EEG channels at all 5 trials of Subject 6.

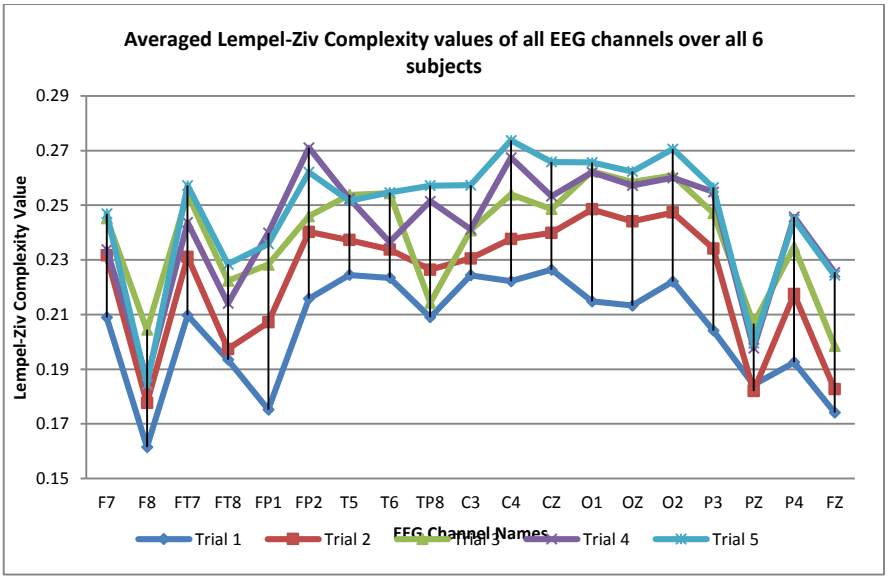

Figure 5.11: Averaged Lempel-Ziv Complexity distribution of all EEG channels for all 6 subjects.

The overall topological frequency spectrum plots of Subject 5 over Trial 1 to Trial 5 are shown in Figure 5.12 (a-e). Similarly, the topological frequency spectrum plots for Subject 6 are shown in Figure 5.13 (a-e). The individual frequency spectrums of channels C3, C4, CZ, O1, OZ, O2, P3, PZ and P4 are plotted in Figure 5.14(a-e) and Figure 5.15(a-i) for Subject 5 and Subject 6 respectively.

5.4 Discussion

5.4.1 LZC distribution

It would be a logical assumption that the since brain activity would decrease and be less complex as the task gets mastered, the LZC values would be shown to decrease with increasing number of trials performed. However, overall LZC values are shown to increase with increasing number of trials (see Figure 5.11). Although this seems counter-intuitive since it shows that the signals get increasingly more complex even though the subject is getting more masterful with the task, one

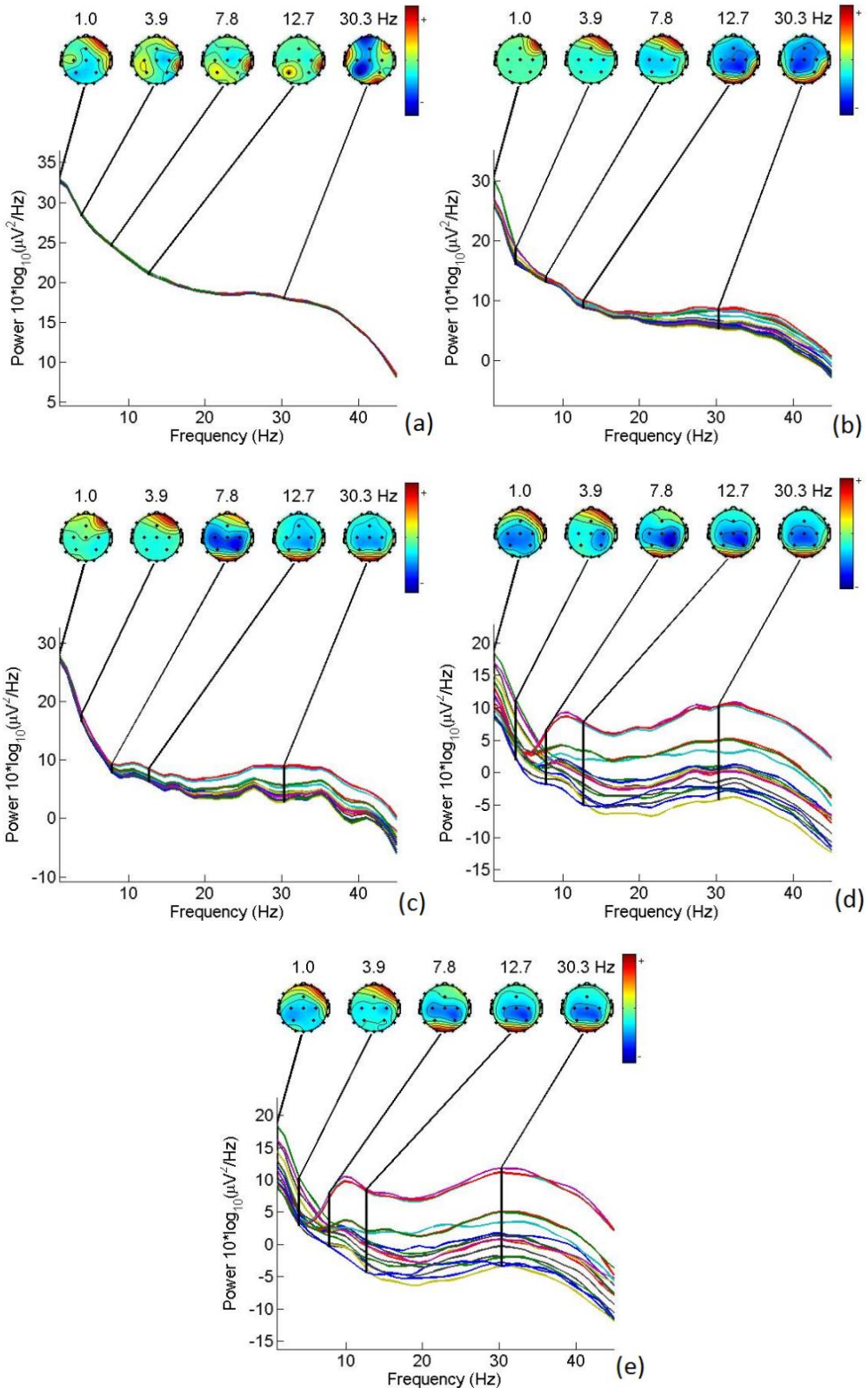

Figure 5.12 (a-e): Channel spectra and topographic maps of Subject 5 for all 5 trials.
The subplots are sequentially lettered from Trial 1 to Trial 5.

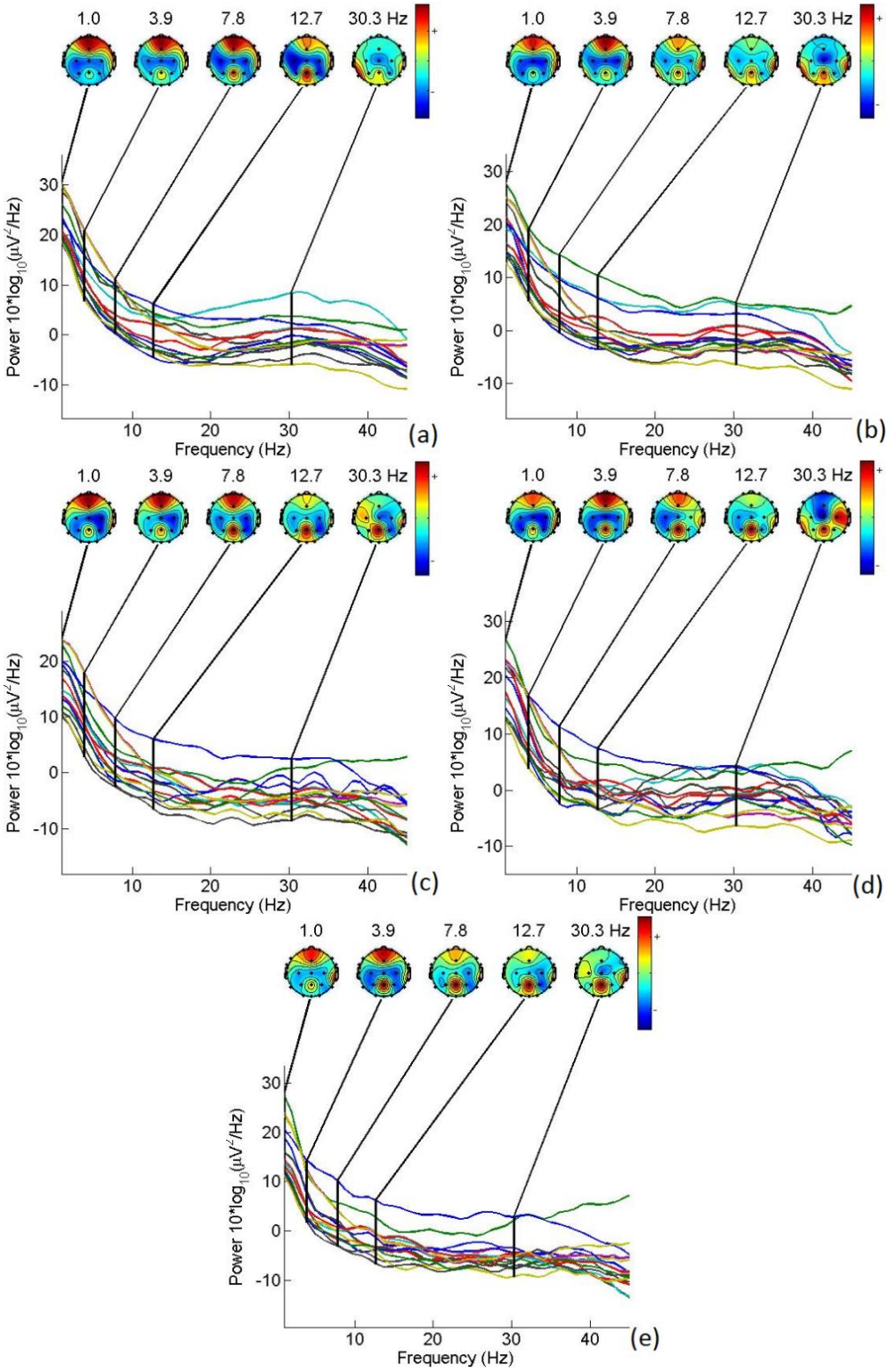

Figure 5.13 (a-e): Channel spectra and topographic maps of Subject 6 for all 5 trials.

The subplots are sequentially lettered from Trial 1 to Trial 5.

suggested possible explanation for this phenomenon is that at high mental concentration, amplitude synchrony triggers the activation of an internal concentration state [116], [117]. The internal concentration state refers to an isolation of the activity in the thalamencephalon cortex [118]. The result of that postulation is that at higher concentration with higher difficulty, the brain waves seemingly become more harmonic and synchronous, leading to lower LZC values. In our case, when the task gets mastered over increasing number of trials, the subjects need to concentrate less, thus the brain waves reduce to a more asynchronous and complex state.

By comparing the trends in LZC values of individuals (Figure 5.5 - Figure 5.10) over the 5 trials against the time taken for each trial, we can occasionally see that the increase in LZC values in some channels seem to mirror the improvement in timings. For example, when we look at Subject 3, the time taken sharply improves significantly from Trial 1 to Trial 2 and similarly we see a large consistent rise in LZC values between Trial 1 to Trial 2. Similarly, for Trial 2 to Trial 5, the improvement in timings tapers off and a similar trend appears in the LZC values of Trials 2 to 5. In addition, a similar corresponding trend is evident with Subject 6 where Subject 6 has relatively little improvement in timings and the LZC trend lines (see Figure 5.10) are also shown to be clustered vertically. However, more studies need to be performed to determine the consistency of this trend as it might possibly be an artifact from the LZC computation due to the different lengths of the trials [56]. Due to the rounding of data points, LZC has also been found to be more sensitive to high frequency components in the EEG signal [119].

Ideally, the LZC distributions should generate a consistently identifiable trend in that mirrors the changes in subject motor performance, meaning that the LZC trend lines of the 5 trials should not overlap each other and ideally be vertically spaced out to reflect the reduction in difficulty of consecutively performing the folding task over

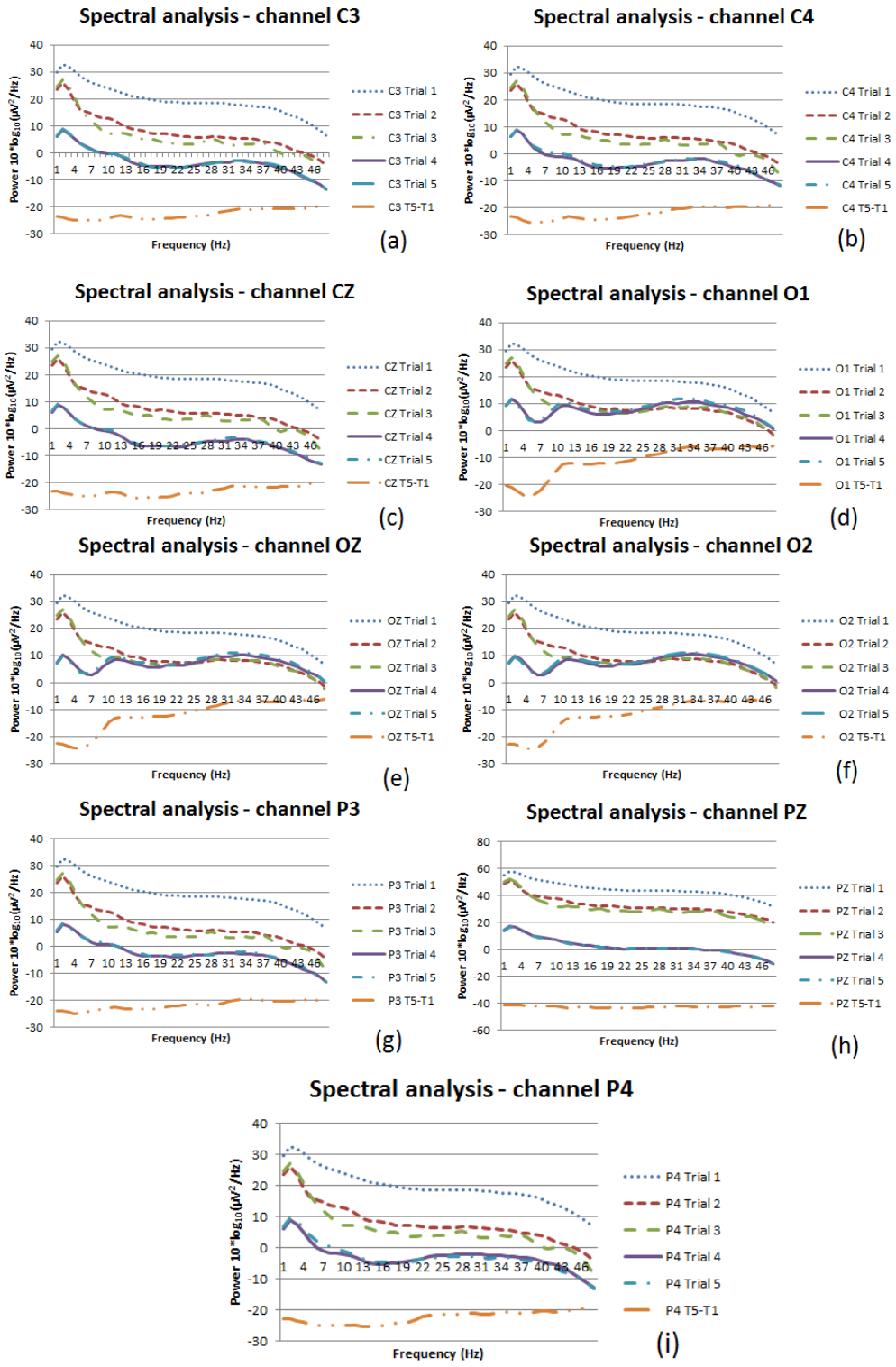

Figure 5.14(a-i): Individual frequency spectrums of channel C3, C4, CZ, O1, OZ, O2, P3, PZ and P4 for Subject 5.

The difference in power between Trial 5 and Trial 1 are plotted in orange for each of the channels.

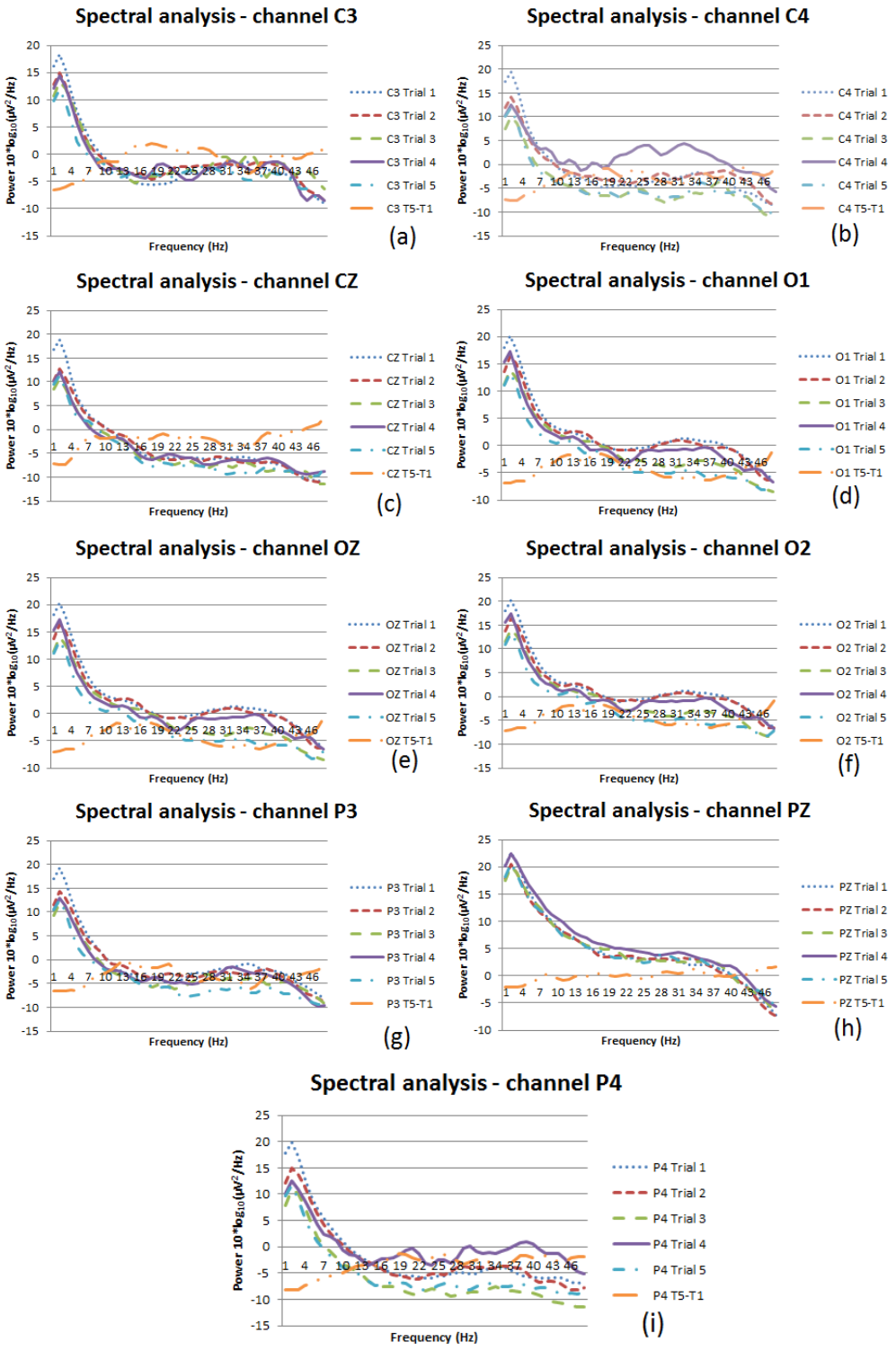

Figure 5.15: (a-i) Individual frequency spectrums of channel C3, C4, CZ, O1, OZ, O2, P3, PZ and P4 for Subject 6.

The difference in power between Trial 5 and Trial 1 are plotted in orange for each of the channels.

increasing number of trials. However, in most individual subject data sets, the LZC trend lines appear clustered together and intersecting at multiple channel locations.

Visually, it was hard to identify any useful LZC trend per individual, but when the LZC values are averaged over all 6 subjects, as shown in Figure 5.11, we can clearly see that channels C3, C4, CZ, O1, OZ, O2, P3, and P4 seem to satisfy our requirements for a useful LZC marker. This result mirrors that found by Hong et. al. whereby their LZC distributions were significantly different at the

occipital and parietal regions when comparing amongst different levels of mental workload using tasks of increasing levels of difficulty [117]. In the following section, we shall compare these channels in the frequency spectrum to see if there is a similar trend present in these channels identified by their LZC distributions.

5.4.2 Spectral Analysis

Unlike the normalized LZC values, frequency spectrums can vary from person to person so we cannot directly average the values across the 6 subjects like in LZC analysis. By looking at the topological spectral analysis plots in Figure 5.12 (a-e) for Subject 5, we can see that the delta (1-3Hz) and theta (4-7Hz) activity are frontally predominant and remain frontally predominant over the 5 trials. Similarly, the beta (14-25) and gamma (25-45Hz) activity are predominantly occipital and persist over the 5 trials. However for the alpha band (8-13Hz), it changes from being frontally dominant to occipital. Overall, the power reduces across the whole spectrum in all the channels when moving from Trial 1 to Trial 5, clearly indicating that brain activity and mental workload was reduced as the task is repeated.

By looking at the topological spectral analysis plots in Figure 5.13(a-e) for Subject 6, we can see similar topological trends as with Subject 5 for the delta and theta range. However, the alpha range remains primarily frontal and parietal (corresponding to area around channel PZ). Similarly the beta and gamma range are

predominantly parietal instead of occipital as in Subject 5. The overall activity level is also lower in Subject 6 as compared to Subject 5, especially in the first 3 trials. These two trends suggest that because Subject 6 has better mastery of the task, he does not need to visually focus as much on the task. Hence it is reflected in lower activity in the occipital region which processes visual information. Thus the parietal region that is responsible for integration of visual and proprioceptive inputs [120] appears relatively more active hence stands out in contrast.

Looking the individual channel frequency spectrums of subjects 5 and 6 (see Figure 5.14 (a-i) and Figure 5.15(a-i) respectively), it is clear that with an increasing number of trials, the activity level of all the individual channels plotted drops. By looking at Subject 5's channel plots (see Figure 5.14(a-i)), we can see that the drop in activity in individual channels is more pronounced in the central channels (C3, C4 and CZ) and parietal channels (P3 and P4) as compared to the occipital channels (O1, O2 and OZ). This is also reflected in the overall channel spectrum trends as shown in Figure 5.12 (a-e). In contrast, the overall activity levels of the individual channel frequency spectrum plots of Subject 6 (see Figure 5.15(a-i)) start out lower than that of Subject 5 but do not drop as much as that in Subject 5 from Trial 1 to Trial 5. This shows that Subject 6's brain activity starts relatively low and remains low over the 5 trials. This trend is mirrored in the time taken for Subject 6 to perform the 5 trials, suggesting that the task seemed naturally easier for Subject 6 as compared to the other subject.

Research on the alpha band (8-13Hz) [121] can be further divided into the slow alpha (8-10Hz) [122] and fast alpha (10-12Hz) range [123]–[126]. Slow alpha while not topographically bound to any brain region, is shown to relate to general attention levels. Whereas theta band activity has been found to be closely related to short term memory load [127]–[129] and sustained attention [130]–[133]. In Figure 5.14(d-f) we can see a sharp drop in the slow alpha and theta bands at the occipital area when we

compare Trial 1 with Trial 5. However, the same trend is much more attenuated in Subject 6 (see Figure 5.15(d-f)). This result suggests that the slower Subject 5 experienced higher levels of short term memory load and attentional demands during the early trial that decreases after more trials. This outcome complements the Fitts and Posner model for skill acquisition [134].

In the Fitts and Posner model, the first cognitive stage is associated with interpreting the nature of the task and trying out different strategies to perform the task which result in highly variable performance and high cognitive load such as attention. The second stage is the associative stage where the person has settled on a strategy and the focus is on refinement of the strategy, biomechanical efficiency and task performance. The third stage is the autonomous stage where the person has achieved muscle memory and automation of the skill, enabling minimal cognitive load for the task and allowing for the attention to be spent on other aspects such as higher order strategic planning. Therefore, classifying and monitoring the cognitive load of the trainee can be used as a method of determining the stage of skill learning where, according to the model, cognitive load and attention level decreases as the trainee advances in skill acquisition [135].

5.5 Summary

The objective of this study was to determine suitable means of gauging mental activity pertinent to the mastery of simple tasks. This study presents our method of integrating EEG in serious games for mental patient's rehabilitation. We have shown in our results and discussion that LZC trends measured using EEG in the central, occipital and parietal regions as well as spectral analysis of those channels, in particular within the theta and low alpha band, have potential to be used as markers for identifying the mental performance of a subject performing a simple training task.

LZC and spectral analysis of EEG data is capable of revealing deeper mental processes that correlate with overall motor performance. These means of classifying cognitive activity enable alternative and more reliable ways of looking at a person's task mastery and hand eye coordination ability.

We have shown that using LZC and spectral analysis in combination can help to reduce the redundant processing of data in the EEG data that we recorded. In retrospect, by looking at the clustered plots of individual channels in Figure 5.14 and Figure 5.15, it is hard to visually identify the same trends found in LZC analysis. This shows that LZC and spectral analysis could be used simultaneously in order to get alternative perspectives on the same EEG data.

Using results from this study enables us to isolate the pertinent EEG markers needed to develop an effective solution through a Serious Game environment that uses both physical kinematics and mental states for the rehabilitation of mental patients. Combining human performance engineering with cognitive science in a computer gaming environment is our ongoing research for mental patient's rehabilitation.

6 Experiment - Tracing and pointing task with robotic guidance

Chapter 6 presents our investigation on the effect of robotic haptic guidance on motor skill mastery of two HEC tasks through a robotic manipulator. The motivation for this experiment is to investigate the efficacy of haptic cues for training of HEC tasks as well as to contrast relative changes in neural activity due to the haptic guidance.

6.1 Background

The traditional dogma of teaching dexterous surgical skill has been the "see one, do one, teach one" system of master-apprentice tutelage as pioneered by William Halsted at Johns Hopkins University over a century ago [136]. After observing the master surgeon perform a surgical procedure several times, the trainee surgeon will attempt the procedure by mimicking the master surgeon's actions while the master surgeon physically steers the trainee with hand-over-hand guidance. Although this method is manpower intensive and limited in opportunity, arguably it provides the best form of guidance to the trainee. With the rapid advancement of surgical techniques together with technological breakthroughs such as laparoscopy as well as ethical and legal perspectives on teaching with real patients and the implementation of work-hour restrictions, the traditional approach has become insufficient to the needs of modern surgical training. This is especially true for laparoscopic training as it has been found that laparoscopic surgery requires significantly different skill sets as compared to open surgery [137] thus specificity in laparoscopic training is required. The skewed eye-hand-instrument axis, fulcrum effect of operating through a fixed trocar port and 2D endoscopic representation of the 3D intra-abdominal workspace

are some of the factors that contribute to a steep learning curve for laparoscopic training [85], [138].

A solution to the problem of the steep learning curve in laparoscopic training is the introduction of laparoscopic simulators that enable self-directed learning outside of the operating theatre. Laparoscopic simulators range from traditional box trainers [139] to virtual reality simulators [140] with a multitude of surgical fidelity and feedback mechanisms such as haptics and quantitative assessment of performance through indicators such as kinematic analysis, time taken, force and torque analysis [141]. However, current laparoscopic simulators have their limitations. It has been postulated the cheaper and simpler box trainers are just as effective as the expensive virtual reality simulators in training basic laparoscopic skill [142] which limits the advantages of the virtual reality trainers to other factors such as fidelity in simulating complex surgical scenarios. However, the range of operative scenarios included with the simulators is also limited and generic. Certain manoeuvres and skills such as tactile soft tissue manipulation cannot be easily taught through observation or virtual reality simulators. Furthermore, standard quantitative assessment of performance in current virtual reality simulators may be able to generalize the competency of the subject but it might not necessarily relate to the qualitative evaluation of laparoscopic skill which requires the expert judgement of experienced surgeons and is still an actively researched and discussed topic [139], [143].

Current laparoscopic simulators can only more or less function as a safe visual and haptic sandbox environment where trainees are free to make mistakes. However, without the traditional critical analysis and hand-over-hand guidance from a master surgeon, they forgo the physical experience of being taught the proper method of performing a procedure. Therefore, in order to reintroduce the missing traditional hand-over-hand guidance, the notion of haptic guidance through a robotic training system for laparoscopy was proposed [104].

A robotic laparoscopy training system that has the same range of motion and degrees of freedom (DOF) as conventional laparoscopic instruments was used in this experiment. This system enables the recording of a master surgeon performing a surgical procedure as a reference for the training of other subjects. Haptic guidance can then be given to the trainee based on the recorded motions of the master surgeon through the actuators on each axis.

The haptic guidance can be tuned to a spectrum of trajectory tolerances with respect to the reference recording ranging from fully controlling the replaying motion or an intermediately assistive type of guidance in which the amount of force the robot uses to correct the trainee's motion is proportional to the deviation from the reference trajectory or a "virtual guide rail" that allows free motion within a certain displacement radius from the reference trajectory. It is hypothesized that the degree of haptic guidance should be in tandem with the amount of experience and confidence of the trainee with the task. The novice trainees should initially experience a fully controlled robotic motion and gradually the amount of haptic guidance can be reduced to allow for greater autonomy once the trainee familiarizes with the elementary stage of the task as described in the Fitts and Posner model for technical skill acquisition [134].

In the Fitts and Posner model, the first cognitive stage is associated with interpreting the nature of the task and trying out different strategies to perform the task which result in highly variable performance and high cognitive load such as attention. The second stage is the associative stage where the person has settled on a strategy and the focus is on refinement of the strategy, biomechanical efficiency and task performance. The third stage is the autonomous stage where the person has achieved muscle memory and automation of the skill, enabling minimal cognitive load for the task and allowing for the attention to be spent on other aspects such as higher order strategic planning.

With haptic guidance, the optimal strategy as defined by the master surgeon's reference trajectory is introduced early to the trainee which we hypothesize that it will directly help to shorten the first two stages where the trainee would be attempting various self-formulated strategies which may not be anywhere near optimal at all.

The initial fully controlled haptic guidance phase complements the notion of observational practice as described by Wulf et al [144] where they highlight that observation and practice can uniquely benefit the learning process. Shea et al [145] also postulates that an observer may develop a unique perspective on the task that is hard to achieve while physically engaged in practicing the task. Therefore, the fully controlled haptic guidance phase enables a way of "haptic observation" whereby the trainee can simultaneously experience the reference motion as an observer and a physical hands-on participant. Once the trainee has advanced past the elementary stage, the haptic guidance will be relaxed in order to motivate the trainee to have more self-guided learning [146] and vested interest in their motion.

In this study, haptic robotic guidance for training of laparoscopic HEC tasks was performed. The hypothesis is that fully controlled haptic guidance will improve training efficacy as compared to unaided practice on two basic laparoscopic HEC training tasks. Fundamentally, the experiment was performed to investigate whether the "haptic observation" of a reference trajectory will improve the early cognitive and associative stages of skill learning. In addition, the EEG readings of the subjects were recorded in order to compare for any difference in neural activation from being taught by a robot and correlate with the motor performance of the subject.

6.2 Materials and Methods

6.2.1 Experimental Setup

The equipment used in this study includes the robotic laparoscopy trainer, a PC that manages the system of actuators and encoders in the robot, a HD webcam (Microsoft LifeCam HD-5000) that represents the endoscopic view of the intracorporeal workspace and an EEG recording system that comprises of a 40 channel EEG electrode cap, PC to record the EEG data and an EEG amplifier (Neuroscan, NuAmps Express). The robotic laparoscopy trainer includes a pair of spherical joint laparoscopic manipulators which can be recorded and replayed through a network of encoder and actuator pairs at each degree of freedom: namely, the roll, pitch and yaw rotation axes, the translational motion associated with withdrawing and inserting the instrument through the trocar and the activation of the tip of the instrument such as a grasper or a pair of scissors.

6.2.2 Laparoscopic tasks

We tested the laparoscopic proficiency of the subjects with two basic laparoscopic tasks adapted from conventional commercial laparoscopic training systems. The first task is a circle pattern tracing game in which the subjects are instructed to follow the black and red lines demarcating a 9 cm diameter circular pattern for two revolutions with a total path length of 131 cm per trial (see Figure 6.1). Subjects were not allowed to rest the manipulator on the task plane as it would create additional frictional forces. The subjects were assessed by their time taken and the consistency of motion by their cumulative path deviation of the tip of the instrument to the circle. The circular tracing pattern is the adaptation of the circular pattern cutting task available in the Fundamentals of Laparoscopic Surgery (FLS) and ProMIS laparoscopic training systems. Although the task seems simplistic, it requires constant manipulation of most DOFs in order to generate the circular pattern which enables a more thorough gauge of laparoscopic proficiency.

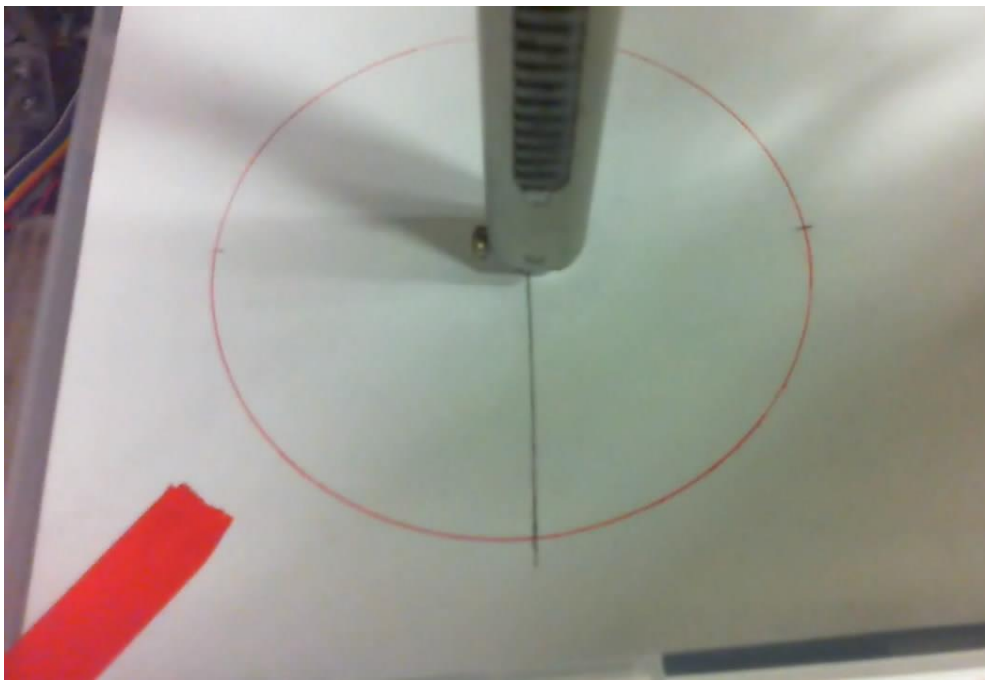

Figure 6.1: Endoscopic view of the circular tracing task.

The second task is a pointing game that is adapted from peg transfer / pick & place tasks. The task is to use the tip of the manipulator to touch the purple markers, in a clockwise manner starting from the top right corner, which are spread out amongst a network of interweaving wires that act as 3D obstacles simulating major vasculature that has to be avoided to prevent haemorrhages (see Figure 6.2). Due to the labyrinth of wires, the subjects have to continually withdraw and insert the manipulator at correct orientations in order to reach the purple markers. Subjects will be assessed by their time taken and the accuracy of the manipulator's trajectory.

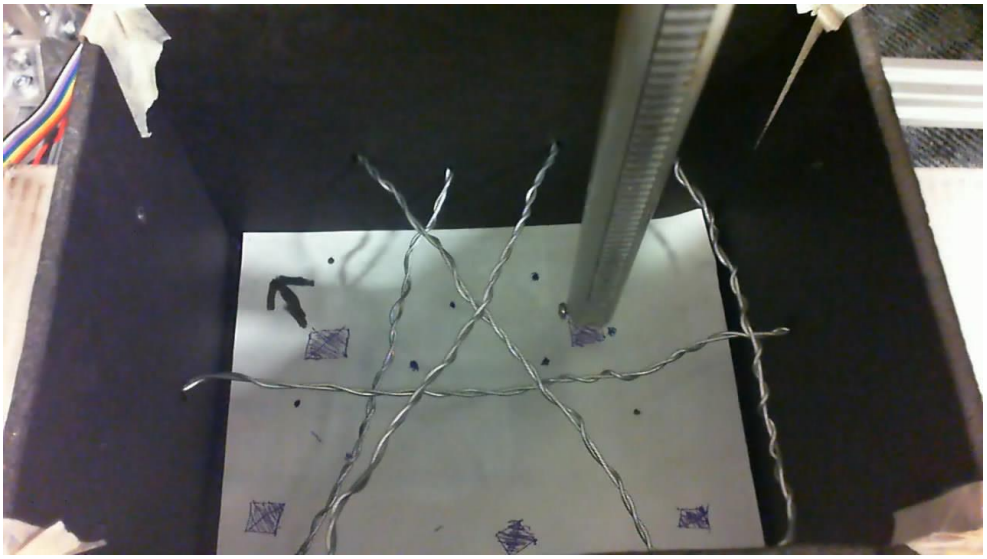

Figure 6.2: Endoscopic view of the pointing task.

6.2.3 Experimental Protocol

In this study, twelve volunteers (10 male, 2 female. Age ranged from 21 to 32 years with a mean of 27 years) from non-medical backgrounds with no prior training with laparoscopy volunteered for this experiment. Participants provided informed consent.

The twelve volunteers were divided into two groups of six. One group was assigned as the control whereby they practiced on the robotic platform with the same two tasks but with no actuators enabled thus no haptic guidance was given to them. The other group was trained on the same robotic platform but with the actuators enabled.

In this study, the mode of haptic guidance was set to fully control the manipulator to move according to a pre-recorded reference trajectory. For the group that was trained with haptic guidance, the reference trajectory used in this study were recorded by iterative manual manipulation of the end effector tip of the robotic instrument to ensure the most direct control over the manipulator trajectory, akin to performing the

tasks like an open surgery procedure whereas the subjects have to perform the tasks laparoscopically.

All subjects performed the experiment with only their dominant hand. For each task, the subjects record a starting baseline performance of the task with no robotic feedback. After which, each group continued with their allocated mode of practice for 5 rounds and a final assessment of their task performance was taken. The order of tasks carried out was alternated with each consecutive subject in order to reduce the effect of familiarity on the results collected.

6.3 Results

Subject task performance of the control group and haptic guided group have been tabulated in Table 6.1 and Table 6.2 respectively. All statistical comparisons were analyzed using an analysis of variance (ANOVA) with statistical significance set at 0.05.

Table 6.1: Subject performance in the circle tracing task

	Haptic guided group		Control group	
	Initial timing	Final timing	Initial timing	Final timing
Mean timings (s)	66.5	61.2	66.1	52
Average percentile improvement (p value)	8.00%	(p=0.65)	21.40%	(p=0.40)
Average percentile reduction in cumulative path deviation (p value)	8.50%	(p=0.11)	29.70%	(p=0.89)

*Corresponding P values are indicated in parenthesis

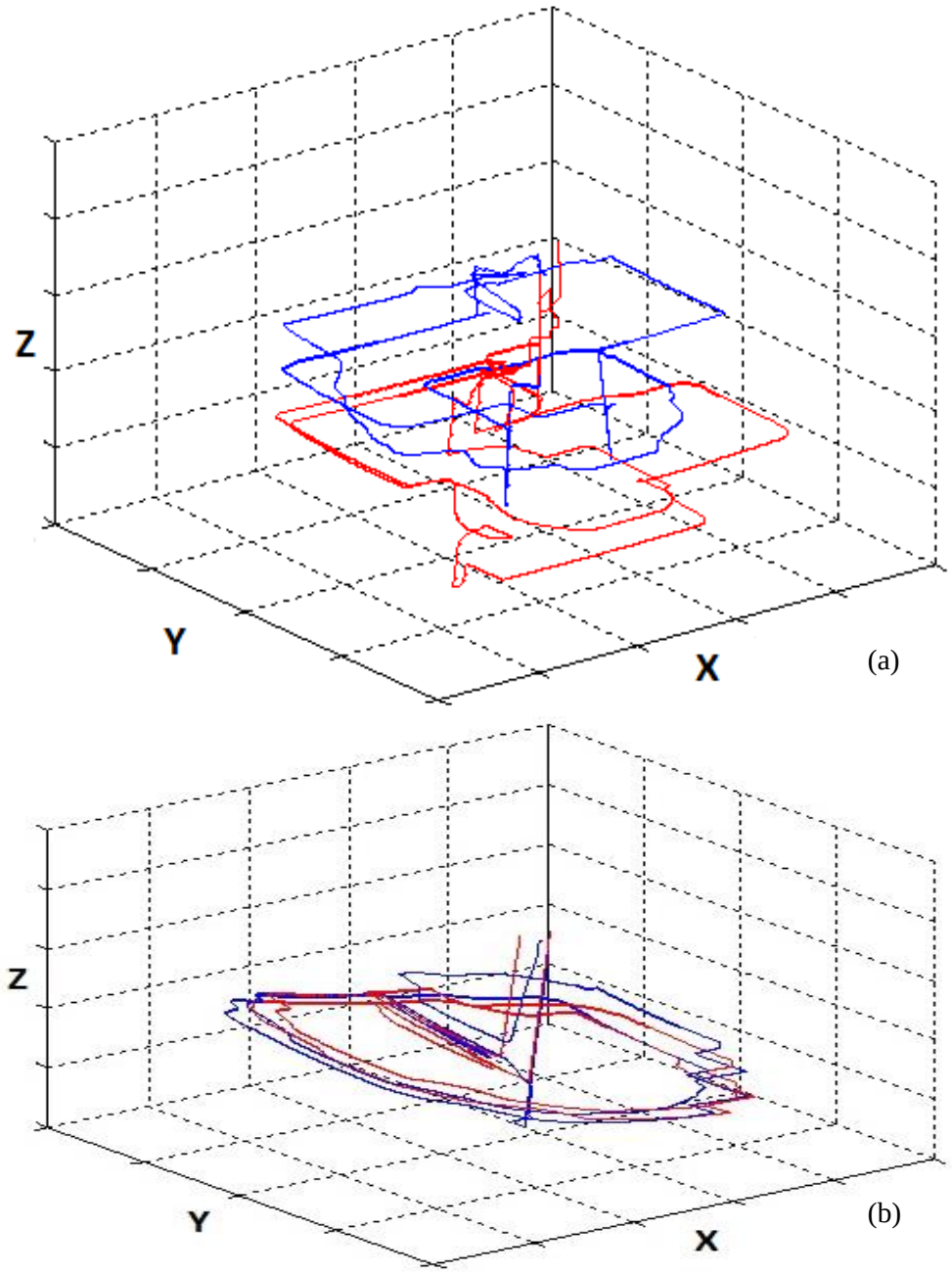

Figure 6.3: Example of the circle tracing trajectory by (a) Subject 8 and (b) Subject 11.

Each grid marking represent 3 cm distance on the actual workspace. The blue line indicates the initial baseline assessment and the red line indicates the final assessment.

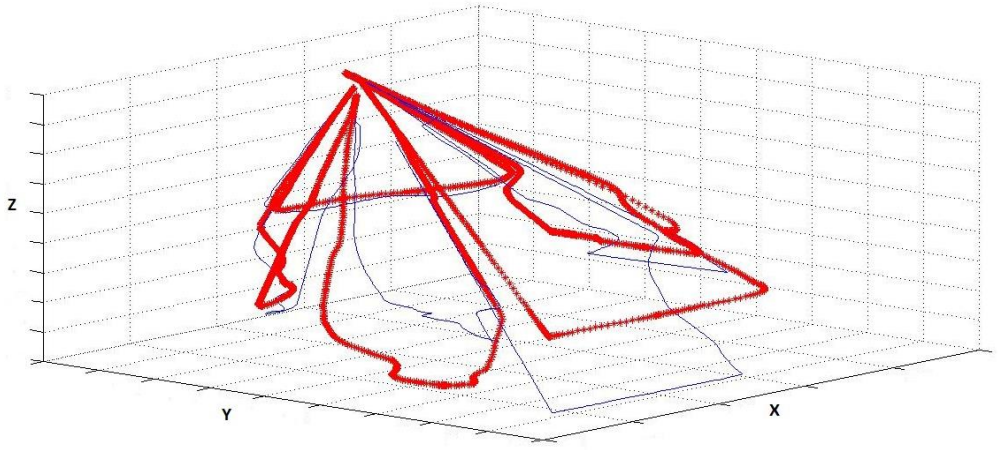

Figure 6.4: Example of the conical workspace of the pointing task trajectory recorded by Subject 1.

The blue line indicates the initial baseline assessment and the red line indicates the final assessment.

Table 6.2: Percentile improvement in performance of the control group

Subject	**yaw**	**pitch**	**translation**
1	-7.17	1.92	-0.08
2	15.37	-9.86	17.17
3	-14.59	6.10	-12.27
4	-8.70	-11.60	-5.24
5	-15.12	6.65	-3.84
6	4.98	-13.33	1.89
Mean	-4.20 (0.80)	-3.35 (0.75)	-0.39 (0.96)

*Corresponding P values are indicated in parenthesis

Table 6.3: Percentile improvement in performance of the haptic guidance group

Subject	**yaw**	**pitch**	**translation**
7	27.00	-1.75	-1.49
8	-17.02	35.88	1.14
9	28.65	17.03	13.24
10	10.59	0.37	10.30
11	20.15	13.11	-24.16
12	19.68	10.61	12.32
Mean	14.84 (0.04)	12.54 (0.22)	1.89 (0.79)

*Corresponding P values are indicated in parenthesis

6.4 Discussion

6.4.1 Circular Tracing task Discussion

The trajectory data of two subjects in the group with haptic guidance (Subject 8 and Subject 10) had to be discarded from analysis as outliers due to ambiguity in interpreting their trajectories as they performed the tracing far elevated above the real task plane (see Figure 6.3 (a)). This skewed their performance as the size and orientation of their traces were no longer similar to the task objectives or the data of the other subjects who managed to remain close to the task plane as instructed.

On average, the control group reduced their time taken for this task by 21.4% ($p=0.40$) from 66.1s initially to 52.0s at the final assessment but their cumulative path deviation increased by 3.94% ($p=0.89$) to 6.7 cm. Whereas, in the group with haptic guidance, their average time taken reduced by 8.0% ($p=0.65$) from 66.5s to 61.2s and their cumulative path deviation also reduced by 8.5% ($p=0.11$) to 3.2 cm. The reference trajectory for the circle task was approximately 50s long.

The results from the cumulative error of motion showed that the control group did not manage to improve their trajectory error whereas the haptic guidance group achieved an almost significant ($p=0.11$) 8.5% reduction in trajectory error. Our assumption is that the reduction in timing relates to the confidence of the subject in performing the task.

The control group reduced their timings by a larger percentage than the haptic guided group, suggesting that autonomous hands-on learning helps the subject get more comfortable with manipulating the instrument faster but the confidence and speed did not correlate with better motor performance. This corresponds to the cognitive stage of the Fitts and Posner model where confidence influences the propensity to try more radical strategies which leads to volatility in performance but also an opportunity to acquire a significantly better strategy. Whereas, the haptic

guidance group showed more restraint than the control group but were able to learn off the reference trajectory to improve both timing and trajectory error.

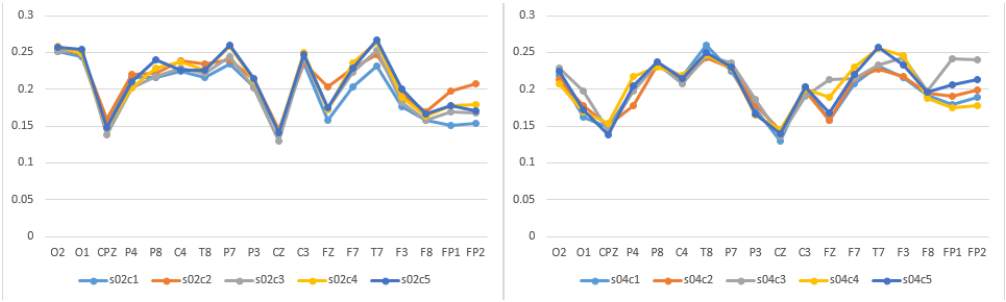

Figure 6.5: Circle task – Control Group (best vs. worst performer).

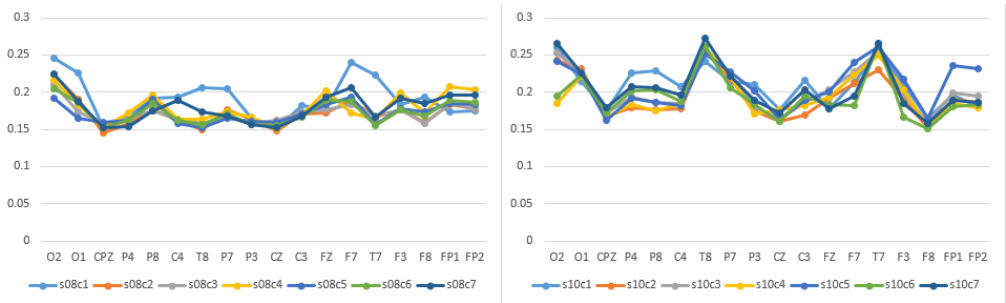

Figure 6.6: Circle task – Haptic Guided Group (best vs. worst performer).

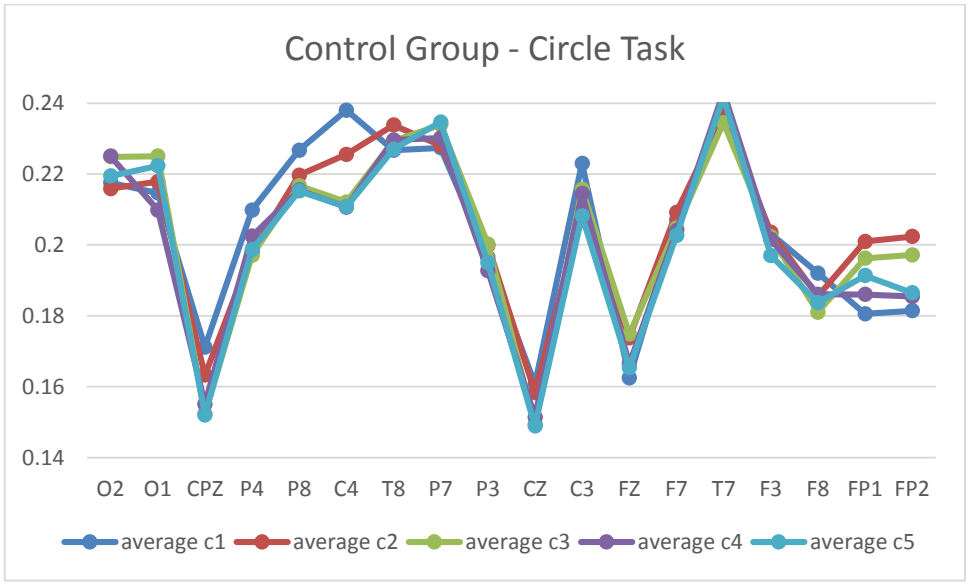

Figure 6.7: Trial Averaged LZC values for Control Group - Circle task.

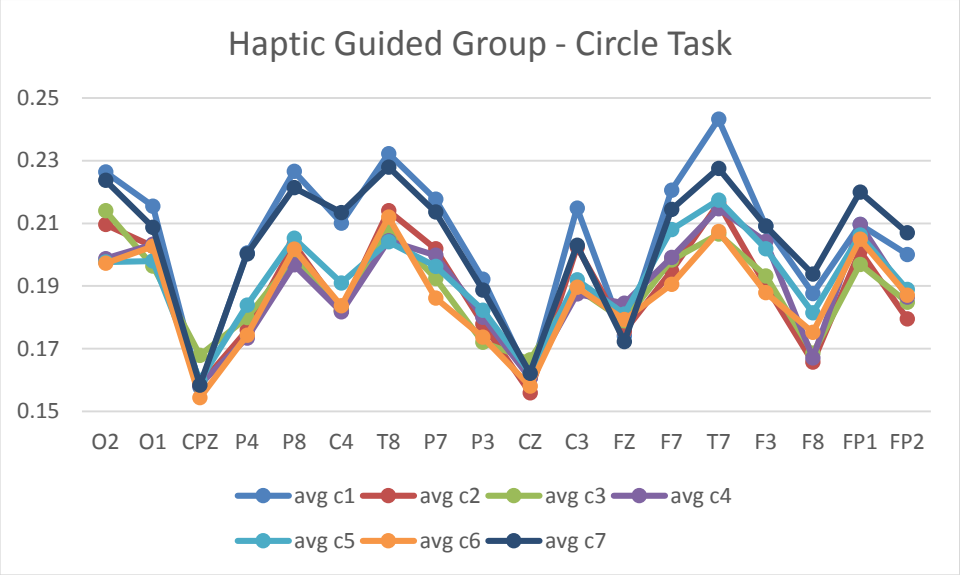

Figure 6.8: Trial Averaged LZC values for Haptic Guided Group - Circle task

In Figure 6.5 and Figure 6.6, the Lempel-Ziv complexity scores of the best and worst performing individuals from the passive training group and active training group are plotted. The difference in LZC scores between individuals was not as pronounced as the LZC results tabulated in Chapter 5. This is accommodated by the fact that the experimental protocol is slightly different between the folding task in Chapter 5 and the experiment in Chapter 6. The subjects practiced the task to mastery in Chapter 5 whereas in Chapter 6, the number of trials is standardized so not all subjects might have mastered the tasks by the last trial. Although, the trend for the highest change in LZC values occurring in the occipital, parietal and central lobes remains consistent.

When the trial averaged LZC values are plot (see Figure 6.7 and Figure 6.8) between the control group and haptic guided group, it is clear in the control group that the LZC values did not vary much across the trials. One possible explanation was that this circle tracing task with the laparoscopic tool was too difficult to master within the limited number of trials set so the subjects were still in the early stages of skill acquisition. In the haptic guided group, there is greater variance in LZC values

especially in the parietal, occipital and temporal regions. This complements the findings in Chapter 4, corresponding to evidence of skill learning having taken place in this group.

6.4.2 Pointing task

Due to the orthogonal arrangement of the encoders, trajectory data from the robotic trainer can be independently analysed in each degree of freedom such as the orientation (pitch and yaw) and translation axes of motion (see Figure 6.4 for path illustration). The percentile improvements in cumulative joint angle motion of orientational and translational axes of motion are listed in Table 6.1 -Table 6.2. A smaller cumulative joint angle motion represents a narrower and more efficient trajectory and a shorter translational motion represents better control of the reach of the instrument indicating the depth perception ability of the subject. The roll axis of motion, which is represented by the twisting orientation of the tool tip, is ignored from the analysis as there is no need for tool tip orientation for these two tasks and the motion in this axis throughout the study was also small and insignificant.

The control group improved their timing by 27.9% (p=0.30) with the mean time taken reduced from 97.3s to 52.5s. The haptic guidance group similarly improved their timing by 25% (p=0.08) with their mean timings reduced from 78.1s to 56.7s. The reference trajectory used was approximately 40s long.

The mean percentile reduction in timing was almost equal in both groups but the haptic guidance group showed prominent improvement in their orientational yaw (14.84%, P=0.04) and pitch (12.54%, P=0.22) joint displacements whereas the control group had a largely unchanged trajectory performance denoted by the small insignificant percentile change in yaw, pitch and translations joint displacements. As the pointing task is fundamentally a test of accuracy of orientation and reach and manipulator path strategy, the contrasting difference in improvement of orientational

joint displacements between the two groups signifies that there is some evidence to the hypothesis of haptic guidance being used to teach a reference trajectory as an optimal strategy in order to shorten the cognitive and associative stages of skill learning.

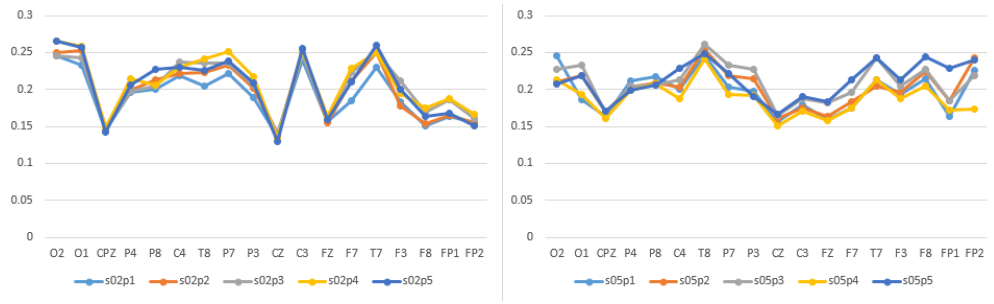

Figure 6.9: Pointing task – Control Group (best vs. worst performer).

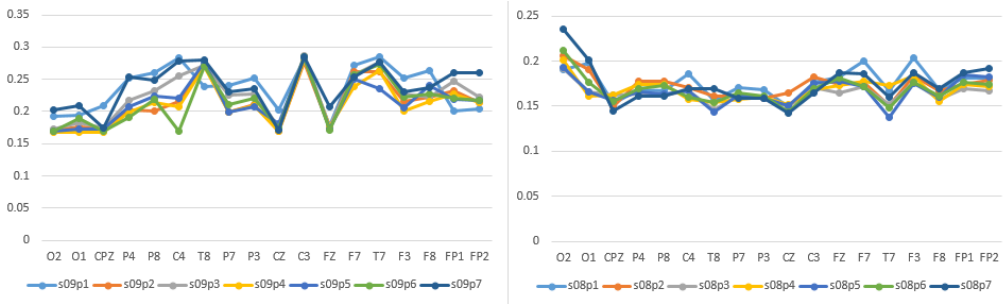

Figure 6.10: Pointing task – Haptic Guided Group (best vs. worst performer)

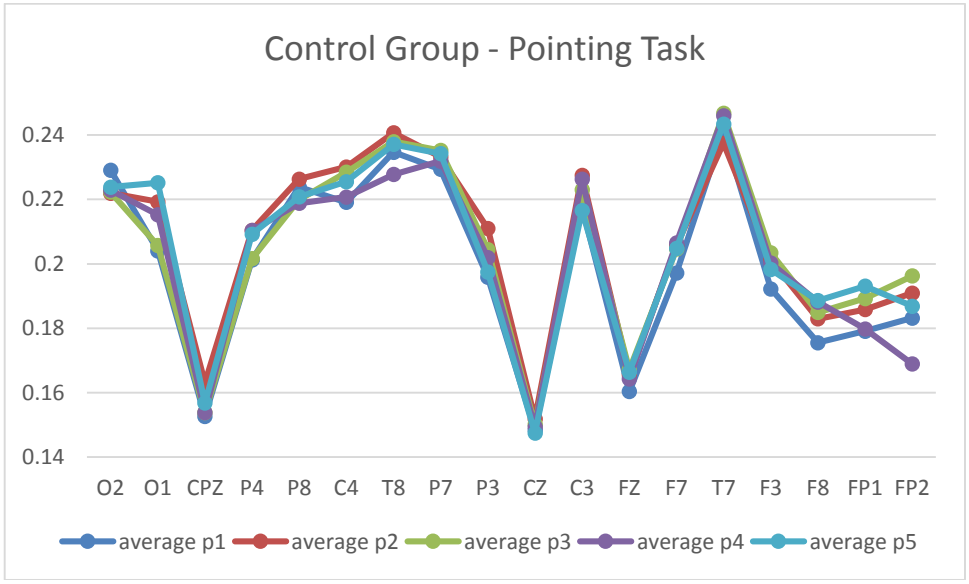

Figure 6.11: Trial Averaged LZC values for Passive Training Group - Pointing task

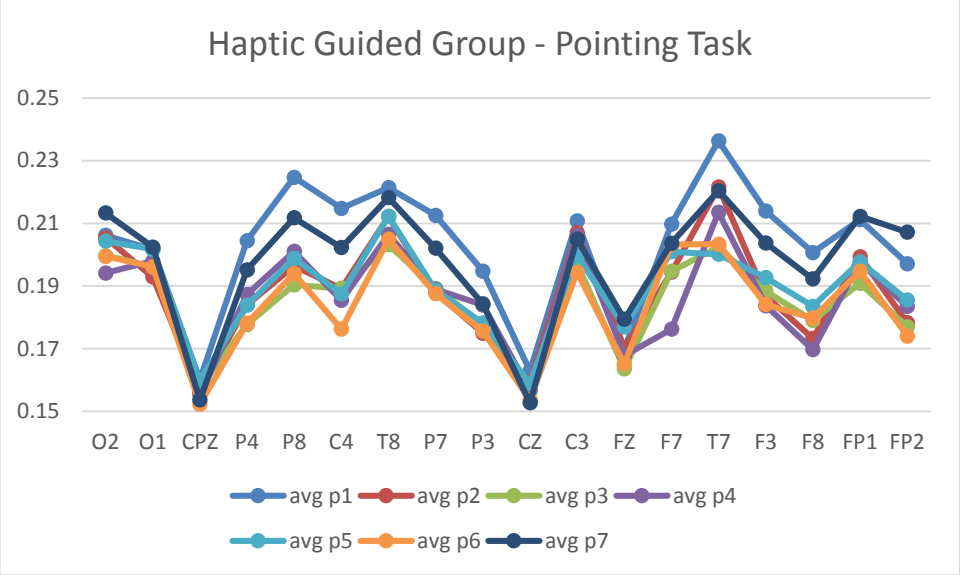

Figure 6.12: Trial Averaged LZC values for Haptic Guided Group - Pointing task

The LZC scores of the best and worst performing individuals for the pointing task are plotted in Figures 6.9 and 6.10. The results are similar to the circular tracing task whereby there are no discernible trends in the LZC scores and the variance in LZC scores across trials are not as pronounced as in the subjects in Chapter 4. When the LZC scores are averaged across subjects within the two groups (see Figure 6.11 - Figure 6.12), it can be seen that the LZC values did not vary much across trials in the Control Group whereas the LZC values in the Haptic Guided Group visibly varied in the parietal, temporal and frontal regions. This trend is similar to that in the circular tracing task (see Figure 6.7 and Figure 6.8).

There is significantly decreased complexity in temporal, parietal and central regions in the Haptic Guided Group vs. the Control Group, corresponding to primary motor cortex (motion) and somatosensory cortex (sensory integration) (see Figure 6.13). By tabulating the variance of Lempel-Ziv complexity values between the passive training group and the active training group (see Figure 6.14), it is evident that the Haptic Guided Group experience higher variance in complexity values at the frontal-temporal-parietal regions as compared to the passive group which did not experience much change in complexity.

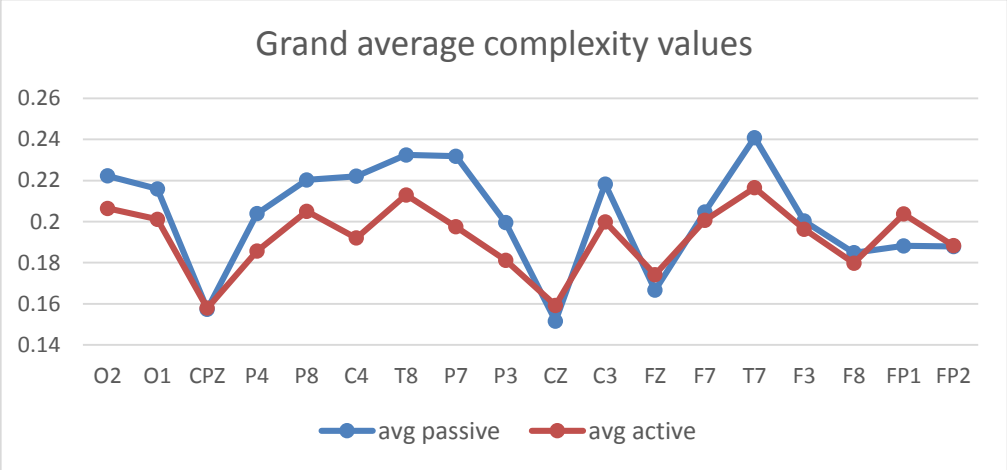

Figure 6.13: Grand Averaged Lempel-Ziv complexity values between the Control Group and Haptic Guided Group.

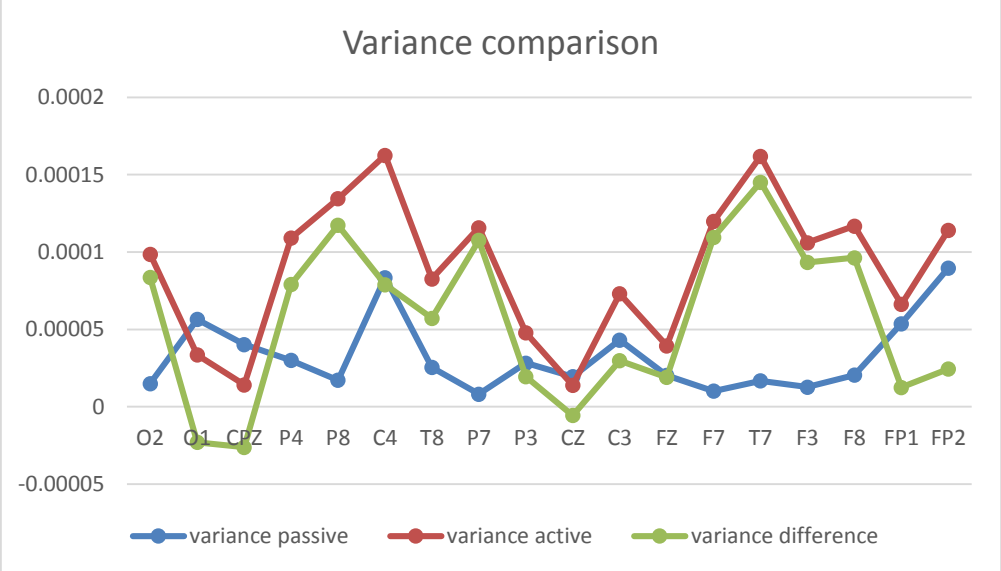

Figure 6.14: Variance in Lempel-Ziv Complexity values

6.5 Summary

Haptic guidance has been used primarily as means of rehabilitation [147] and even as assistive virtual fixtures during robotic surgery [148]. However, its application for laparoscopic training, to our knowledge, is novel. As shown by the favourable results for both tasks in the haptic guidance group over the control group, the initial assessment of the concept of robotic assistance in laparoscopic motor skill learning is promising.

In this preliminary study, we have arbitrarily enrolled 12 volunteers within a three week recruitment window. Therefore, the sample size might be too small to conclude statistically significant results. Data from this preliminary study will be used for power analysis calculation of the minimum sample size of future studies. Another factor that affects this study is the motivation towards the training. Motivational factors have been found to affect training efficacy [144], [149]. In this study, we have enrolled non-medical students hence they might not have the same attitude and interest in laparoscopic training as surgical trainees.

The two tasks used were adapted from conventional laparoscopic partial task trainers which have been used as platforms for practicing technical skill for open surgery before the era of laparoscopy. The common presumption is that actual surgical procedures can be broken down into partial tasks and that mastery of the partial tasks has transferability to the clinical setting [150]. However, it is still unclear whether haptic guidance of laparoscopic training can be applicable to full complex surgical procedures and eventually unto clinical proficiency. As future work, we intend to explore this notion further with simulations of realistic surgical scenarios along with the reference trajectories recorded from experienced senior surgeons.

In addition, EEG based neural sensing has been used to classify and monitor the cognitive load of the trainee which can be used as a method of indirectly determining

the stage of skill learning where, according to the Fitts and Posner model, cognitive load and attention level decreases as the trainee advances in skill acquisition [135].

In the control group, it has been shown that the LZC values did not vary much as compared to the Haptic Guided Group. This suggests that the difference in motor performance mirrors the LZC trends, highlighting the difference in skill acquisition between the two groups. One limitation of this study was the limited number of trials. The number was fixed according to the average number of trials needed for the mastery of the box folding task. However, as shown by the LZC trends in the Control Group, the limited number of trials seemed to not be enough to induce significant change in neural complexity in the passively trained group whereas the Haptic Guidance Group showed significant changes in neural complexity and significant improvement in motor performance within the same number of trials.

As future work, the degree of haptic guidance can be dynamically adjusted according to the cognitive state of the trainee. Adaptive haptic guidance enables the robot to gently rein in control of the motion during a particularly difficult phase of the procedure, enabling the trainee to pay less attention to his own motion and concentrate on understanding the haptic guidance's reference motion as a "haptic observer". Such adaptive haptic guidance would be useful for complex surgical procedures with varied intermittent difficulties.

7 Experiment - Sequential Pointing task

In this chapter, a platform was developed that encompasses a sequential planar pointing task that was implemented on a touchscreen. The objective was to develop an integrated platform between the simulation game and EEG recording system to enable epoched inter-task neural analysis at a much shorter time scale.

7.1 Background

Sequential pointing is a classic task for HEC research [151]. Studies have been performed to look at how the continual goal driven rapid eye saccade/fixation have a neural coupling with rapid hand movements [152]. The performance can be affected by factors such as length of target distance and performance feedback [153]. Bock et al showed that arm motion is controlled in the motor cortex and parietal cortex by independent direction and movement amplitude than position for sequential planar motions [154] which mirrors Harris and Wolpert's postulation of signal dependent neural noise being proportional to signal amplitude [39]. The effects of gaze restriction on the accuracy of HEC has also been investigated [155] to reveal that the feedforward model based on foveal motion efference enabling an eye-hand lead time of about 200ms is critical in the accuracy of hand-eye coordinated motion.

In this study, the overall objective was to incorporate the classic sequential pointing task used for HEC studies with the principles of epoched event-related potential (ERP) analysis of EEG [156] such that a platform for measuring intra-trial performance can be developed. In particular, the hypothesis is that the spatial-temporal changes between epoched windows of neural activity can potentially be used to differentiate successful pointing events against failed events. In addition, the latencies of epoched EEG can also potentially be used to reflect changes in saccade and reach reaction times that has been postulated to correlate with movement speed

and accuracy [157]. In addition, task mastery of the sequential pointing game should derive similar trends in LZC values as discovered in Chapters 5 and 6.

In an additional exploratory aim, the effect of colour on the simulation game was investigated. The colour of the background, target crosshair and balloons were modified to red, green or blue (see Figure 7.7). Previously, in the visual cue experiment performed in Chapter 4, Colour was shown to be an important indirect visual cue for HEC. The colour red, in particular, has been shown to affect physical performance [158]. The exploratory hypothesis was that by changing the colour scheme of the simulation game, subject performance could be influenced.

Another exploratory aspect of the simulation game in Chapter 7 is the implementation of a dyadic avatar using Matlab Simulink. The objective of this implementation was to automatically generate a dyadic avatar that simulated and mirrored a user in an allocentric frame of view, providing the user with a companion for dyadic training. This form of training has been proven to improve training effectiveness [159], [160] by increasing the simulation's interactiveness and providing a motivational companion for the subject.

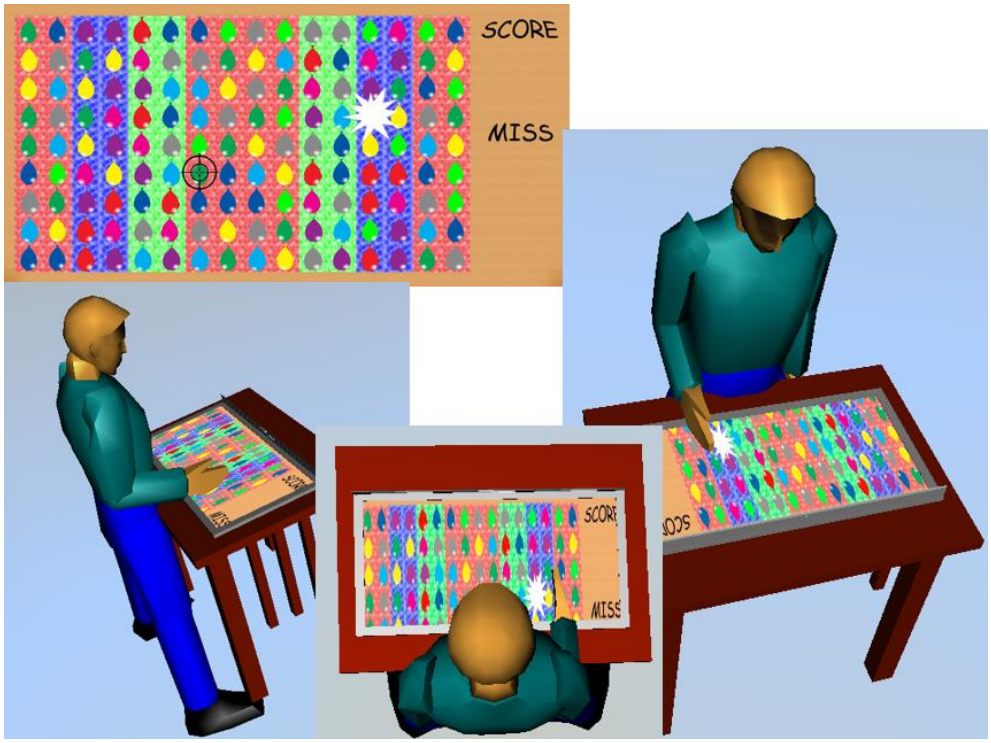

Figure 7.1 Simulated dyadic avatar designed to mirror and accompany the subjects performing the sequential pointing task.

7.2 Materials and Methods

7.2.1 Experimental setup

The experimental setup (see Figure 7.2 and Figure 7.3) consists of several CMOS webcams (Microsoft LifeCam HD-5000) arranged to the side and top of the subject to record the subject's arm motion. Several joint markers were placed on the subject's shoulder, elbow and wrist as visual tracking markers. A 40 channel NuAmps EEG amplifier (Neuroscan, Scan NuAmps Express) and EEG electrode cap was used to record the neural activity of the subjects. A touchscreen monitor (Acer, T230H) was used as a planar target workspace for the subject to directly interact with the sequential pointing simulation game created.

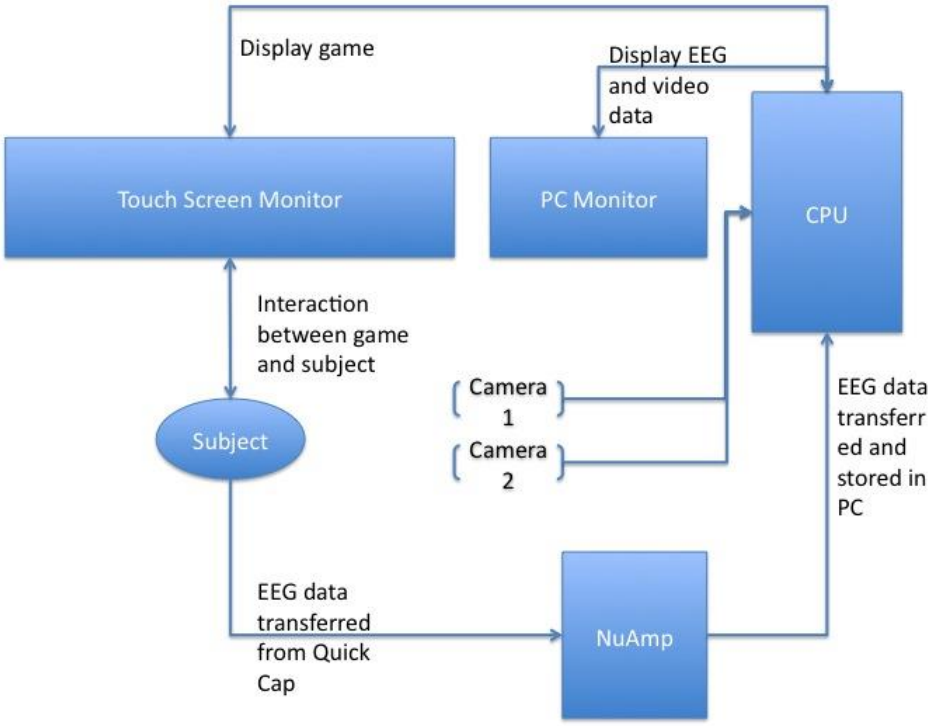

Figure 7.2: Schematic layout of the experimental setup.

A PC was used to run both the simulation game as well as the EEG recording with automated event timestamp markers for latency reduction which is essential for epoched analysis of EEG events.

7.2.2 Experimental task

In Chapters 5 and 6, the experimental tasks chosen were too long and unsegmentable which made them unsuitable for epochal analysis methods like ERP and PLV. In this study, the sequential pointing task was designed specifically for sequential epoch generation. In order to execute the sequential pointing task with the touchscreen monitor interface, a simple "whack-a-mole" simulation game (see Figure 7.4) was written in Visual Basic. In order to appeal to the subjects, the simulation game disguised the sequential pointing task to resemble the balloon popping game commonly seen in carnivals (see Figure 7.5).

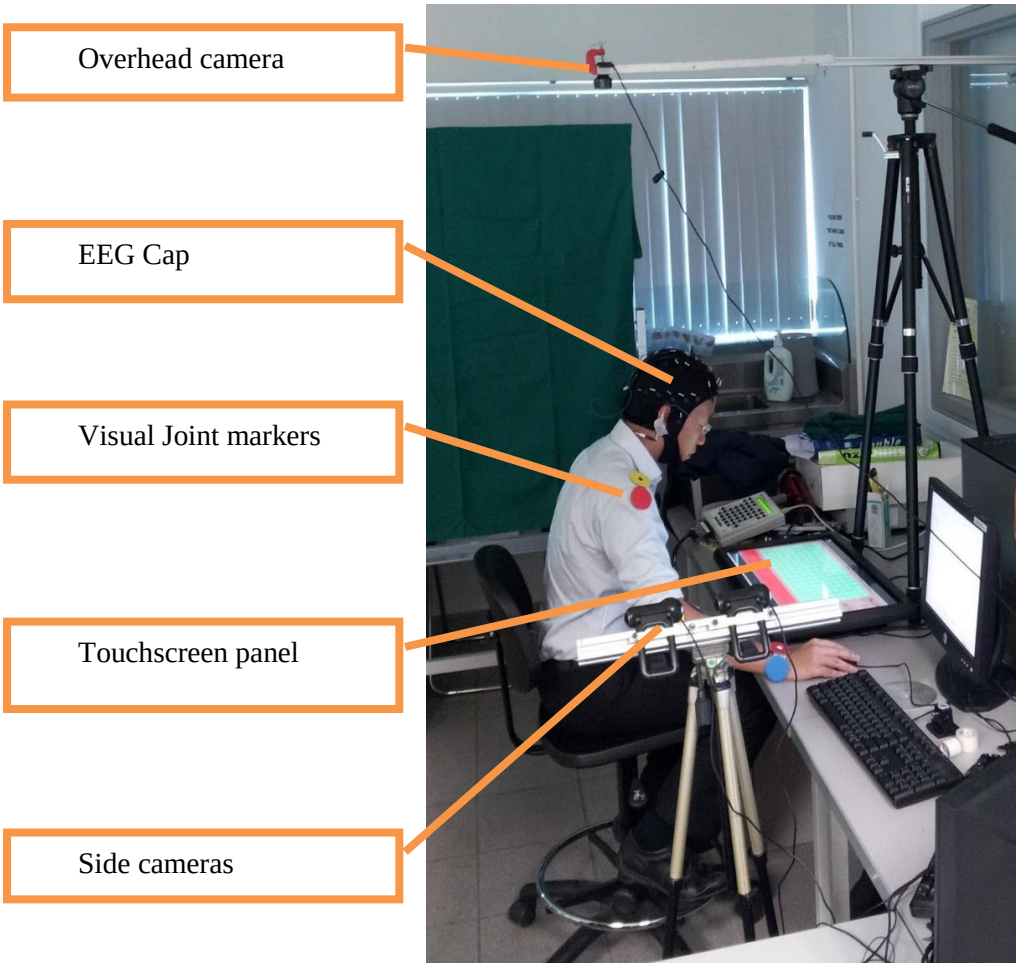

Figure 7.3: Layout of the experimental setup.

The subject is tasked to manipulate visual targets on the touchscreen while cameras record his motion. An EEG cap is also worn to record the neural activity of the subject.

The logical workflow for the simulation game is presented in Figure 7.6. When initiated, the game presents the subject with a crosshair on a randomly chosen balloon and a 1 second window for the subject to successfully tap the balloon with crosshair is initiated. As the simulation game was implemented on a touchscreen, the subject only needs to directly tap the target on the screen to register their input. The planar (x, y) pixel locations of the subject's taps are automatically recorded together with the classification of whether the tap was a successful or failed attempt on the EEG signal data (see Figure 7.8). If the subject taps on the wrong balloon or no attempt was made before the time window lapses, the event was logged as either failed or no attempt

respectively. At the start of the next time window, a new target crosshair then appears on the next randomly chosen balloon until 25 targets have been presented to the subject.

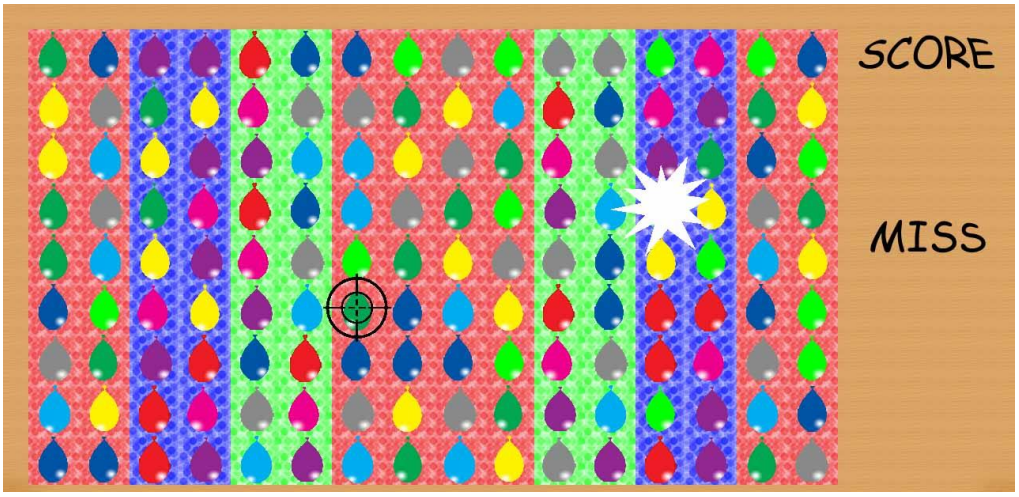

Figure 7.4: Screenshot of the simulation game.

The target crosshair (shown in black) is displayed over a balloon icon as a visual cue to the subject. If the correct balloon is successfully pressed within the allowed time window of 1 second, the balloon popping icon will be shown and the score will be reflected.

Figure 7.5: The balloon popping carnival dart game.[5]

[5]Photo credit: D.H. Parks. https://www.flickr.com/photos/parksdh/6141149497/

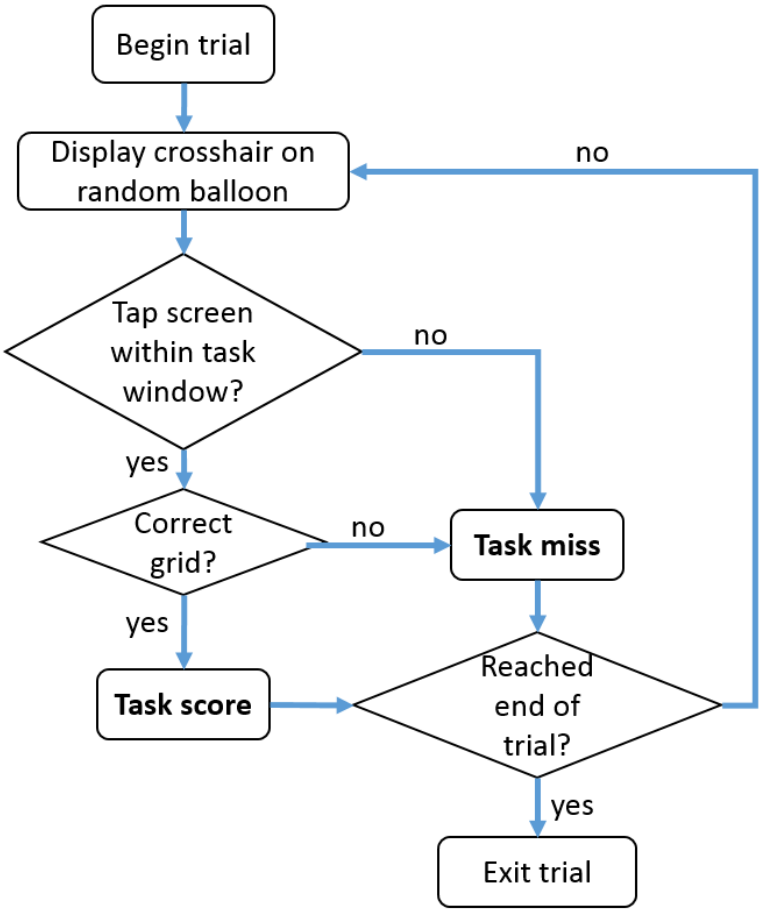

Figure 7.6: Schematic for the logical workflow of the simulation game.

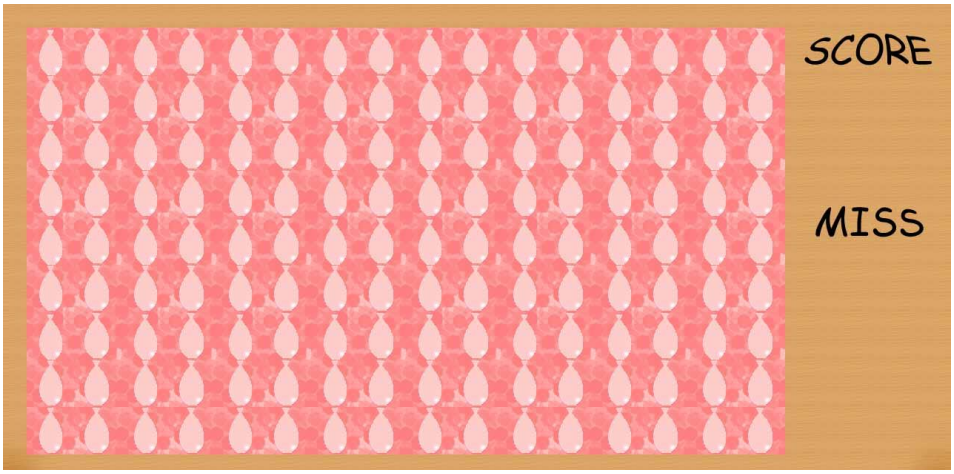

Figure 7.7: The sequential pointing simulation game with a modified red colour scheme.

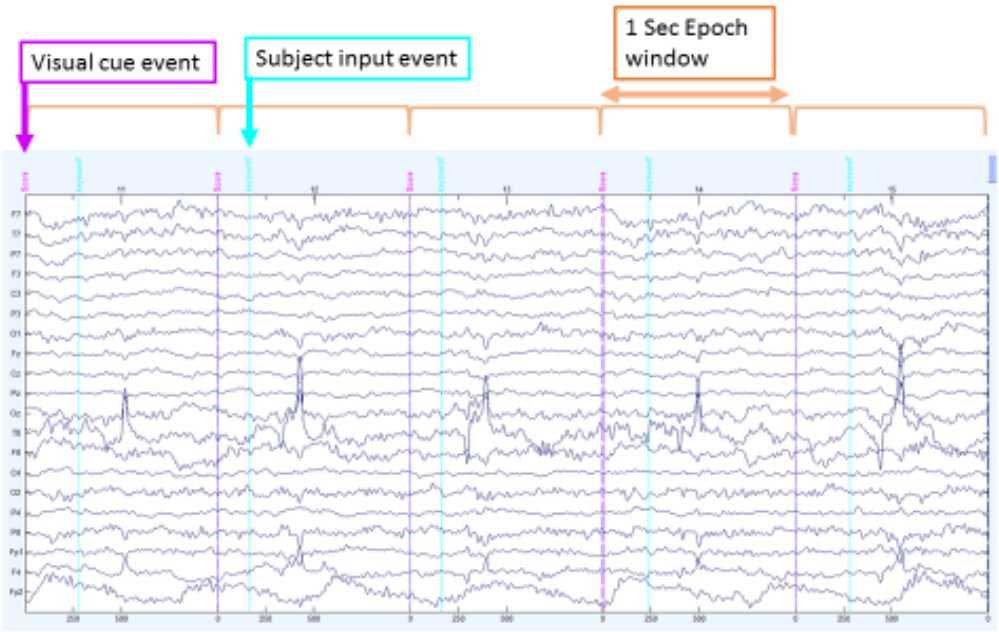

Figure 7.8: Automated task event labelling and classification on the EEG data stream.

7.2.3 Experimental Protocol

In total, 18 healthy volunteer subjects between the ages of 20 to 28 were recruited for this study (11 male and 7 female). All but two of the subjects had right master hands so all subjects were standardized to use only their right hands for this study. To aid post-experiment video review of the experimental procedure, visual tracking markers were placed on the subjects' right shoulder, elbow and wrist.

Ten trials were conducted per subject. Each sequential pointing trial consists of 25 targets, totalling 250 targets per subject. The 10 trials were sequentially conducted within a single session but the subjects were allowed to rest whenever desired.

Before and after the 10 sequential pointing trials, single observational trials were performed where the subjects would observe the trial but not move to tap on the crosshair, the subject was instructed to click on a mouse to acknowledge the identification of the crosshair. The rationale for the observational trials was to record EEG epochs with less motor noise before and after the 10 trials and use these epochs

as noise cancellation. However, the EEG epochs from the observational trials were eventually not used as it was found that the subjects performed the clicks much faster (<~200ms) than the typical finger tapping action in the 10 trials so this means of noise cancellation could not be implemented.

An additional set of exploratory trials was performed on the same sequential pointing task but with modified colour schemes of red, green and blue. Subjects were tasked to perform a practice observational trial and an actual trial for each colour scheme twice so a total of 12 trials of modified colour schemes were conducted per subject.

Similar to the EEG pre-processing steps done for studies in Chapters 4, 5 and 6, raw EEG data recorded from the Nuamps EEG system was imported into Matlab and the extraneous recordings at the before and after the actual trials were trimmed. Next, the data was band-pass filtered with a linear finite impulse response (FIR) filter between 1Hz to 50Hz. Subsequently, the data was passed through an ICA decomposition (see Section 2.5 for details) and noise-related components were manually removed from the EEG signal. Afterwards, the filtered data was manually scanned and sections of the data were removed if there were regions containing significant noise artifacts.

7.3 Results

The spectral maps and ICA component maps of all the subjects have been plot (see Appendix A for sample of spectral maps and ICA component maps). A typical example of the spectral map and ICA component map of a subject is shown in Figure 7.9– Figure 7.11.

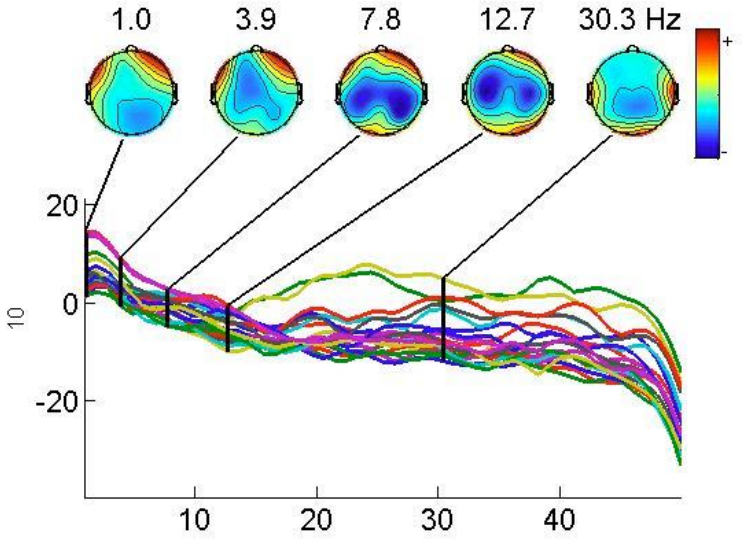

Figure 7.9: Spectral map for Subject 7 during the first sequential pointing trial.

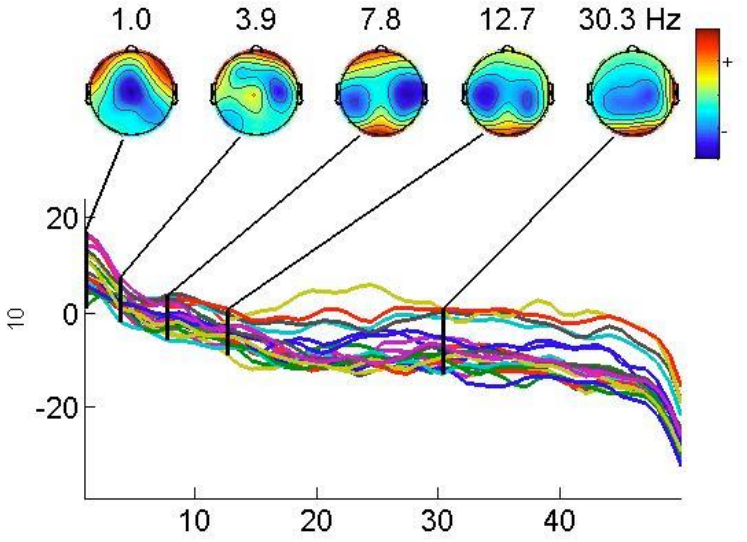

Figure 7.10: Spectral map for Subject 7 during the last sequential pointing trial.

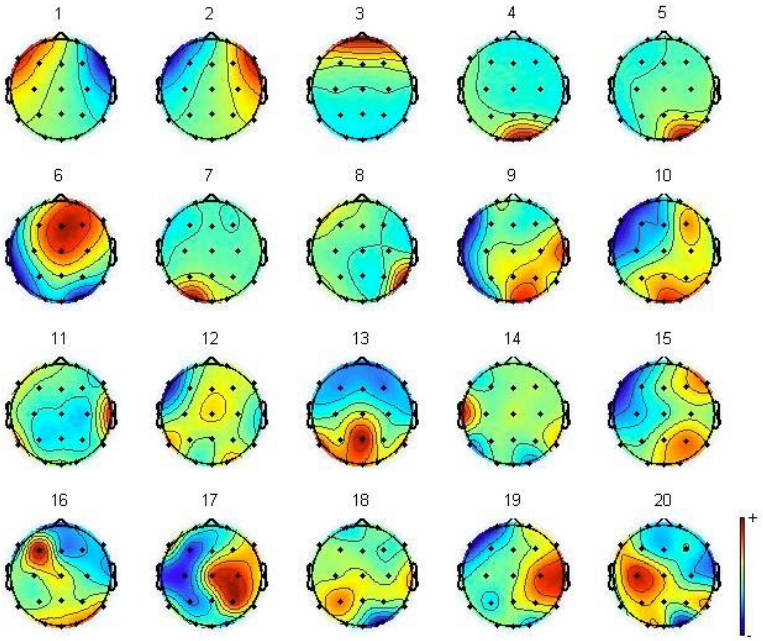

Figure 7.11: ICA component map for Subject 8 during the first sequential pointing task.

By inspecting the spectral maps of the subjects, it is observed that there is a trend of alpha band (8-13Hz) oscillatory activity (see Figure 7.9 and Figure 7.10) being attenuated at the frontal region. Attenuation of frontal alpha power has been shown to relate to decreased cognitive workload [161] and increased task mastery, mirroring the Spectral Analysis findings in Chapter 5.4.2 for the box folding task. Slow wave Delta (1-3Hz) and theta (4-7Hz) activity are frontally predominant and remain frontally predominant over the 10 trials. Whereas the beta (14-25) and gamma (25-45Hz) band activity are predominantly occipital and persist over the occipital regions throughout the trials.

ICA component maps (see Figure 7.11) are sorted in decreasing order of significance. As the sequential pointing task is predominantly a visuomotor task, typical ICA component maps generated show the largest contributions from eye motion (component 1 and 2 in Figure 7.11), and visual cognition (component 3, 4 and 5 in Figure 7.11).

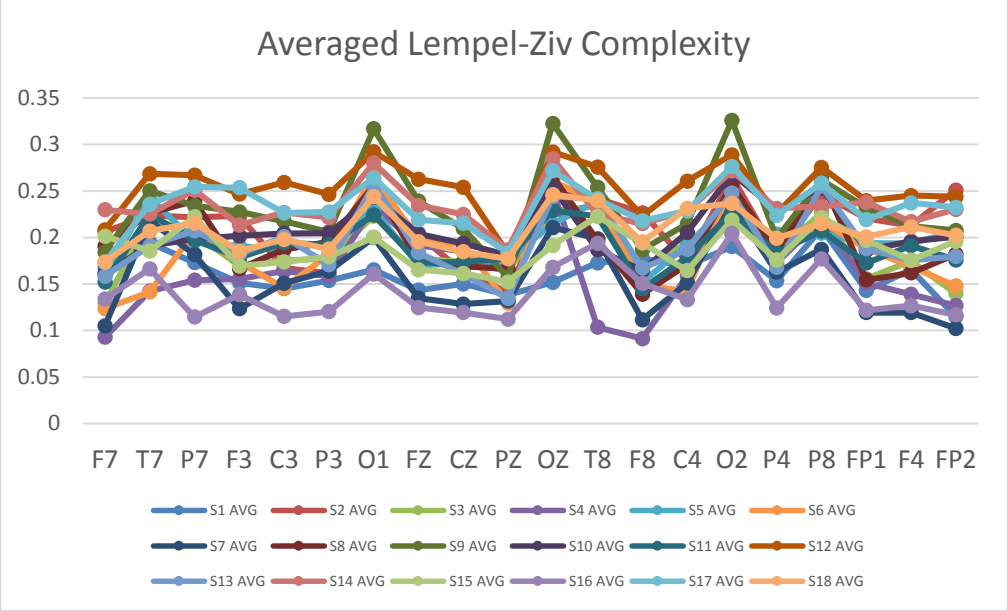

Figure 7.12: Averaged Lempel-Ziv Complexity values amongst subjects across all sequential pointing trials.

The averaged Lempel-Ziv Complexity values of all subjects across all sequential pointing trials is shown in Figure 7.12. The range of LZC values in this experiment are similar to those calculated for the previous experiments in Chapters 4, 5 and 6. It is observed that there are consistent spikes in complexity at the three occipital nodes (O1, O2 and OZ) in all subjects. This trend is to be expected since the sequential pointing task is a rapid-fire sequence of visual cues, the occipital region, which is responsible for visual processing, continually remains very active throughout the whole trial.

As a sample, the individual LZC plots of the first and last trials for two subjects are tabulated in the Appendix A. An example of the LZC plot is shown in Figure 7.13. It is observed that the largest changes in complexity occur in the frontal, parietal and occipital regions for most subjects. However, not all subjects exhibit the same trend (see Figure 7.14).

In most subjects, the difference in complexity values is not plainly different. LZC values averaged across all subjects (see Figure 7.15) show that there is very little

difference (<10%) between the first and last trial at most electrode channels. In order to further extrapolate the difference in LZC values between the first and last trial, the variance of the averaged values was calculated (see Figure 7.16).

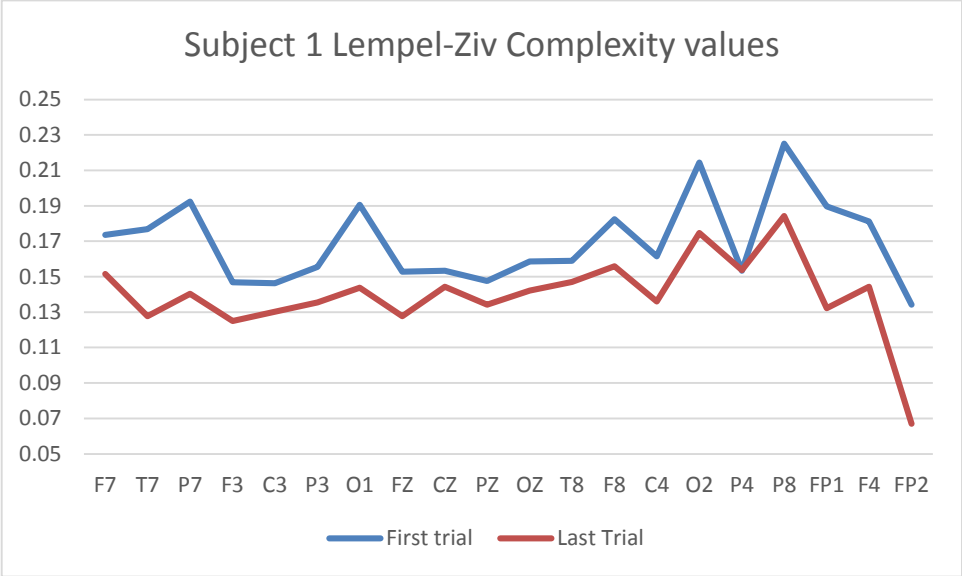

Figure 7.13: Lempel-Ziv Complexity values for Subject 1.

The complexity values for the first sequential pointing trial are plot in blue. The complexity values for the last sequential pointing trial are plot in red.

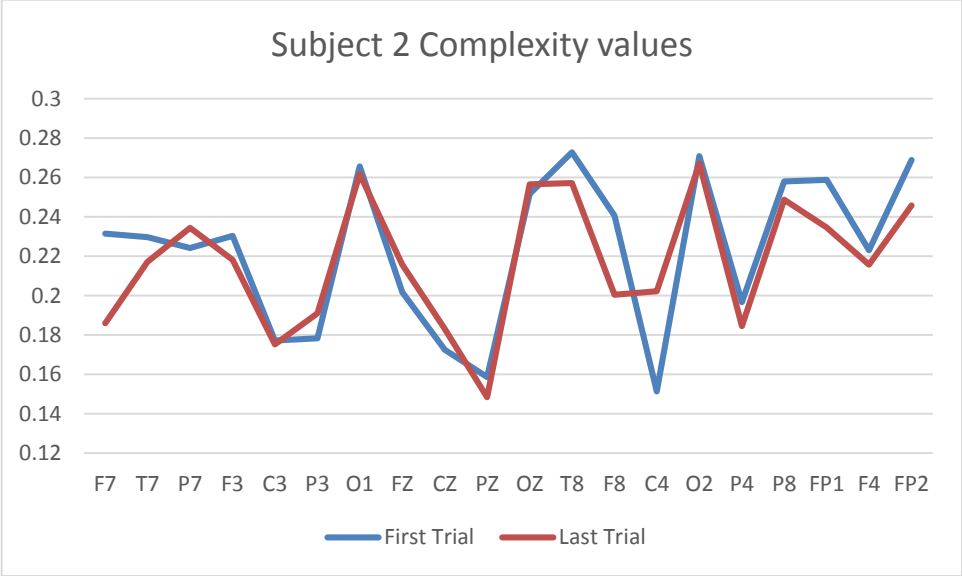

Figure 7.14: Lempel-Ziv Complexity values for Subject 2.

The complexity values for the first sequential pointing trial are plot in blue. The complexity values for the last sequential pointing trial are plot in red.

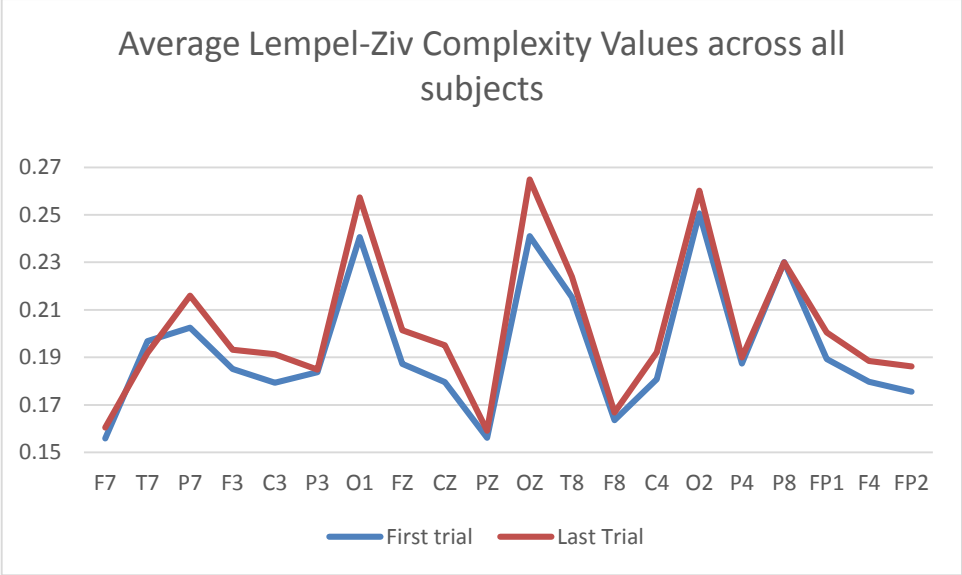

Figure 7.15: Averaged Lempel-Ziv Complexity values across all subjects.

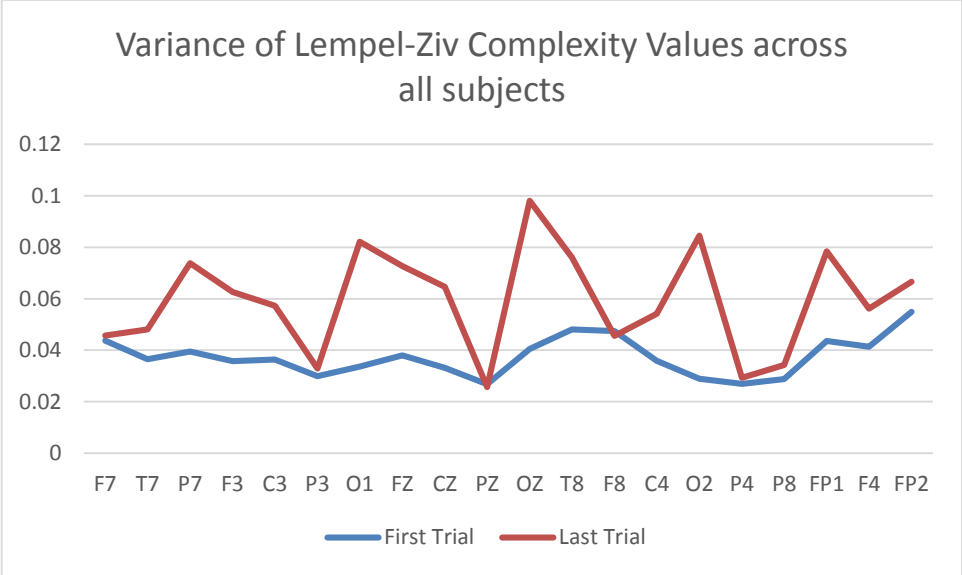

Figure 7.16: Variance of the averaged Lempel-Ziv Complexity values across all subjects.

Event-Related Potentials (ERP) have been generated for most subjects by creating a time-locked 1 second window beginning at the start of each visual cue generated by the simulation game (see Appendix A for two sample plots). Due to the time and noise sensitive nature of ERP analysis, approximately half of all trials

recorded were discarded due to factors such as high noise level and mismatches between simulation and user generated event timestamps.

By grouping and averaging the 1 second windows at the onset of every visual cue, the differences in a subject's time-locked cognitive response to a visual cue at every EEG electrode (see Figure 7.17) can be observed. On a broader scope, the collation of the individual ERP channels can be view for topological trends (see Figure 7.18). Throughout all subjects, it is observed that the anterior channels (FP1, FP2, F7 and F8) tend to be slow wave (~1Hz) dominant. Whereas the posterior channels (O1 and O2) are composed of higher frequency waves (~10 to 30Hz).

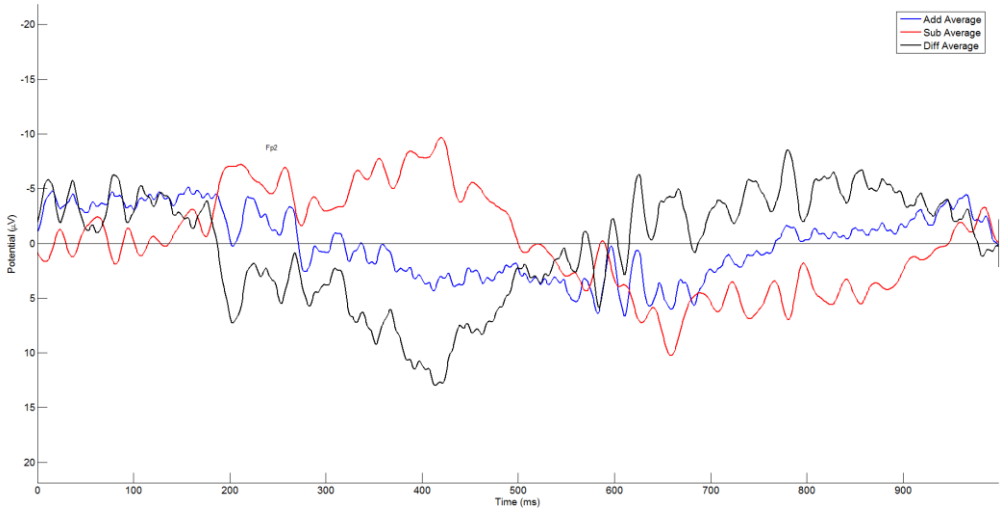

Figure 7.17: ERP plot of Subject 1 at channel FP2.

The blue line indicates the averaged ERP signal of all successfully completed tasks. The red line indicates the averaged ERP signal of all failed tasks. The black line is the computed difference between the successful and unsuccessful tasks.

ERP data for all subjects have been categorized under two different scenarios. The first scenario is the comparison between all successfully completed tasks and unsuccessfully completed tasks across all 10 trials per subject. The second scenario is the comparison between the successfully completed tasks in the first 5 trials and last 5 trials of each subject (see Figure 7.19).

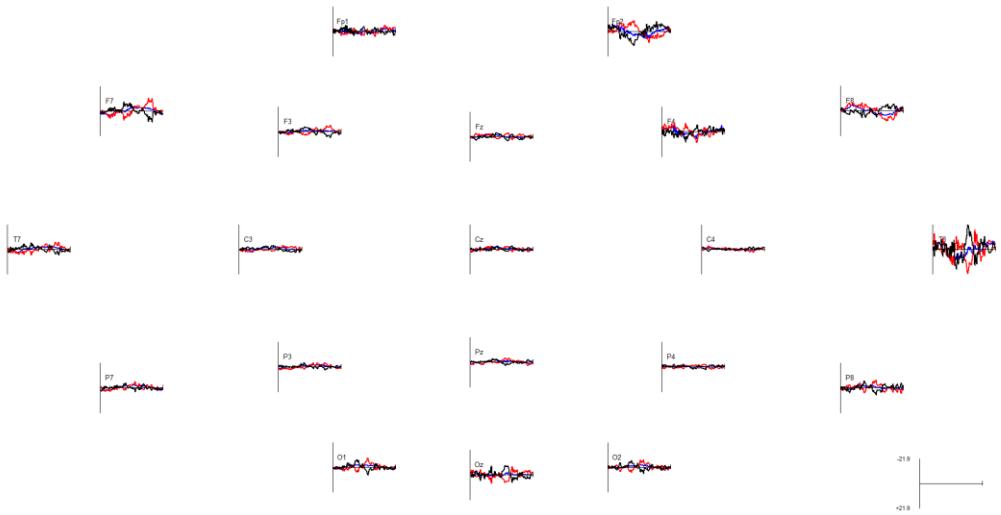

Figure 7.18: Collation of all ERP channels for Subject 1.

The Blue lines indicate the average of all successful tasks and the red lines indicate the average of all unsuccessful tasks. The black lines are the calculated difference between the successful and unsuccessful tasks.

The first scenario provides a grand averaged comparison of the difference in cognitive response between a successful task and unsuccessful task at each electrode channel. Although the trends were slightly different in every subject, it was observed that ERP signals were attenuated in the central channels like C3, C4, CZ, P3, P4, PZ, F3, F4 and FZ.

Peripheral channels, such as the frontal polar (FP1 and FP2), frontal (F7 and F8), temporal (T7 and T8) and occipital (O1 and O2) channels, exhibit significantly different amplitudes and waveforms when comparing between a successfully completed task and unsuccessfully completed task. In some channels, the waveform polarity was completely reversed for large parts of the epoch time window (see Figure 7.17).

This finding directly supports the main hypothesis of this experiment, showing that ERP-based analysis of the peripheral channels might be used to differentiate whether the subject has successfully performed a task. A simple way of leveraging

and implementing this novel information is to sample the peak amplitudes and corresponding latencies of ERP signals at the peripheral channels as inputs for classification.

The second scenario is the comparison between the successfully completed tasks in the first 5 trials and last 5 trials of each subject (see Figure 7.19). This comparison was implemented to identify any difference in cognitive response to visual task cues due to the effect of task mastery. However, it was found that in most subjects, there was no consistently discernible difference to be observed. This could be due to the fact that the subjects might not have had sufficient training to exact a difference in their ERP since this experiment was conducted within a single 30 minute session. In some subjects, some of the peripheral channels showed increased amplitudes in the later trials. However, this is most likely due to increased noise from electrode displacement than neural activity.

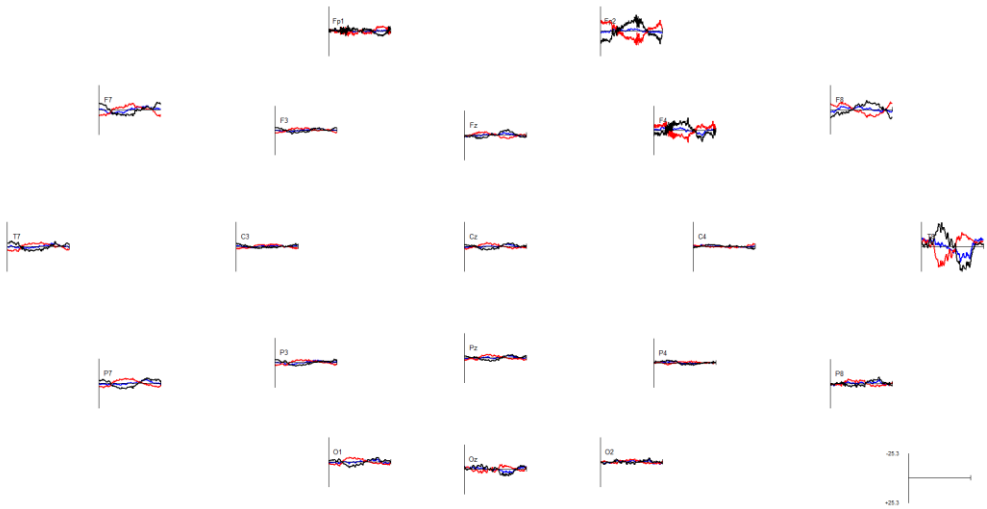

Figure 7.19: Collation of all ERP channels for Subject 1.

The Blue lines indicate the average of the successfully completed tasks in the first 5 trials and the red lines indicate the average of successfully completed tasks in the last 5 trials. The black lines are the calculated difference between the first 5 trials and last 5 trials.

The subjects' averaged game performances per trial are plot in Figure 7.20 to Figure 7.22. The first six trials recorded were from the exploratory modified colour scheme trials. Each of the three modified colour schemes (red, green and blue) was performed twice, totalling six trials. The following ten trials were then conducted with the standard colour scheme.

It can be seen that the subjects exhibited a typical logarithmic learning curve whereby the first few trials had poor scores and high levels of null-attempts and wrongly-keyed tasks. As the subjects performed more trials, the average score rapidly improved and plateaued at 22 points out of a possible 25, which is an approximately 90% success rate. This was achieved by the reduction in both null-attempts and wrongly-keyed tasks (see Figure 7.21 and Figure 7.22).

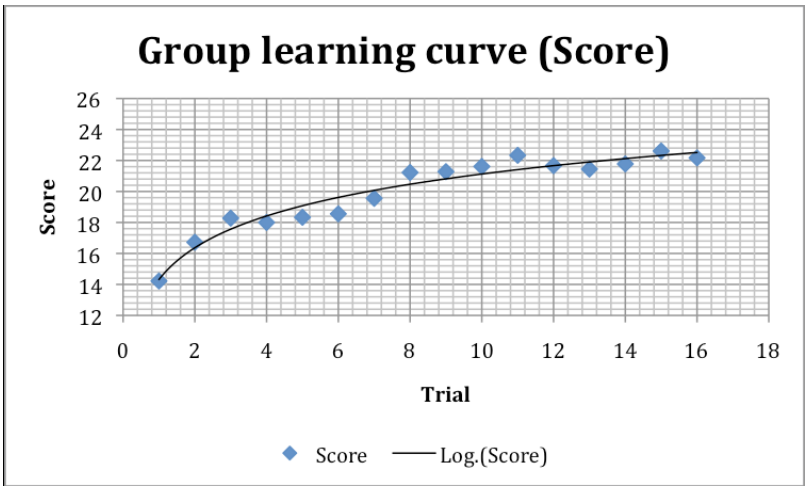

Figure 7.20: Average score of all subjects per trial.

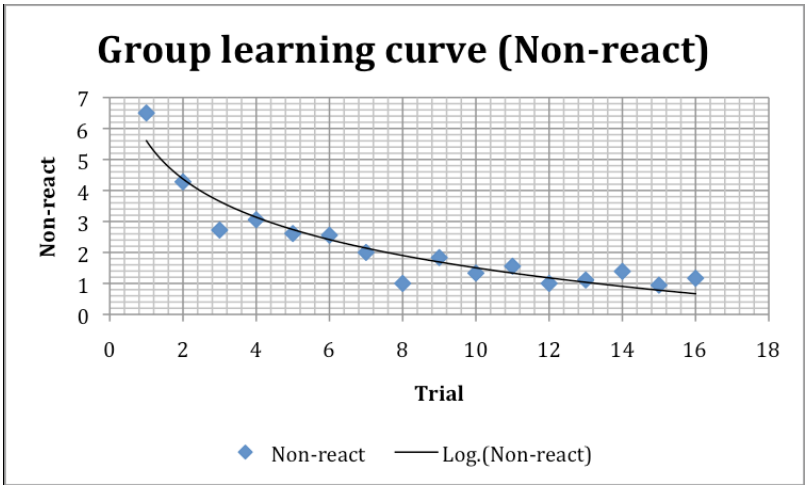

Figure 7.21: Average number of tasks with no user input for all subjects per trial.

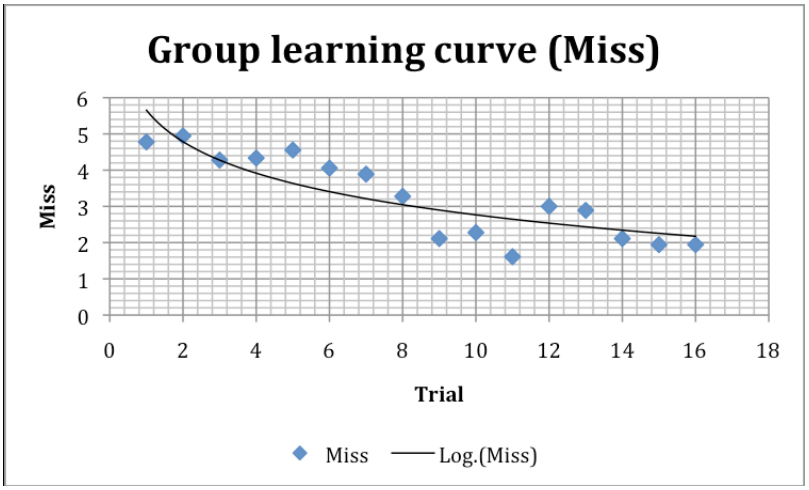

Figure 7.22: Average number of tasks with erroneous inputs for all subjects per trial.

7.4 Discussion

Similar to previous Chapters 4 and 5, the spectral plots of the subjects exhibited predominantly slow wave delta (1-3Hz) and theta (4-7Hz) activity in the anterior electrode channels, across all trials. This trend of slow wave dominance is also clearly evident in the 1 second ERP epochs of the anterior channels (see Figure 7.16 - Figure 7.18). Fast waves in the beta (14-25) and gamma (25-45Hz) bands remain predominantly in the posterior channels. When comparing the first few trials against the last few trials of every subject, alpha band (8-13Hz) attenuation at the frontal

channels was observed for some subjects. This load-related attenuation reflects the reduction in task difficulty as subjects got familiar with the sequential pointing task.

However, as compared to the other experiments, there is constantly high alpha band activity in the occipital region. It is postulated that the occipital region remains continually in high activity due to the rapid-fire randomized visual cue sequence of the sequential pointing task in this experiment. Comparatively, the visual cues provided for the experimental tasks in the other chapters were static and relatively constant so the subject's reliance on the visual cues becomes diminished once the task is learned after a few trials and the alpha band activity in the occipital region becomes attenuated.

The plot of averaged Lempel-Ziv Complexity values (see Figure 7.15) showed that the complexity of the signals was slightly increased after the 10 trials. The channels that exhibited the largest changes in complexity were the peripheral channels such as T7, P7, O1, O2, FP1 and FP2.

It is postulated that the small changes in LZC values are due to the relatively short overall trial lengths as compared to the trials conducted for the other experiments in Chapters 4, 5 and 6. Each of the trials conducted in this experiment lasted approximately 50 seconds and the total amount of time each subject took to complete this experiment was approximately 25 minutes, inclusive of intermittent resting periods. The cumulative amount of subject experimentation time is approximately half of what subjects took to complete the other experiments in Chapters 4, 5 and 6.

Taking into account that LZC algorithm utilizes the entire length of the EEG trial recording to generate the LZC value, it is a relatively tonic representation of the subject's EEG signal. Since the trials in this experiment are much shorter than other

experiments, this may explain why the LZC values in this experiment are relatively insensitive to change.

The Event-Related Potential is an important derivative of this study. Typical ERP studies in literature utilize the ERP components for analysis. ERP components are the approximate amplitudes of the ERP waveform at different latencies. For example, the P200 ERP component is the positive peak amplitude of the ERP waveform at approximately 200ms after the onset of the stimuli. Another widely researched ERP component is the P300 ERP component which is the peak positive amplitude of the ERP waveform at 300ms after the onset of an external stimulus. Other ERP components include the N100 and LPP (late positive potential) which represented the remaining waveform beyond the P300 peak. Miller et al reported that ERP components at central channels (CZ, PZ and FZ) were found to be correlated with cognitive workload [80], [81]. The larger the cognitive workload, the more attenuated the ERP components like P200 and P300 components became.

In the perspective of our sequential pointing task experiment, it is expected that the ERP components become less attenuated with more trials, to reflect the gradual reduction in cognitive workload and improved task mastery. This trend was found to be present for most of the subjects in this experiment (see two sample Figures in Appendix) and it was found to occur in many peripheral channels (such as F7, F8, T7 and T8) in addition to the central channels (CZ, PZ and FZ) reported by Miller et. al. [81].

7.5 Summary

Consistent with the other experiments, Spectral Analysis and Lempel-Ziv Complexity analysis were performed on the EEG data. Spectral analysis showed that there was attenuation of the alpha band at the frontal channels with increased task

mastery. In contrast, alpha band activity at the occipital region remained high due to continual visual cue information. The LZC plots showed that most channels did not exhibit significant changes in complexity. This may be attributable to the short duration of the overall experiment and the short length of each trial.

ERP analysis of the EEG data revealed novel information. Activity in the central channels was comparatively attenuated whereas the amplitude and waveform of ERP signals in the peripheral channels were found to vary between successful and unsuccessful tasks. This finding supports the primary hypothesis of this experiment that is; properly contextualized ERP analysis of EEG could be used to investigate differences in subject intra-trial performance.

The design and implementation of the simulation system was a challenging process. Due to the time sensitive nature of ERP analysis, various system operations had to be carried out in synchrony. User generated data and events had to be continually transmitted from the simulation game to the EEG recording software. However, even with meticulous planning, approximately half of all ERP epochs had to be discarded due to noise artifacts and data synchrony mismatches. It was noticed that in some of those trials that were discarded, the CPU utilization was intermittently high. This could be due to buffering or memory leaks from the video capturing software or EEG recording software.

The parameters of the sequential pointing task were also carefully investigated prior to the experimentation with subjects. The game task parameters had to be well-tuned to provide a proper level of difficulty such that novice subjects were able to demonstrate the distinct logarithmic learning curve and plateau in performance within the limited amount of trials planned. Visual cue parameters such as balloon shape and size, balloon grid size and density, crosshair shape, size and colour were all recursively investigated to fine-tune the game difficulty. The 1 second task window

was another important game parameter that was adjusted to match the ERP epoch generation and provided a uniform time window for comparison.

Building on the weaknesses of the current platform, to reduce the amount of data lost to de-synchronization, the interface between the EEG software and simulation game could be further optimized by reducing the communication latency between the two systems in the future. Better marker-less motion capturing systems will be implemented to integrate motion analysis. Excessive motion of the head and torso can also be used as a cue for automated noise removal in the EEG data.

The current simulation game parameters are static. This provides a consistent level of difficulty to all subjects, enabling comparisons across the whole cohort. However, in some subjects, their high level of HEC ability trivializes the game's default difficulty, reducing the ability for the system to track any improvement in score and task mastery. One possible solution is to enable the game parameters to be dynamically derived from past performance and ERP components that correlate with cognitive workload. This will enable an adaptable game that will continually adjust its difficulty to be challenging to the subject.

8 Conclusions

The overall objective of this thesis is to investigate the visual, motor and neural aspects of HEC through neural and motor performance analysis of subjects performing visual cue driven HEC tasks such as pointing and tracing.

In Chapter 4, the effect of visual cues on HEC was investigated. By attenuating or augmenting the illumination, colour and depth cues to the subjects, the influence of visual cues on subject HEC performance was investigated and quantified. A novel way of augmenting depth cues through endoscopic dynamic shadowing was also developed. Key findings include:

- The effect of depth cues was independent of the effect of colour on the performance of a subject.
- Visual cues, when applied incorrectly, can have a negative compounding effect on subject performance. When dynamic shadowing was applied with 3D visualization, subject performance was degraded even though both techniques were depth cue augmentations.

In Chapter 5, the neural activity of subjects performing a box folding task was investigated. The objective was to evaluate suitable neural analysis methods to gauge mental activity that is pertinent to the mastery of simple HEC tasks. Key findings include:

- Spectral analysis showed that activity in the theta and low alpha band of the channels in the central, occipital and parietal regions corresponded well to task mastery.
- LZC values within the central, occipital and parietal regions correspond with subjects' task performance.

- LZC values tend to vary inversely to task mastery. The complexity of the signal increases with reduced cognitive load. It was postulated that this is due to a phenomena whereby different regions of the brain synchronize in a concentrated state of high attention during high cognitive workloads, leading to a more harmonic mental state and reducing the complexity of the signal.
- Combined Spectral analysis and LZC analysis can be a tool to greatly reduce the dimensionality of the captured EEG data into more manageable and relevant information.

In Chapter 6, a robotic haptic guidance platform was used to train subjects in HEC tasks. The objective was to compare the training efficacy of automated haptic guidance and investigate the effects of the haptic guidance on the neural activity of the subjects. Key findings include:

- Subjects in the control group reduced their time taken to perform the tasks but the accuracy of the motion suffered. Whereas subjects in the haptic guidance group improved in both timing and motion accuracy.
- By comparing the experimental tasks and protocol in Chapter 5 and 6, the magnitude of change in LZC values in subjects tend to correlate with overall experimental task duration and training duration. A more intensive training task and longer duration of exposure will elicit a larger change in LZC. The largest change in LZC occurs in the occipital, parietal and central regions.
- There is a larger change in LZC values in the haptic guidance group as compared to the control group. The greatest difference in LZC values between the two groups are located at the EEG channels corresponding to

the Primary Motor Cortex (responsible for motion control) and Somatosensory Cortex (responsible for sensory integration).

In Chapter 7, a platform that implemented a sequential planar pointing task simulation was developed. The objective was to create a system suitable for performing inter-task neural analysis through ERPs and investigate whether ERP analysis could be used for differentiating the neural activity between subject task performances. Key findings include:

- In some subjects, spectral analysis showed attenuation at the alpha band in the frontal region during the initial trials, suggesting cognitive load related attenuation.
- The alpha band activity in the occipital region remains high despite increased task mastery as the simulation demands continual visual cue processing.
- LZC is insensitive to the change in task mastery due to the limited length of the trials. This suggests that LZC analysis fares better for comparing the tonic changes in neural activity.
- ERP components at the peripheral channels are significantly different between successfully completed tasks and unsuccessfully completed tasks.
- The attenuation of ERP components corresponded with larger cognitive workload at multiple peripheral channels and central channels.
- Neural synchrony through PLV analysis did not generate any observable trends. This may be due to the limited number of trials and presence of noise artifacts.

The results of this study contribute to the further understanding of HEC and their underlying aspects. The inclusion of EEG provides with a novel insight into the

neural mechanisms of HEC and learning, providing the foundations for the development of EEG-based supervisory guidance, as described in Chapter 3, for autonomous training platforms for HEC related skills. The comprehensive analysis and correlation of trends in neural activity with motor task performance and task mastery will enable a better understanding to a person's HEC ability, allowing for more efficient training and better causal feedback, more akin to human supervision.

9 Future Work

We are investigating the application of autonomous EEG-based supervisory guidance into rehabilitation of mental patients. It is not uncommon to have mental illnesses manifest as deficiencies in hand eye coordination. For example, in schizophrenic patients, they can feel physically dissociated between their sensory feedback and motor execution [71]. Therefore, they feel as if the body is not their own to control and this paranoia further affects their emotive capability to recover. From this observation, it is speculated that schizophrenia affects the forward model from providing a proper reafference signal that offsets the proprioceptive feedback sensation of self-motion. Thus the two asynchronous signals end up negatively manifesting on the patient.

One possible way of applying the framework for schizophrenic patients is to rehabilitate patients with situations that mimic the causal relationship of the forward model. The subjects can be trained with a simple object manipulation computer simulation with varying degrees of latency from the input to the virtual environment so as to let the schizophrenic patient have an opportunity in a controlled environment to familiarize and cope with his condition. Another way would be the brain conditioning approach to help the patient cope with the paranoia of suffering from a schizophrenic episode.

Another possible example for applying the hand eye coordination framework is the rehabilitation of mental depression. Although, physically, the motor function of patients with mental depression may not be inherently impaired, the cognitive state of the subject may affect proper implementation of HEC. During several occupational therapy (OT) cooking classes conducted for mental patients, it was observed that patients that suffered from depression lacked the confidence in performing tasks. This resulted in purposefully slow, tensed and doubtful actions that impaired their motor performance and memory. Rather than focusing on the performance of the patient,

OT staffs take a gentler approach of positive reinforcement that in one way help to calm the patients' state of mind and also guide the patient to complete the task successfully. From this observation, motor performance may not necessarily be the highest priority in rehabilitation and neurofeedback on the cognitive state of the subject will help in determining an efficient positive reinforcement protocol to provide feedback cues to the subject.

10 BIBLIOGRAPHY

[1] S. Kumar, A. Abhayambika, A. N. E. Sundaram, and J. A. Sharpe, "Posterior reversible encephalopathy syndrome presenting as Balint syndrome.," *J Neuroophthalmol*, vol. 31, no. 3, pp. 224–227, 2011.

[2] J. P. Piek and M. J. Dyck, "Sensory-motor deficits in children with developmental coordination disorder, attention deficit hyperactivity disorder and autistic disorder," *Hum. Mov. Sci.*, vol. 23, no. 3–4 SPE. ISS., pp. 475–488, 2004.

[3] S. Suzuki, F. Harashima, and K. Furuta, "Human control law and brain activity of voluntary motion by utilizing a balancing task with an inverted pendulum," *Adv. Human-Computer Interact.*, 2010.

[4] E. Dayan and L. G. Cohen, "Neuroplasticity subserving motor skill learning," *Neuron*, vol. 72, no. 3. pp. 443–454, 2011.

[5] L. Masia, M. Casadio, G. Sandini, and P. Morasso, "Eye-Hand Coordination during Dynamic Visuomotor Rotations," *PLoS One*, vol. 4, no. 9, p. e7004, 2009.

[6] R. A. Abrams, D. E. Meyer, and S. Kornblum, "Eye-hand coordination: oculomotor control in rapid aimed limb movements.," *J. Exp. Psychol. Hum. Percept. Perform.*, vol. 16, pp. 248–267, 1990.

[7] P. van Donkelaar and J. Staub, "Eye-hand coordination to visual versus remembered targets.," *Exp. Brain Res.*, vol. 133, pp. 414–418, 2000.

[8] P. Bédard, A. Thangavel, and J. N. Sanes, "Gaze influences finger movement-related and visual-related activation across the human brain," *Exp. Brain Res.*, vol. 188, no. 1, pp. 63–75, 2008.

[9] C. C. a M. Gielen, T. M. H. Dijkstra, I. J. Roozen, and J. Welten, "Coordination of gaze and hand movements for tracking and tracing in 3D," *Cortex*, vol. 45, no. 3, pp. 340–355, 2009.

[10] D. Srinivasan and B. J. Martin, "Eye-hand coordination of symmetric bimanual reaching tasks: Temporal aspects," *Exp. Brain Res.*, vol. 203, no. 2, pp. 391–405, 2010.

[11] H. Bekkering and U. Sailer, "Commentary: Coordination of eye and hand in time and space," in *Progress in Brain Research*, vol. Volume 140, D. P. M. W. H. J. Hyona and R. Radach, Eds. Elsevier, 2002, pp. 365–373.

[12] M. Hayhoe and D. Ballard, "Eye movements in natural behavior," *Trends Cogn. Sci.*, vol. 9, no. 4, pp. 188–194, Jul. 2005.

[13] N. Moray, "Designing for attention.," in *Attention: Selection, awareness, and control: A tribute to Donald Broadbent*, A. D. B. L. Weiskrantz, Ed. New York, NY, US: Clarendon Press/Oxford University Press, 1993, pp. 111–134.

[14] E. D. Guestrin and M. Eizenman, “General theory of remote gaze estimation using the pupil center and corneal reflections,” *Biomed. Eng. IEEE Trans.*, vol. 53, no. 6, pp. 1124–1133, 2006.

[15] M. Marmor, M. Brigell, D. McCulloch, C. Westall, and M. Bach, “ISCEV standard for clinical electro-oculography (2010 update),” *Doc. Ophthalmol.*, vol. 122, no. 1, pp. 1–7, 2011.

[16] E. Criswell, *Cram’s Introduction to Surface Electromyography*. 2011.

[17] “Standards for Reporting EMG Data,” *J. Electromyogr. Kinesiol.*, vol. 24, no. 2, pp. I–II, Apr. 2014.

[18] M. B. I. Reaz, M. S. Hussain, and F. Mohd-Yasin, “Techniques of EMG signal analysis: detection, processing, classification and applications (Correction).,” *Biol. Proced. Online*, vol. 8, p. 163, 2006.

[19] K. Jerbi, T. Ossandón, C. M. Hamamé, S. Senova, S. S. Dalal, J. Jung, L. Minotti, O. Bertrand, A. Berthoz, P. Kahane, and J.-P. Lachaux, “Task-related gamma-band dynamics from an intracerebral perspective: Review and implications for surface EEG and MEG,” *Hum. Brain Mapp.*, vol. 30, no. 6, pp. 1758–1771, 2009.

[20] E. Niedermeyer and F. L. da Silva, *Electroencephalography: Basic Principles, Clinical Applications, and Related Fields*. Lippincott Williams & Wilkins, 2004.

[21] T. P. Jung, S. Makeig, M. Westerfield, J. Townsend, E. Courchesne, and T. J. Sejnowski, “Removal of eye activity artifacts from visual event-related potentials in normal and clinical subjects,” *Clin. Neurophysiol.*, vol. 111, no. 10, pp. 1745–1758, 2000.

[22] S. E. Henderson, D. A. Sugden, and A. Barnett, *Movement Assessment Battery for Children*, Second Edi. Psychological Corporation, 2007.

[23] L. Johnston and P. Watter, “Movement Assessment Battery for Children (Movement ABC),” *Aust. J. Physiother.*, vol. 52, no. 1, p. 68, Jan. 2006.

[24] H. Van Waelvelde, W. De Weerdt, P. De Cock, and B. C. M. Smits-Engelsman, “Aspects of the validity of the Movement Assessment Battery for Children.,” *Hum. Mov. Sci.*, vol. 23, no. 1, pp. 49–60, Jun. 2004.

[25] S. Houwen, C. Visscher, K. A. P. M. Lemmink, and E. Hartman, “Motor skill performance of school-age children with visual impairments,” *Dev. Med. Child Neurol.*, vol. 50, no. 2, pp. 139–145, 2008.

[26] K. Caeyenberghs, A. Leemans, M. Geurts, T. Taymans, C. Vander Linden, B. C. M. Smits-Engelsman, S. Sunaert, and S. P. Swinnen, “Brain-behavior relationships in young traumatic brain injury patients: Fractional anisotropy measures are highly correlated with dynamic visuomotor tracking performance,” *Neuropsychologia*, vol. 48, no. 5, pp. 1472–1482, 2010.

[27] M. Vassiliou, G. Ghitulescu, L. Feldman, D. Stanbridge, K. Leffondré, H. Sigman, and G. Fried, "The MISTELS program to measure technical skill in laparoscopic surgery," *Surg. Endosc.*, vol. 20, no. 5, pp. 744–747, 2006.

[28] Z. Lian, C.-K. Chui, and S.-H. Teoh, "A biomechanical model for real-time simulation of PMMA injection with haptics," *Comput. Biol. Med.*, vol. 38, no. 3, pp. 304–312, Jul. 2008.

[29] C.-K. Chui, J. S. K. Ong, Z.-Y. Lian, Z. Wang, J. Teo, J. Zhang, C.-H. Yan, S.-H. Ong, S.-C. Wang, H.-K. Wong, C.-L. Teo, and S.-H. Teoh, "Haptics in computer-mediated simulation: Training in vertebroplasty surgery," *Simul. Gaming* , vol. 37 , no. 4 , pp. 438–451, Dec. 2006.

[30] S. Omata, Y. Murayama, and C. E. Constantinou, "Real time robotic tactile sensor system for the determination of the physical properties of biomaterials," *Sensors Actuators A Phys.*, vol. 112, no. 2–3, pp. 278–285, 2004.

[31] J. Anderson, C.-K. Chui, Y. Cai, Y. Wang, Z. Li, X. Ma, W. Nowinski, M. Solaiyappan, K. Murphy, P. Gailloud, and A. Venbrux, "Virtual Reality Training In Interventional Radiology: The Johns Hopkins and Kent Ridge Digital Laboratory Experience," *Semin Interv. Radiol*, vol. 19, no. 02, pp. 179–186, 2002.

[32] N. Stylopoulos, S. Cotin, S. K. Maithel, M. Ottensmeyer, P. G. Jackson, R. S. Bardsley, P. F. Neumann, D. W. Rattner, and S. L. Dawson, "Computer-enhanced laparoscopic training system (CELTS): bridging the gap," *Surg. Endosc.*, vol. 18, no. 5, pp. 782–789, 2004.

[33] F. M. M. O. Campos and J. M. F. Calado, "Approaches to human arm movement control--A review," *Annu. Rev. Control*, vol. 33, no. 1, pp. 69–77, 2009.

[34] P. M. Fitts, "The information capacity of the human motor system in controlling the amplitude of movement," *J Exp Psychol Gen*, vol. 47, no. 6, pp. 381–391, 1954.

[35] T. Flash and N. Hogan, "The coordination of arm movements: an experimentally confirmed mathematical model," *J. Neurosci.* , vol. 5 , no. 7 , pp. 1688–1703, Jul. 1985.

[36] J. J. Craig, *Introduction to Robotics: Mechanics and Control*, 3rd Editio. Pearson/Prentice Hall, 2005.

[37] E. J. Todorov Michael I., "Smoothness Maximization Along a Predefined Path Accurately Predicts the Speed Profiles of Complex Arm Movements," *J. Neurophysiol.*, vol. 80, no. 2, pp. 696–714, Aug. 1998.

[38] Y. Uno, M. Kawato, and R. Suzuki, "Formation and control of optimal trajectory in human multijoint arm movement," *Biol. Cybern.*, vol. 61, no. 2, pp. 89–101, 1989.

[39] C. M. Harris and D. M. Wolpert, “Signal-dependent noise determines motor planning,” *Nature*, vol. 394, no. 6695, pp. 780–784, Aug. 1998.

[40] E. Todorov and M. I. Jordan, “Optimal feedback control as a theory of motor coordination,” *Nat Neurosci*, vol. 5, no. 11, pp. 1226–1235, Nov. 2002.

[41] M. J. T. Fitzgerald, G. Gruener, and E. Mtui, *Clinical Neuroanatomy and Neuroscience*. Elsevier Health Sciences, 2007.

[42] R. C. Miall, D. J. Weir, D. M. Wolpert, and J. F. Stein, “Is the cerebellum a smith predictor?,” *J. Mot. Behav.*, vol. 25, pp. 203–216, 1993.

[43] D. M. Wolpert, R. C. Miall, and M. Kawato, “Internal models in the cerebellum,” *Trends Cogn. Sci.*, vol. 2, no. 9, pp. 338–347, 1998.

[44] M. Kawato and H. Gomi, “The cerebellum and VOR/OKR learning models,” *Trends Neurosci.*, vol. 15, no. 11, pp. 445–453, Nov. 1992.

[45] M. Kawato, K. Furukawa, and R. Suzuki, “A hierarchical neural-network model for control and learning of voluntary movement,” *Biol. Cybern.*, vol. 57, no. 3, pp. 169–185, 1987.

[46] D. M. Wolpert and M. Kawato, “Multiple paired forward and inverse models for motor control,” *Neural Networks*, vol. 11, no. 7–8, pp. 1317–1329, Oct. 1998.

[47] M. Haruno, D. M. Wolpert, and M. Kawato, “Mosaic model for sensorimotor learning and control.,” *Neural Comput.*, vol. 13, pp. 2201–2220, 2001.

[48] M. Berniker and K. Kording, “Bayesian Models of Motor Control,” in *Encyclopedia of Neuroscience*, R. S. Larry, Ed. Oxford: Academic Press, 2009, pp. 127–133.

[49] K. P. Kording and D. M. Wolpert, “Bayesian integration in sensorimotor learning,” *Nature*, vol. 427, no. 6971, pp. 244–247, Jan. 2004.

[50] D. M. Wolpert, “Probabilistic models in human sensorimotor control,” *Hum. Mov. Sci.*, vol. 26, no. 4, pp. 511–524, 2007.

[51] M. B. Sterman and L. Friar, “Suppression of seizures in an epileptic following sensorimotor EEG feedback training.,” *Electroencephalogr. Clin. Neurophysiol.*, vol. 33, pp. 89–95, 1972.

[52] M. B. Sterman, “Basic concepts and clinical findings in the treatment of seizure disorders with EEG operant conditioning.,” *Clin. Electroencephalogr.*, vol. 31, pp. 45–55, 2000.

[53] S. Vanhatalo, J. Voipio, and K. Kaila, “Full-band EEG (fbEEG): a new standard for clinical electroencephalography.,” *Clin. EEG Neurosci.*, vol. 36, pp. 311–317, 2005.

[54] U. Leins, G. Goth, T. Hinterberger, C. Klinger, N. Rumpf, and U. Strehl, “Neurofeedback for children with ADHD: A comparison of SCP and

Theta/Beta protocols," *Appl. Psychophysiol. Biofeedback*, vol. 32, pp. 73–88, 2007.

[55] M. Talebinejad, A. D. C. Chan, and A. Miri, "A Lempel-Ziv complexity measure for muscle fatigue estimation," *J. Electromyogr. Kinesiol.*, vol. 21, pp. 236–241, 2011.

[56] H. Jing, G. Jianbo, and J. C. Principe, "Analysis of Biomedical Signals by the Lempel-Ziv Complexity: the Effect of Finite Data Size," *Biomed. Eng. IEEE Trans.*, vol. 53, no. 12, pp. 2606–2609, 2006.

[57] L.-Y. Zhang and C.-X. Zheng, "Lempel-Ziv complexity changes and physiological mental fatigue level during different mental fatigue state with spontaneous EEG," *Health (Irvine. Calif).*, vol. 1, no. 1, p. 35+, 2009.

[58] X. S. Zhang, R. J. Roy, and E. W. Jensen, "EEG complexity as a measure of depth of anesthesia for patients," *Biomed. Eng. IEEE Trans.*, vol. 48, no. 12, pp. 1424–1433, 2001.

[59] D. Abásolo, R. Hornero, C. Gómez, M. García, and M. López, "Analysis of EEG background activity in Alzheimer's disease patients with Lempel-Ziv complexity and central tendency measure," *Med. Eng. Phys.*, vol. 28, no. 4, pp. 315–322, 2006.

[60] A. J. Ibáñez-Molina, S. Iglesias-Parro, M. F. Soriano, and J. I. Aznarte, "Multiscale Lempel-Ziv complexity for EEG measures," *Clinical Neurophysiology*, 2014.

[61] J. Hu, J. Gao, and J. C. Principe, "Analysis of biomedical signals by the Lempel-Ziv complexity: The effect of finite data size," *IEEE Trans. Biomed. Eng.*, vol. 53, pp. 2606–2609, 2006.

[62] R. Nagarajan, "Quantifying physiological data with Lempel-Ziv complexity-certain issues," *Biomed. Eng. IEEE Trans.*, vol. 49, no. 11, pp. 1371–1373, 2002.

[63] A. J. Haufler, T. W. Spalding, D. L. Santa Maria, and B. D. Hatfield, "Neuro-cognitive activity during a self-paced visuospatial task: Comparative EEG profiles in marksmen and novice shooters," *Biol. Psychol.*, vol. 53, no. 2–3, pp. 131–160, 2000.

[64] S. P. Deeny, C. H. Hillman, C. M. Janelle, and B. D. Hatfield, "Cortico-cortical communication and superior performance in skilled marksmen: An EEG coherence analysis.," *J. Sport Exerc. Psychol.*, vol. 25, pp. 188–204, 2003.

[65] T.-M. Hung, T. W. Spalding, D. L. S. Maria, and B. D. Hatfield, "Assessment of Reactive Motor Performance With Event-Related Brain Potentials: Attention Processes in Elite Table Tennis Players," *J. Sport Exerc. Psychol.*, vol. 26, no. 2, pp. 317–337, 2004.

[66] B. D. Hatfield, A. J. Haufler, T.-M. Hung, and T. W. Spalding, “Electroencephalographic Studies of Skilled Psychomotor Performance,” *J. Clin. Neurophysiol.*, vol. 21, no. 3, pp. 144–156, 2004.

[67] J. Baumeister, K. Reinecke, H. Liesen, and M. Weiss, “Cortical activity of skilled performance in a complex sports related motor task,” *Eur. J. Appl. Physiol.*, vol. 104, no. 4, pp. 625–631, 2008.

[68] S. P. Deeny, A. J. Haufler, M. Saffer, and B. D. Hatfield, “Electroencephalographic coherence during visuomotor performance: a comparison of cortico-cortical communication in experts and novices.,” *J. Mot. Behav.*, vol. 41, no. 2, pp. 106–116, 2009.

[69] D. Landers, M. Han, W. Salazar, and S. Petruzzello, “Effects of learning on electroencephalographic and electrocardiographic patterns in novice archers,” *Int. J. Sport Psychol.*, vol. 25, no. 3, pp. 313–330, 1994.

[70] M. E. Smith, L. K. McEvoy, and A. Gevins, “Neurophysiological indices of strategy development and skill acquisition,” *Cogn. Brain Res.*, vol. 7, no. 3, pp. 389–404, 1999.

[71] S. S. Shergill, G. Samson, P. M. Bays, C. D. Frith, and D. M. Wolpert, “Evidence for Sensory Prediction Deficits in Schizophrenia,” *Am J Psychiatry*, vol. 162, no. 12, pp. 2384–2386, 2005.

[72] E. Murakami and T. Matsui, “Human Control Modeling Based on Multimodal Sensory Feedback Information,” *Proceedings of the 5th International Conference on Foundations of Augmented Cognition. Neuroergonomics and Operational Neuroscience: Held as Part of HCI International 2009*. Springer-Verlag, San Diego, CA, pp. 192–201, 2009.

[73] S. P. Kelly, P. Dockree, R. B. Reilly, and I. H. Robertson, “EEG alpha power and coherence time courses in a sustained attention task,” *First Int. IEEE EMBS Conf. Neural Eng. 2003. Conf. Proceedings.*, pp. 1–4, 2003.

[74] L. a Mrotek and J. F. Soechting, “Target interception: hand-eye coordination and strategies.,” *J. Neurosci.*, vol. 27, no. 27, pp. 7297–7309, 2007.

[75] M. Wilson, M. Coleman, and J. McGrath, “Developing basic hand-eye coordination skills for laparoscopic surgery using gaze training,” *BJU Int.*, vol. 105, no. 10, pp. 1356–1358, 2010.

[76] J. R. Anderson, *Cognitive psychology and its implications*, vol. 6. 2010.

[77] R. S. Huang, T. P. Jung, and S. Makeig, “Multi-scale EEG brain dynamics during sustained attention tasks,” *ICASSP, IEEE Int. Conf. Acoust. Speech Signal Process. - Proc.*, vol. 4, pp. 1173–1176, 2007.

[78] F. F. Zhu, J. P. Maxwell, Y. Hu, Z. G. Zhang, W. K. Lam, J. M. Poolton, and R. S. W. Masters, “EEG activity during the verbal-cognitive stage of motor skill acquisition,” *Biol. Psychol.*, vol. 84, no. 2, pp. 221–227, 2010.

[79] D. Stefanidis, J. R. Korndorffer, F. W. Black, J. B. Dunne, R. Sierra, C. L. Touchard, D. a. Rice, R. J. Markert, P. R. Kastl, and D. J. Scott, "Psychomotor testing predicts rate of skill acquisition for proficiency-based laparoscopic skills training," *Surgery*, vol. 140, no. 2, pp. 252–262, 2006.

[80] S. Deeny, C. Chicoine, L. Hargrove, T. Parrish, and A. Jayaraman, "A Simple ERP Method for Quantitative Analysis of Cognitive Workload in Myoelectric Prosthesis Control and Human-Machine Interaction.," *PLoS One*, vol. 9, no. 11, p. e112091, Jan. 2014.

[81] M. W. Miller, J. C. Rietschel, C. G. McDonald, and B. D. Hatfield, "A novel approach to the physiological measurement of mental workload," *Int. J. Psychophysiol.*, vol. 80, pp. 75–78, 2011.

[82] M. Hayhoe and D. Ballard, "Eye movements in natural behavior," *Trends Cogn. Sci.*, vol. 9, no. 4, pp. 188–194, Jul. 2005.

[83] A. A. Shah, "Minimally Invasive Surgery," *Indian J. Pediatr.*, vol. 75, no. 9, pp. 925–929, 2008.

[84] J. Heemskerk, R. Zandbergen, J. G. Maessen, J. W. Greve, and N. D. Bouvy, "Advantages of advanced laparoscopic systems," *Surg. Endosc.*, vol. 20, no. 5, pp. 730–733, 2006.

[85] T. A. Emam, G. Hanna, and A. Cuschieri, "Ergonomic principles of task alignment, visual display, and direction of execution of laparoscopic bowel suturing," *Surg. Endosc.*, vol. 16, no. 2, pp. 267–271, 2002.

[86] C. S. Lee, "Simulation Gaming for Laparoscopy," Final Year Project Thesis, National University of Singapore, 2009.

[87] S. Manasnayakorn, A. Cuschieri, and G. Hanna, "Hand-assisted laparoscopic surgery is associated with enhanced depth perception in novices," *Surg. Endosc.*, vol. 24, no. 11, pp. 2694–2699, 2010.

[88] N. Taffinder, S. G. Smith, J. Huber, R. C. Russell, and A. Darzi, "The effect of a second-generation 3D endoscope on the laparoscopic precision of novices and experienced surgeons," *Surg. Endosc.*, vol. 13, no. 11, pp. 1087–1092, 1999.

[89] Y. Yamauchi, "Clinical Demands and Evaluations of 3D and Augmented Visualization," *Medical Image Computing and Computer Assisted Intervention (MICCAI)*. 2002.

[90] S.-H. Kong, B.-M. Oh, H. Yoon, H. Ahn, H.-J. Lee, S. Chung, N. Shiraishi, S. Kitano, and H.-K. Yang, "Comparison of two- and three-dimensional camera systems in laparoscopic performance: a novel 3D system with one camera," *Surg. Endosc.*, 2009.

[91] J. Hofmeister, T. G. Frank, A. Cuschieri, and N. J. Wade, "Perceptual Aspects of Two-dimensional and Stereoscopic Display Techniques in Endoscopic Surgery: Review and Current Problems," *Surg. Innov.*, vol. 8, no. 1, pp. 12–24, 2001.

[92] P. Storz, G. Buess, W. Kunert, and A. Kirschniak, “3D HD versus 2D HD: surgical task efficiency in standardised phantom tasks,” *Surg. Endosc.*, vol. 26, no. 5, pp. 1454–1460, 2012.

[93] R. Smith, A. Day, T. Rockall, K. Ballard, M. Bailey, and I. Jourdan, “Advanced stereoscopic projection technology significantly improves novice performance of minimally invasive surgical skills,” *Surg. Endosc.*, vol. 26, no. 6, pp. 1522–1527, 2012.

[94] R. K. Mishra, G. B. Hanna, S. I. Brown, and A. Cuschieri, “Optimum Shadow-Casting Illumination for Endoscopic Task Performance,” *Arch Surg*, vol. 139, no. 8, pp. 889–892, 2004.

[95] M. Nicolaou, A. James, B. P. L. Lo, A. Darzi, and G.-Z. Yang, “Invisible Shadow for Navigation and Planning in Minimal Invasive Surgery,” in *Medical Image Computing and Computer-Assisted Intervention – MICCAI 2005*, vol. 3750, J. Duncan and G. Gerig, Eds. Springer Berlin / Heidelberg, 2005, pp. 25–32.

[96] R. T. Shimotsu and C. G. L. Cao, “The Effect of Color-Contrasting Shadows on a Dynamic 3-D Laparoscopic Surgical Task,” *Syst. Man Cybern. Part A Syst. Humans, IEEE Trans.*, vol. 37, no. 6, pp. 1047–1053, 2007.

[97] M. H. P. H. van Beurden, A. Kuijsters, and W. A. Ijsselsteijn, “Performance of a path tracing task using stereoscopic and motion based depth cues,” in *Quality of Multimedia Experience (QoMEX), 2010 Second International Workshop on*, 2010, pp. 176–181.

[98] E. B. Johnston, B. G. Cumming, and A. J. Parker, “Integration of depth modules: Stereopsis and texture,” *Vision Res.*, vol. 33, no. 5–6, pp. 813–826, 1993.

[99] D. Kersten, P. Mamassian, and D. C. Knill, “Moving cast shadows induce apparent motion in depth,” *Perception*, vol. 26, no. 2, pp. 171–192, 1997.

[100] L. Marcucci, J. Freeman, T. Quinn, M. Hopmeier, R. Milner, J. Friedberg, and J. Buyske, “Infrared imaging in minimally invasive surgery,” in *Engineering in Medicine and Biology Society, 1998. Proceedings of the 20th Annual International Conference of the IEEE*, 1998, vol. 2, pp. 926–927 vol.2.

[101] E. M. Sevick-Muraca, “Translation of near-infrared fluorescence imaging technologies: emerging clinical applications.,” *Annu. Rev. Med.*, vol. 63, pp. 217–31, 2012.

[102] T. Matsushita, T. Miyati, K. Nakayama, T. Hamaguchi, Y. Hayakawa, A. G. Farman, and S. Ohtake, “Qualitative near-infrared vascular imaging system with tuned aperture computed tomography,” *J. Biomed. Opt.*, vol. 16, no. 7, pp. 76004–76005, 2011.

[103] A. Lee, D. Elson, M. Neil, S. Kumar, B. Ling, F. Bello, and G. Hanna, “Solid-state semiconductors are better alternatives to arc-lamps for efficient and uniform illumination in minimal access surgery,” *Surg. Endosc.*, vol. 23, no. 3, pp. 518–526, 2009.

[104] L. Chun Siong, Y. Liangjing, Y. Tao, C. Chee-Kong, L. Jiang, H. Weimin, S. Yi, S. K. Y. Chang, and C. K. Chui, "Designing an Active Motor Skill Learning Platform with a Robot-Assisted Laparoscopic Trainer," in *Engineering in Medicine and Biology Society,EMBC, 2011 Annual International Conference of the IEEE*, 2011, pp. 4534–4537.

[105] S. J. Westerman and T. Cribbin, "Individual differences in the use of depth cues: implications for computer- and video-based tasks," *Acta Psychol. (Amst).*, vol. 99, no. 3, pp. 293–310, 1998.

[106] X. Li, B. Hu, T. Zhu, J. Yan, and F. Zheng, "Towards affective learning with an EEG feedback approach," *Proceedings of the first ACM international workshop on Multimedia technologies for distance learning*. ACM, Beijing, China, pp. 33–38, 2009.

[107] P. N. Friel, "EEG Biofeedback in the Treatment of Attention Deficit / Hyperactivity Disorder," *Altern. Med. Rev.*, vol. 12, no. 2, p. 6, 2007.

[108] W. Klimesch, H. Schimke, and G. Pfurtscheller, "Alpha frequency, cognitive load and memory performance," *Brain Topogr.*, vol. 5, no. 3, pp. 241–251, 1993.

[109] L. I. Aftanas, V. I. Koshkarov, V. L. Pokrovskaja, N. V Lotova, and Y. N. Mordvintsev, "Pre- and post-stimulus processes in affective task and event-related desynchronization (ERD): Do they discriminate anxiety coping styles?," *Int. J. Psychophysiol.*, vol. 24, no. 3, pp. 197–212, 1996.

[110] V. J. Monastra, S. Lynn, M. Linden, J. F. Lubar, J. Gruzelier, and T. J. LaVaque, "Electroencephalographic Biofeedback in the Treatment of Attention-Deficit/Hyperactivity Disorder," *Appl. Psychophysiol. Biofeedback*, vol. 30, no. 2, pp. 95–114, 2005.

[111] A. Lempel and J. Ziv, "On the Complexity of Finite Sequences," *Inf. Theory, IEEE Trans.*, vol. 22, no. 1, pp. 75–81, 1976.

[112] V. D.Gusev and L. A.Nemytikova, "On the complexity measures of genetic sequences," *Bioinformatics*, vol. 15, no. 12, pp. 994–999, 1999.

[113] X. Chen, S. Kwong, and M. Li, "A compression algorithm for DNA sequences and its applications in genome comparison," *Proceedings of the fourth annual international conference on Computational molecular biology*. ACM, Tokyo, Japan, p. 107, 2000.

[114] D. Abásolo, R. Hornero, C. Gómez, M. García, and M. López, "Analysis of EEG background activity in Alzheimer's disease patients with Lempel–Ziv complexity and central tendency measure," *Med. Eng. & Phys.*, vol. 28, no. 4, pp. 315–322, 2006.

[115] A. Delorme and S. Makeig, "EEGLAB: an open source toolbox for analysis of single-trial EEG dynamics including independent component analysis," *J. Neurosci. Methods*, vol. 134, no. 1, pp. 9–21, 2004.

[116] Y. Li, S. Tong, D. Liu, Y. Gai, X. Wang, J. Wang, Y. Qiu, and Y. Zhu, "Abnormal EEG complexity in patients with schizophrenia and depression," *Clin. Neurophysiol.*, vol. 119, no. 6, pp. 1232–1241, 2008.

[117] J. Hong, X. Li, F. Xu, Y. Jiang, and X. Li, "The mental workload judgment in visual cognition under multitask meter scheme," *Int. J. Phys. Sci.*, vol. 7, no. 5, pp. 787–796, 2012.

[118] T. Fernández, T. Harmony, M. Rodríguez, J. Bernal, J. Silva, A. Reyes, and E. Marosi, "EEG activation patterns during the performance of tasks involving different components of mental calculation," *Electroencephalogr. Clin. Neurophysiol.*, vol. 94, no. 3, pp. 175–182, 1995.

[119] R. Ferenets, L. Tarmo, A. Anier, V. Jantti, S. Melto, and S. Hovilehto, "Comparison of entropy and complexity measures for the assessment of depth of sedation," *Biomed. Eng. IEEE Trans.*, vol. 53, no. 6, pp. 1067–1077, 2006.

[120] W. P. Medendorp, H. C. Goltz, T. Vilis, and J. D. Crawford, "Gaze-Centered Updating of Visual Space in Human Parietal Cortex," *J. Neurosci.*, vol. 23, no. 15, pp. 6209–6214, 2003.

[121] W. Klimesch, R. Freunberger, P. Sauseng, and W. Gruber, "A short review of slow phase synchronization and memory: Evidence for control processes in different memory systems?," *Brain Res.*, vol. 1235, no. 0, pp. 31–44, 2008.

[122] W. Klimesch, "EEG alpha and theta oscillations reflect cognitive and memory performance: A review and analysis," *Brain Res. Rev.*, vol. 29, no. 2–3, pp. 169–195, 1999.

[123] W. Klimesch, H. Schimke, and J. Schwaiger, "Episodic and semantic memory: an analysis in the EEG theta and alpha band," *Electroencephalogr. Clin. Neurophysiol.*, vol. 91, no. 6, pp. 428–441, 1994.

[124] W. Klimesch, M. Doppelmayr, T. Pachinger, and B. Ripper, "Brain oscillations and human memory: EEG correlates in the upper alpha and theta band," *Neurosci. Lett.*, vol. 238, no. 1–2, pp. 9–12, 1997.

[125] W. Klimesch, M. Doppelmayr, H. Schimke, and B. Ripper, "Theta synchronization and alpha desynchronization in a memory task," *Psychophysiology*, vol. 34, no. 2, pp. 169–176, 1997.

[126] M. Doppelmayr, W. Klimesch, W. Stadler, D. Pöllhuber, and C. Heine, "EEG alpha power and intelligence," *Intelligence*, vol. 30, no. 3, pp. 289–302, 2002.

[127] O. Jensen and C. D. Tesche, "Frontal theta activity in humans increases with memory load in a working memory task," *Eur. J. Neurosci.*, vol. 15, no. 8, pp. 1395–1399, 2002.

[128] S. Raghavachari, M. J. Kahana, D. S. Rizzuto, J. B. Caplan, M. P. Kirschen, B. Bourgeois, J. R. Madsen, and J. E. Lisman, "Gating of human theta oscillations by a working memory task," *J. Neurosci.*, vol. 21, no. 9, pp. 3175–3183, 2001.

[129] W. Klimesch, M. Doppelmayr, J. Schwaiger, P. Auinger, and T. Winkler, "'Paradoxical' alpha synchronization in a memory task," *Cogn. Brain Res.*, vol. 7, no. 4, pp. 493–501, 1999.

[130] T. Ishihara and N. Yoshii, "Multivariate analytic study of EEG and mental activity in Juvenile delinquents," *Electroencephalogr. Clin. Neurophysiol.*, vol. 33, no. 1, pp. 71–80, 1972.

[131] R. Ishii, K. Shinosaki, S. Ukai, T. Inouye, T. Ishihara, T. Yoshimine, N. Hirabuki, H. Asada, T. Kihara, S. E. Robinson, and M. Takeda, "Medial prefrontal cortex generates frontal midline theta rhythm," *Neuroreport*, vol. 10, no. 4, pp. 675–679, 1999.

[132] Y. Kubota, W. Sato, M. Toichi, T. Murai, T. Okada, A. Hayashi, and A. Sengoku, "Frontal midline theta rhythm is correlated with cardiac autonomic activities during the performance of an attention demanding meditation procedure," *Cogn. Brain Res.*, vol. 11, no. 2, pp. 281–287, 2001.

[133] L. I. Aftanas and S. A. Golocheikine, "Human anterior and frontal midline theta and lower alpha reflect emotionally positive state and internalized attention: high-resolution EEG investigation of meditation," *Neurosci. Lett.*, vol. 310, no. 1, pp. 57–60, 2001.

[134] P. M. Fitts and M. I. Posner, *Human Performance*. Belmont, CA: Brooks Cole, 1967.

[135] A. Shumway-Cook and M. H. Woollacott, *Motor control : translating research into clinical practice*, 3rd ed. Philadelphia: Lippincott Williams & Wilkins, 2007.

[136] J. L. Cameron, "William Stewart Halsted. Our surgical heritage.," *Ann. Surg.*, vol. 225, no. 5, pp. 445–458, May 1997.

[137] J. H. Peters, G. M. Fried, L. L. Swanstrom, N. J. Soper, L. F. Sillin, B. Schirmer, K. Hoffman, and S. F. L. S. C. the, "Development and validation of a comprehensive program of education and assessment of the basic fundamentals of laparoscopic surgery," *Surgery*, vol. 135, no. 1, pp. 21–27, 2004.

[138] J. Heemskerk, R. Zandbergen, J. G. Maessen, J. W. Greve, and N. D. Bouvy, "Advantages of advanced laparoscopic systems," *Surg Endosc*, vol. 20, no. 5, pp. 730–733, 2006.

[139] G. M. Fried, L. S. Feldman, M. C. Vassiliou, S. A. Fraser, D. Stanbridge, G. Ghitulescu, and C. G. Andrew, "Proving the value of simulation in laparoscopic surgery," *Ann Surg*, vol. 240, no. 3, p. 518, 2004.

[140] D. T. Woodrum, P. B. Andreatta, R. K. Yellamanchilli, L. Feryus, P. G. Gauger, and R. M. Minter, "Construct validity of the LapSim laparoscopic surgical simulator," *Am J Surg*, vol. 191, no. 1, pp. 28–32, 2006.

[141] C. E. Reiley, H. C. Lin, D. D. Yuh, and G. D. Hager, “Review of methods for objective surgical skill evaluation,” *Surg. Endosc.*, vol. 25, no. 2, pp. 356–366, 2011.

[142] D. L. Diesen, L. Erhunmwunsee, K. M. Bennett, K. Ben-David, B. Yurcisin, E. P. Ceppa, P. A. Omotosho, A. Perez, and A. Pryor, “Effectiveness of laparoscopic computer simulator versus usage of box trainer for endoscopic surgery training of novices,” *J Surg Educ*, vol. 68, no. 4, pp. 282–289, 2011.

[143] S. B. Issenberg and W. C. McGaghie, “Clinical skills training – practice makes perfect,” *Med. Educ.*, vol. 36, no. 3, pp. 210–211, 2002.

[144] G. Wulf, C. Shea, and R. Lewthwaite, “Motor skill learning and performance: a review of influential factors,” *Med. Educ.*, vol. 44, no. 1, pp. 75–84, 2010.

[145] C. H. Shea, C. Whitacre, and G. Wulf, “Enhancing Training Efficiency and Effectiveness Through the Use of Dyad Training,” *J. Mot. Behav.*, vol. 31, no. 2, p. 119, 1999.

[146] R. Brydges, H. Carnahan, O. Safir, and A. Dubrowski, “How effective is self-guided learning of clinical technical skills? It’s all about process,” *Med. Educ.*, vol. 43, no. 6, pp. 507–515, 2009.

[147] L. Kahn, M. Zygman, W. Rymer, and D. Reinkensmeyer, “Robot-assisted reaching exercise promotes arm movement recovery in chronic hemiparetic stroke: a randomized controlled pilot study,” *J. Neuroeng. Rehabil.*, vol. 3, no. 1, pp. 1–13, 2006.

[148] J. Abbott, P. Marayong, and A. Okamura, “Haptic Virtual Fixtures for Robot-Assisted Manipulation,” in *Robotics Research*, vol. 28, S. Thrun, R. Brooks, and H. Durrant-Whyte, Eds. Springer Berlin / Heidelberg, 2007, pp. 49–64.

[149] C. B. Guest, G. Regehr, and R. G. Tiberius, “The life long challenge of expertise,” *Med. Educ.*, vol. 35, no. 1, pp. 78–81, 2001.

[150] S. Tsuda, D. Scott, J. Doyle, and D. B. Jones, “Surgical Skills Training and Simulation,” *Curr Probl Surg*, vol. 46, no. 4, pp. 271–370, 2009.

[151] D. H. Ballard, M. M. Hayhoe, F. Li, and S. D. Whitehead, “Hand-eye coordination during sequential tasks.,” *Philos. Trans. R. Soc. Lond. B. Biol. Sci.*, vol. 337, pp. 331–338; discussion 338–339, 1992.

[152] G. Blohm, A. Z. Khan, and J. D. Crawford, “Spatial Transformations for Eye-Hand Coordination,” in *Encyclopedia of Neuroscience*, 2010, pp. 203–211.

[153] A. Ma-Wyatt, M. Stritzke, and J. Trommershäuser, “Eye-hand coordination while pointing rapidly under risk,” *Exp. Brain Res.*, vol. 203, pp. 131–145, 2010.

[154] O. Bock, M. Dose, D. Ott, and R. Eckmiller, “Control of arm movements in a 2-dimensional pointing task,” *Behav. Brain Res.*, vol. 40, pp. 247–250, 1990.

[155] K. Wilmut, J. P. Wann, and J. H. Brown, “How active gaze informs the hand in sequential pointing movements,” *Exp. Brain Res.*, vol. 175, pp. 654–666, 2006.

[156] T. W. Picton, “The P300 wave of the human event-related potential.,” *J. Clin. Neurophysiol.*, vol. 9, pp. 456–479, 1992.

[157] H. L. Dean, D. Martí, E. Tsui, J. Rinzel, and B. Pesaran, “Reaction Time Correlations during Eye–Hand Coordination: Behavior and Modeling,” *J. Neurosci.* , vol. 31 , no. 7 , pp. 2399–2412, Feb. 2011.

[158] R. A. Hill and R. A. Barton, “Psychology: Red enhances human performance in contests,” *Nature*, vol. 435, no. 7040, p. 293, May 2005.

[159] G. Wulf, C. Shea, and R. Lewthwaite, “Motor skill learning and performance: A review of influential factors,” *Medical Education*, vol. 44. pp. 75–84, 2010.

[160] C. H. Shea, G. Wulf, and C. Whltacre, “Enhancing Training Efficiency and Effectiveness Through the Use of Dyad Training,” *Journal of Motor Behavior*, vol. 31. pp. 119–125, 1999.

[161] V. Kolev, J. Yordanova, M. Schürmann, and E. Başar, “Increased frontal phase-locking of event-related alpha oscillations during task processing,” *Int. J. Psychophysiol.*, vol. 39, no. 2–3, pp. 159–165, Jan. 2001.

APPENDIX: EEG Analysis results from the sequential pointing experiment

Spectral Analysis

In the following Figure A1 - Figure A2, the channel spectra topographical maps and ICA component scalp maps of two subjects at the first and last trial are shown.

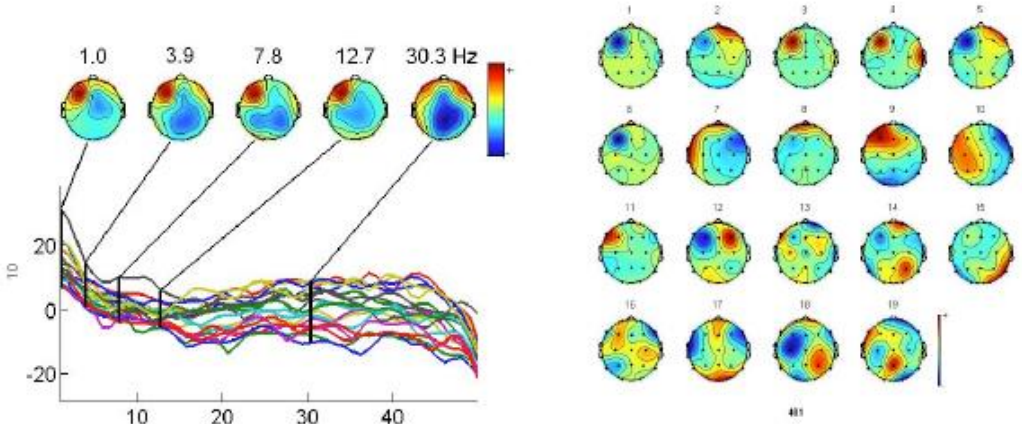

Subject 1 Trial 1 (a) Channel spectral scalp map (b) Component scalp map

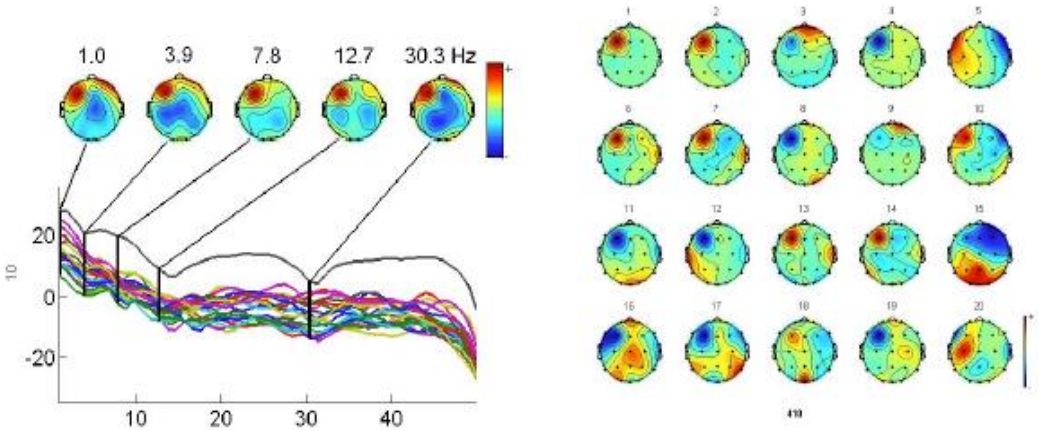

Subject 1 Trial 10 (a) Channel spectral scalp map (b) Component scalp map

Figure A1: Subject 1 Trial 1 and 10 (a) Channel spectral scalp map (b) Component scalp map

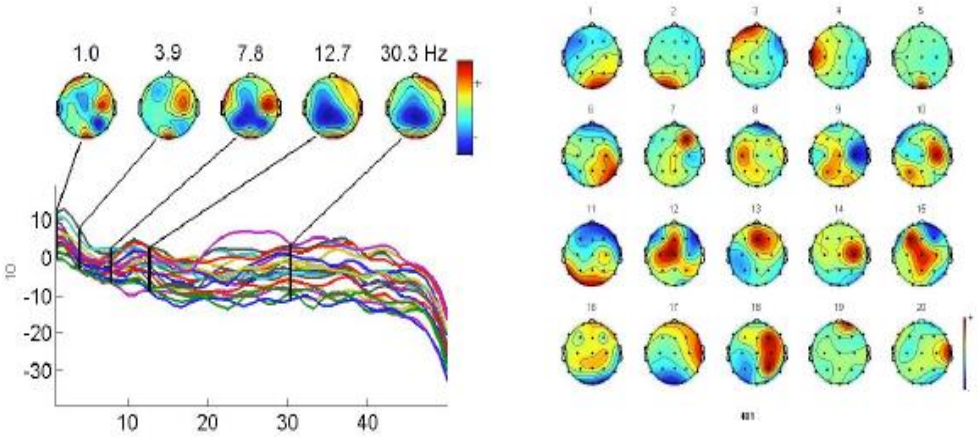

Subject 2 Trial 1 (a) Channel spectral scalp map (b) Component scalp map

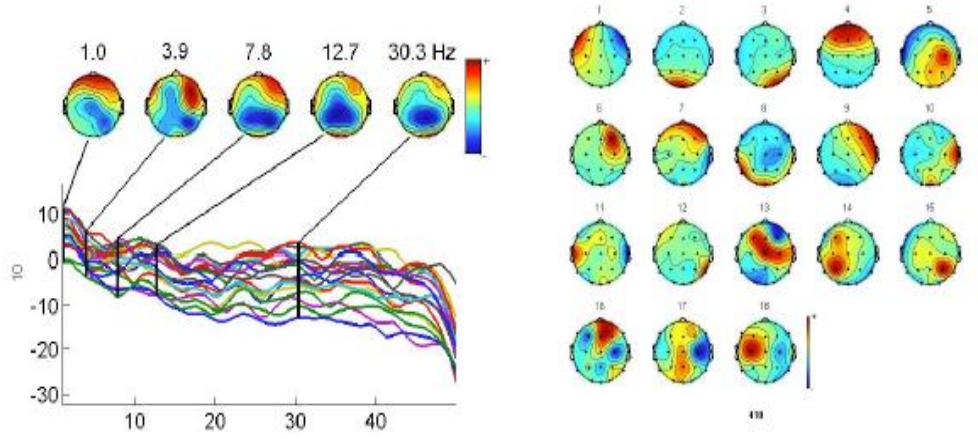

Subject 2 Trial 10 (a) Channel spectral scalp map (b) Component scalp map

Figure A2: Subject 2 Trial 1 and 10 (a) Channel spectral scalp map (b)

Component scalp map

LZC complexity

In the following Figure A3 - Figure A4, the complexity values each of the 18 subjects in the sequential pointing experiment detailed in Chapter 7 are shown. The complexity values for the first sequential pointing trial are plot in blue. The complexity values for the last sequential pointing trial are plot in red.

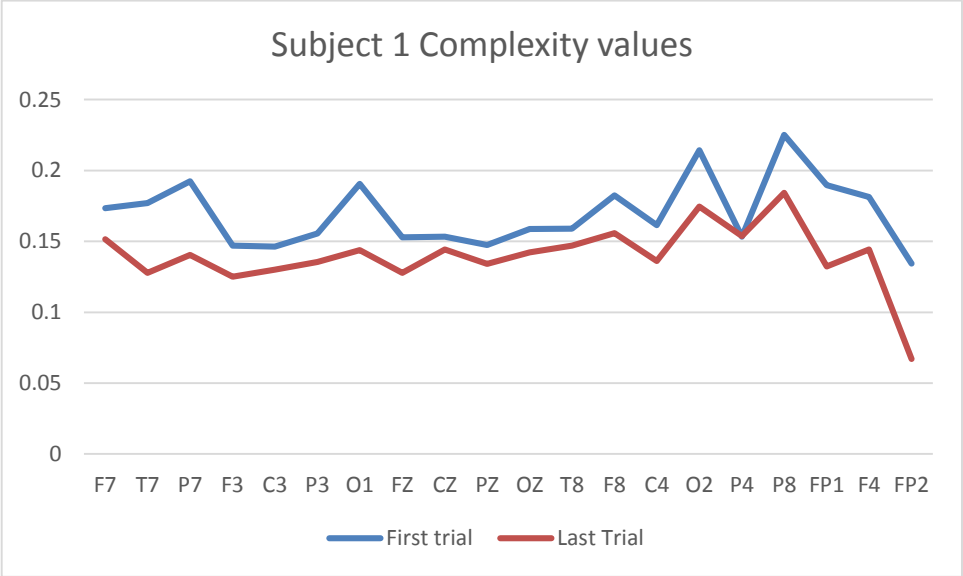

Figure A3: Lempel-Ziv Complexity values for Subject 1.

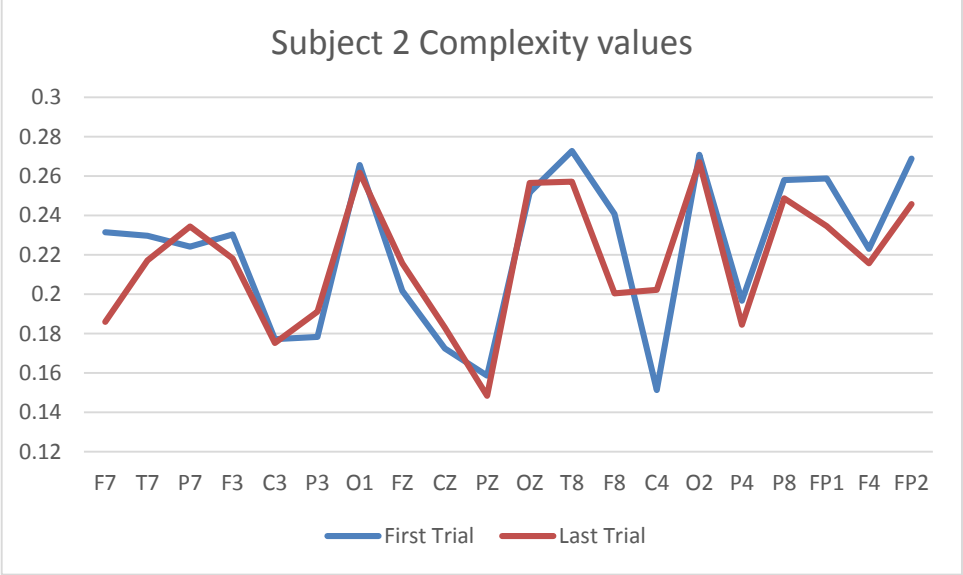

Figure A4: Lempel-Ziv Complexity values for Subject 2.

Event-Related Potential

In the following Figure A5 - Figure A6, The ERP plots comparing the subjects' ERP from the first half of the experiment and the second half of the experiment is shown. The blue lines indicate the average ERP of the successfully completed tasks in the first 5 trials. The red lines indicate the average ERP of the successfully completed tasks in the last 5 trials.

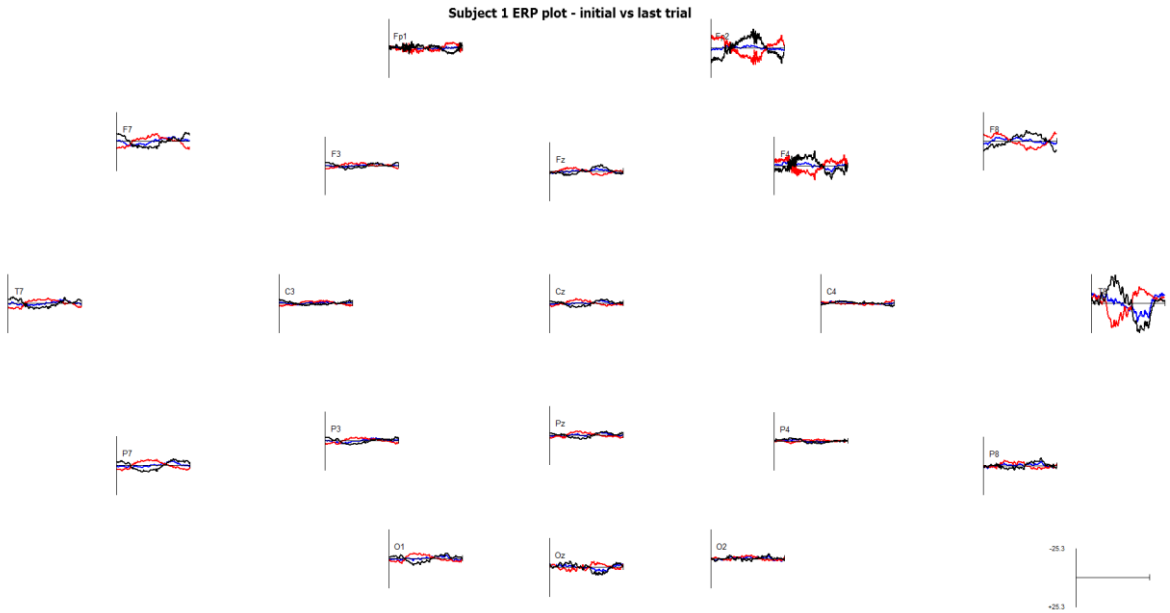

Figure A5: Subject 1 ERP plot – comparison of initial vs last trials.

The Blue lines indicate the average of the successfully completed tasks in the first 5 trials and the red lines indicate the average of successfully completed tasks in the last 5 trials. The black lines are the calculated difference between the first 5 trials and last 5 trials.

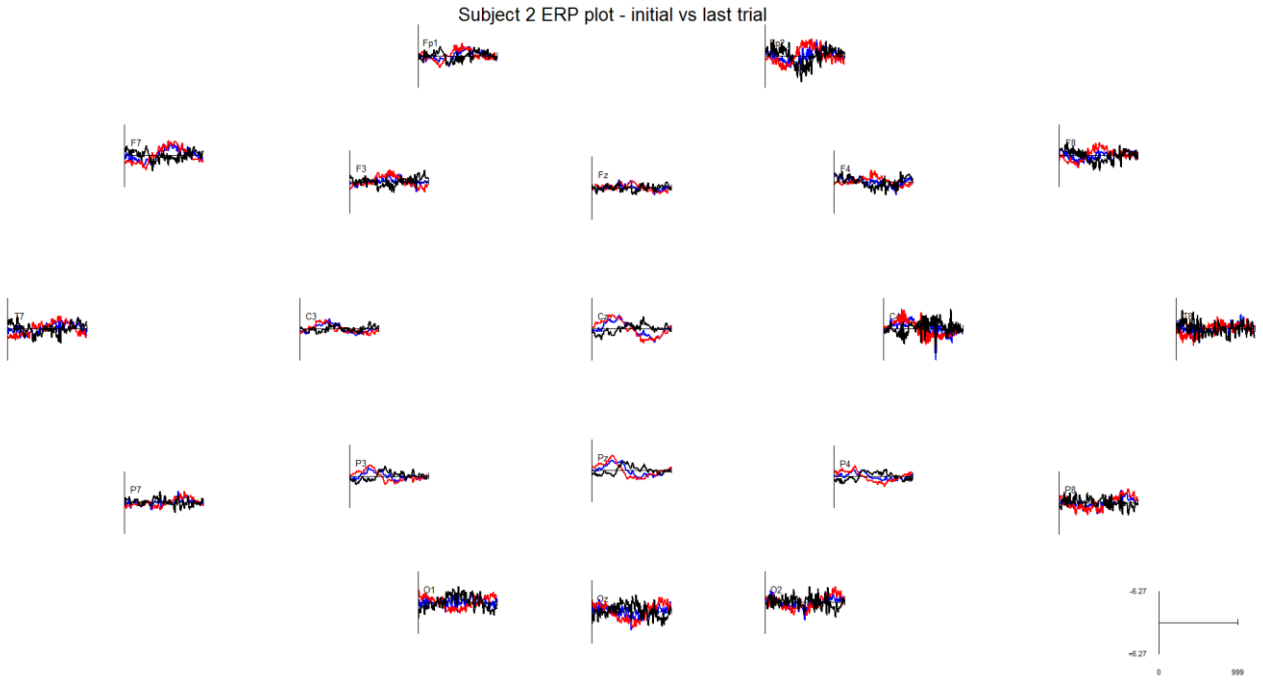

Figure A6: Subject 2 ERP plot – comparison of initial vs last trials.

The Blue lines indicate the average of the successfully completed tasks in the first 5 trials and the red lines indicate the average of successfully completed tasks in the last 5 trials. The black lines are the calculated difference between the first 5 trials and last 5 trials.

In the following Figure A7-Figure A8, The ERP plots comparing the subjects' ERP from the successfully completed tasks against unsuccessfully completed tasks is shown. The blue lines indicate the average ERP of the successfully completed tasks. The red lines indicate the average ERP of the unsuccessfully completed tasks. The black lines are the calculated difference between the blue and red lines.

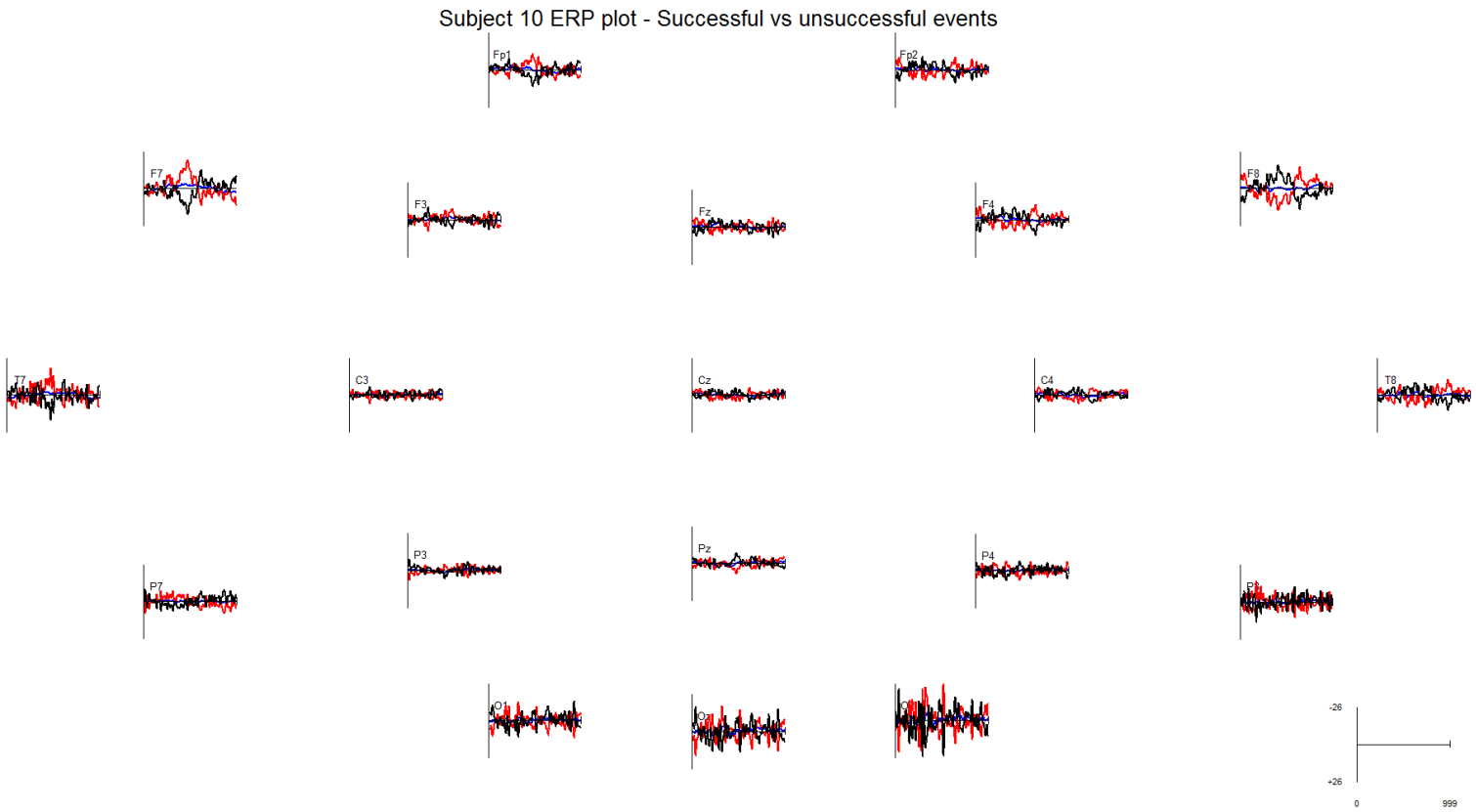

Figure A7: Subject 10 ERP plot – Comparison of successfully completed tasks vs unsuccessfully completed tasks.

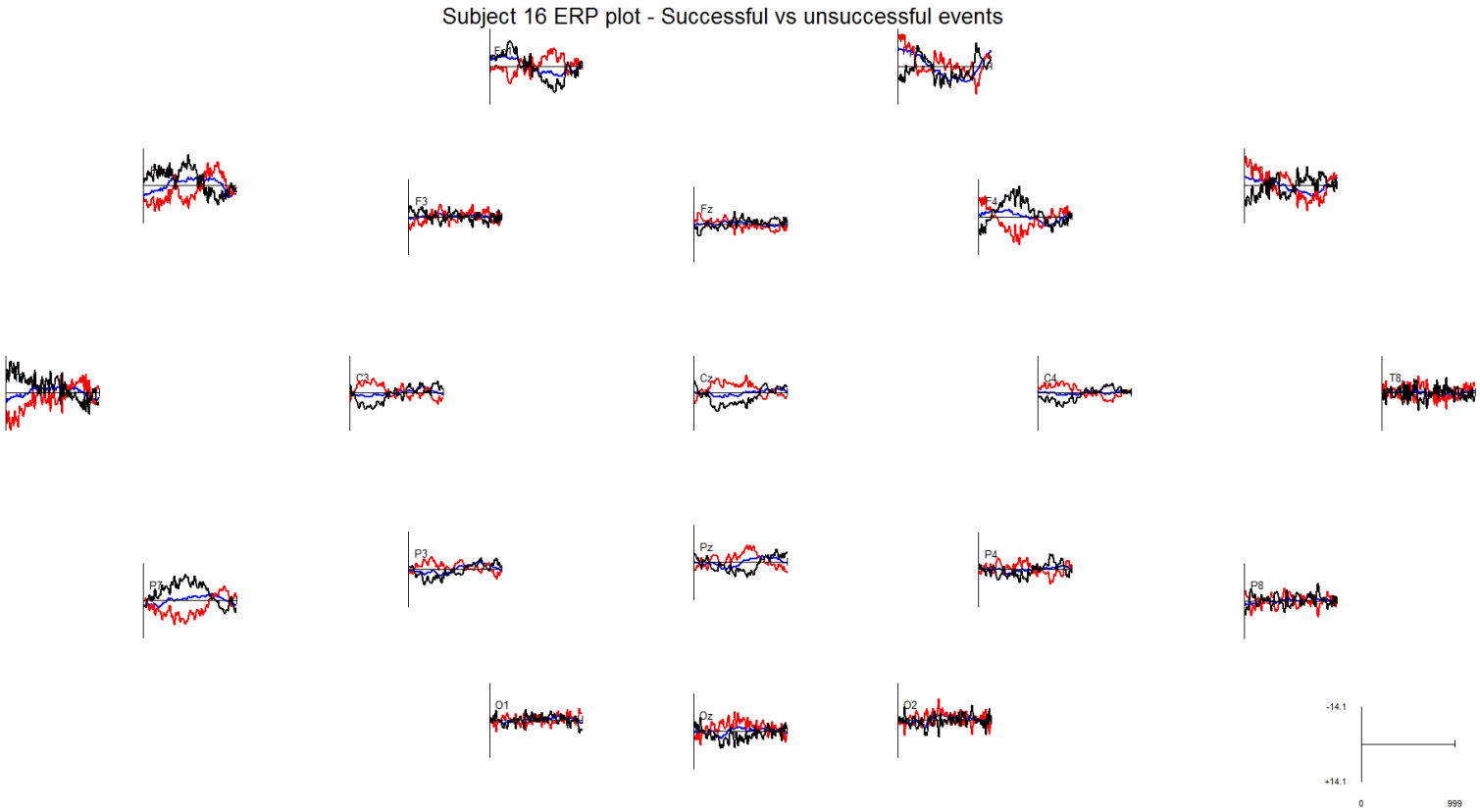

Figure A8: Subject 16 ERP plot – Comparison of successfully completed tasks vs unsuccessfully completed tasks.